Department of Precision and Microsystems Engineering

Compliant Continuous-Locking Micro Mechanism
Design of a Locking Mechanism for Frequency Tuning

Sjoerd van Bracht

TUDelft
Delft
University of
Technology

Challenge the future

Compliant Continuous-Locking Micro Mechanism

Design of a Locking Mechanism for Frequency Tuning

by

S. van Bracht

in partial fulfillment of the requirements for the degree of

Master of Science
in Mechanical Engineering

at the Delft University of Technology,
to be defended publicly on Thursday November 12, 2015 at 13:30.

Student number:	1515683	
Daily Supervisor:	Dr. N. Tolou,	TU Delft
Professor:	Prof. dr. ir. J.L. Herder,	TU Delft
Thesis committee:	Dr. M.K. Ghatkesar,	TU Delft
	Dr. J.J. van den Dobbelsteen,	TU Delft

This thesis is confidential and cannot be made public until December 31, 2022.

An electronic version of this thesis is available at `http://repository.tudelft.nl/`.

PREFACE

Since I can remember I have always loved to design, create, 'improve' or 'repair' mechanism. In my childhood this only involved Legos, but growing older everything my dad's toolbox allowed underwent inspection. Since my start at the TU Delft this 'urge' is used for more constructive projects such as building electric race cars at FS Team Delft (DUT), maintaining my motorcycle(s) or working at the student walk-in workshop. In the first year of my master Just and Nima introduced me to a different type of mechanism. This mechanism does not suffer from all conventional downsides such as lubrication and play which are usually the main reasons for me to disassemble and/or fix it in the first place. These 'Compliant Mechanisms' are not only very cool looking, but when used correct also very useful as I hope to show with the final design presented in this thesis.

This project started with an internship at Flexous BV, but after multiple interesting discussions, feedback sessions, brainstorms and random activities with not only my supervisors Just and Nima but also Jan, Wout, Maarten, Rik, Sybren, Davood, Gerard, Giuseppe, Ásphór, Milton, Minchang, Jelle, Wouter, Sander, Bart-Jan, Rogier, Oleg and Tom it transformed into the project it is now. Without this group it wouldn't have been this much fun and I would like to thank all!

Finally I would like to thank my family and friends for their help, support and interest along the way while dealing with a technical vocabulary describing designs using words such as 'dingen', 'pielen', 'jetsers' and 'apparaten'.

Sjoerd van Bracht
Delft, November 2015

iii

CONTENTS

1

INTRODUCTION

This document contains all relevant readings related to the thesis 'Compliant Continuous-Locking Micro Mechanism'. Main content of this thesis can be found in a thesis paper in Part I.

Prior to this research, a literature study is conducted with main objective to identify different ways to tune frequency on micro-scale (Part II). This result is used to find a suitable solution to change the frequency for an initial case study (Chapter 2).

The process from frequency tuning towards a compliant continuous-locking micro mechanism is described in part III starting with the evaluation of different methods of tuning frequency in Chapters 4 to 6. Next the main system functions for the desired tuning method are discussed (Chapter 7). Based on the main system function evaluation the essence of the problem appears not to be the frequency tuning as investigated in the first part of this technical report but fixation of the move that is used to tune frequency. The research topic is therefore adapted to a micro locking mechanism, resulting in the paper presented in this document. Additional readings considering detailed design, large and small scale prototyping and prototype testing as presented in Part I can be found in Chapters 8 to 11.

I

THESIS PAPER

Compliant Continuous-Locking Micro Mechanism

S. van Bracht, N. Tolou and J.L. Herder

Faculty of Mechanical, Maritime and Materials Engineering

Delft University of Technology, Delft, The Netherlands

Abstract—**Micro-electromechanical systems (MEMS) often require tuning to correct for fabrication errors such as changed dimensions or to adapt for a different scenario such as changed temperature. To prevent continuous power consumption for maintaining system behavior, a locking system can be added which does not require any power during operation. A new comb finger locking mechanism design is proposed using an orthogonal spring force on a moving shuttle to generate a locking force in the motion direction through friction. Multiple contact points are placed in line with the spring force to increase the locking force in a volumetric efficient way. The spring is optimized for high locking force but low sensitivity to fabrication errors. Mechanism design is illustrated and successfully tested using a case study example.**

Index Terms—**Locking mechanism, compliant, continuous, friction contact, MEMS**

I. INTRODUCTION

MICRO-electromechanical systems (MEMS) are widely produced using different etching techniques. Depending on the technique used and phenomena like under- and over-etching, the final product tends to show some deviations from the desired geometry. Especially for devices that obtain their accuracy from this geometry such as a ratchet mechanism [1] or positioning using interlocking teeth [2], deviations affect system performance. Therefore small tuning corrections are required to compensate for these fabrication errors. A second application for tuning is to adjust a device for different tasks, e.g. an accelerometer with tuning capability to improve sensor resolution [3], changing the resonance frequency of an piezoelectric vibration energy harvester for improved harvesting performance [4], and changing a resonators resonance frequency for wide multiband frequency applications [5].

Nowadays tuning is accomplished by changing specific components in the device, resulting in a tuned system with the desired characteristics. A variety of tuning methods is reported in literature, such as heating compliant members resulting in a deformed structure with different characteristics [6], using a comb finger electrostatic actuator [7] or a magnetic field [8, 9] to change the system stiffness. Since MEMS are often monolithic, changing these components in the device will result in deformation of compliant members. These compliant members will deliver a counter force. In order to maintain the tuned system characteristics an actuator applying a tuning force should remain active resulting in continuous power consumption. An actuator and power source including the required space for both is therefore required, limiting the applicability of such a design.

Chiu et al. [10] and Santeri and Sami [11] report methods to bond MEMS structures. Bonding techniques are a method to permanently secure the relative position of tuned components. However, when a new error is introduced in the system after bonding, tuning is not possible anymore resulting in a dysfunctional system.

A method that does not permanently secure the tuning position is the use of a locking mechanism after tuning, ensuring no relative motion between system components when the tuning force is removed. A locking mechanism needs to be added, but after tuning no power is consumed and system functionality is independent of a power source. The second advantage of a locking mechanism is the ability to unlock the system and readjust it. Multiple monolithic locking mechanisms do exist such as interlocking teeth mechanisms [2, 12], providing a high locking force for a large range of motion. The locking positions are however limited by teeth position and interval. The tuning resolution is therefore limited by the fabrication resolution of these teeth. Besides that, an extra degree of freedom (DOF) is required to overcome the teeth height during tuning. A mechanism that can provide a high locking force while not relying on an additional DOF is presented in [13]. It uses two stable positions providing two tuning positions. A similar principle is also shown in [14]. However, these solutions only allow tuning for two preset positions instead of a continuous range. A mechanism that does provide a continuous range is demonstrated in [15]. First two hook elements are aligned (tuned) with respect to each other. Finally, the surfaces are pressed together creating a friction contact between both, locking the relative position.

Downside of this design is the small stroke which is limited by the hook design.

The referenced works obtain useful properties but no mechanism is encountered that combines a large continuous range of motion without an additional actuator exclusive to the locking mechanism.

The goal of this paper is to design a compliant continuous-locking mechanism for a large range of motion, capable of withstanding internal and external forces without power consumption once the system is tuned.

The new locking mechanism principle will be presented in Section II. Test results on a case study using this principle will be shown in Section III and discussed in Section IV. A conclusion regarding this new locking mechanism design is given in Section V.

II. METHODS

The proposed locking mechanism is based on two main working principles: 1) friction locking via a preloaded spring and 2) increasing the amount of friction contact points to increase the total locking force. A case study is used to evaluate the presented working principles.

A. Friction Locking

To ensure the system behavior after tuning is maintained, a locking mechanism is required to withstand both internal forces F_i due to deformation of compliant members, as well as external forces F_e such as shocks, resulting in a minimum locking force F_L:

$$F_L \geq |F_i + F_e| \tag{1}$$

The proposed locking mechanism generates a normal force in y-direction on an initially actuated shuttle to provide a locking force in the x-direction due to friction (fig. 1). This normal force is generated by a spring-structure with stiffness k_s which is prestressed via the actuated shuttle by tuning motion u_x. This tuning motion causes deformation of compliant members in the structures with stiffness k_i resulting in F_i.

The locking force can be determined according to eq. (2) with friction coefficient μ while $k_s \delta_s = F_s$.

$$F_L = \mu k_s \delta_s \tag{2}$$

This working principle uses the main actuation motion to prestress the spring via the shuttle geometry creating a normal force on this shuttle. The friction force generated by this normal force acts as a locking force in x-direction, thus eliminating the need for a second locking actuator.

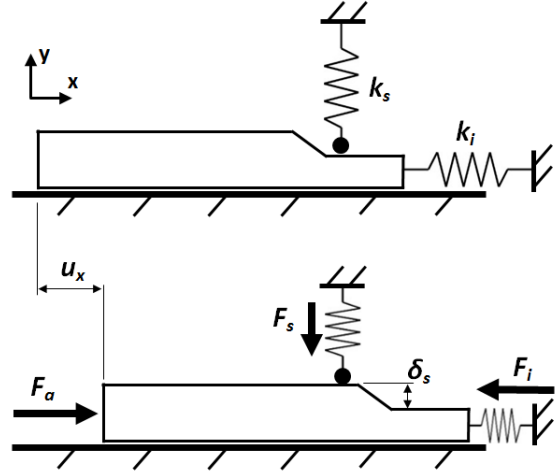Readjusting the shuttle position after initial tuning can be accomplished by again applying F_a, reversing

Fig. 1. Schematic representation of locking by prestressing a spring structure via an actuated shuttle: Actuator force F_a displaces the shuttle over distance u_x causing the spring to deform with distance δ_s resulting in F_s. This spring force generates a normal force between the shuttle and the base, which generates a friction force that acts as the locking force F_L.

its direction for opposed movement or lifting the spring causing the the shuttle to move back to its original position due to force F_i.

B. Spring Design

The function of the spring is to deliver the required normal and therefore locking force, while the design is constrained by a maximum design stress σ_{max}, available area A_{max} and fabrication limitations. When designing for micro-structures in materials such as silicon, having a high Young's Modulus, only a small amount of deformation is allowed before the stress constraint is violated. As a consequence the spring is prone to becoming very stiff resulting in a small prestress displacement δ_s before the required spring force F_s is obtained. Such a system is therefore sensitive to fabrication errors since a small offset in the prestress displacement will result in either a high spring force and high stresses or a low spring force and insufficient locking force. Therefore the spring is optimized to be as soft as possible until a minimum δ_s is obtained.

A 5-control point Bézier curve is used to generate spring geometries. Each control point is defined by an x- and y-coordinate. The first control point is fixed (base), resulting in a total 8 DOFs. An additional DOF is added by the in-plane thickness of the spring which is constant over its length. Stiffness characteristics of the locking spring in y-direction are determined using a finite element analysis (FEA).
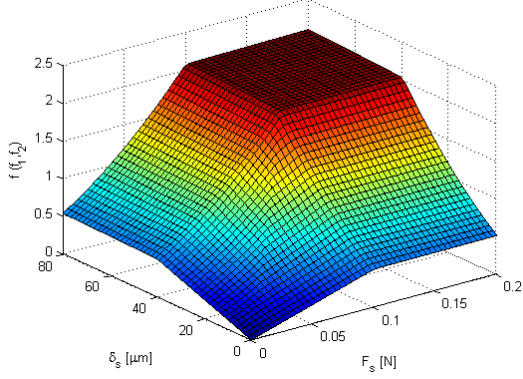
Fig. 2. Spring optimization objective function $f(f_1, f_2)$ where $f_1(F_s)$ and $f_2(\delta_s)$

A genetic optimization process, using these 9 parameters, is executed according to the optimization function in eq. 3. The objective is to maximize the spring force F_s and prestress displacement δ_s according to objective function $f(x)$ with $x = x(f_1, f_2)$, where $f_1(F_s)$ and $f_2(\delta_s)$ (eq. 4). A graphical representation of this objective is presented in fig. 2.

$$\min_{x} \quad f(x) \qquad\qquad (3)$$
$$\text{s.t.} \quad \sigma \leq \sigma_{max}$$
$$A \leq A_{max}$$

$$f(x) = (-f_1 - f_2)\left(1 + \left|\frac{\min(x)}{\max(x)}\right| \max(x)\right) \quad (4)$$

C. Multiple Friction Contact Points

If the optimized spring cannot deliver the required friction force within the given constraints, multiple contact points can be added. Friction will occur at every contact point increasing the total locking force. The number of contact points can be increased by
1) increasing the number of springs n_F (contact forces) in parallel resulting in eq. (5),

$$F_L = \sum_{i=1}^{n_F} \mu \cdot F_{s,i} \qquad\qquad (5)$$

2) increasing the number of contact friction points n_μ in line with a spring force, assuming equal force at each contact, yielding eq. (6).

$$F_L = n_\mu \cdot \mu \cdot F_s \qquad\qquad (6)$$
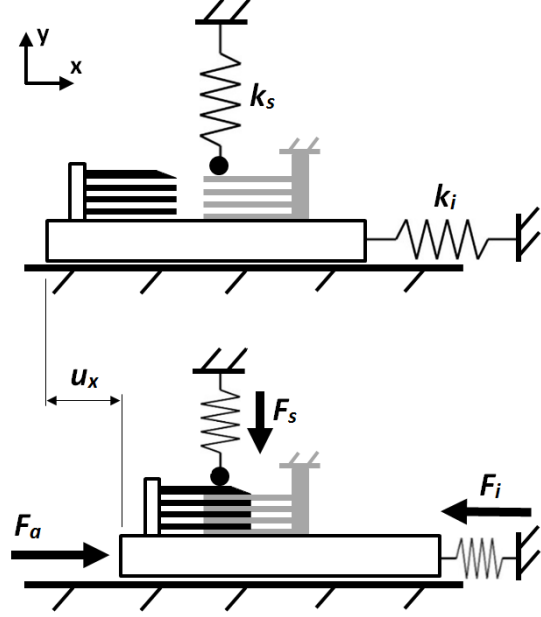
or 3) a combination of both eq. (7):

Fig. 3. Schematic representation of locking mechanism with 8 additional contact points via an orthogonal loaded flexible comb structure

$$F_L = \sum_{i=1}^{n_F} n_{\mu,i} \cdot \mu_i \cdot F_{s,i} \qquad\qquad (7)$$

Adding multiple soft springs, insensitive to fabrication errors, consumes a relatively large area, whereas adding contact points in series with a single spring could be accomplished with higher volumetric efficieny using e.g. a orthogonal loaded comb structure (fig. 3).

Main advantages of this principle are the volumetrically efficient increase in locking force and the adjustability of this force by addition or removal of comb fingers independent of the spring characteristics.

D. Case Study

A case study is conducted for a silicon structure with $h = 525\mu m$, produced using Deep Reactive Ion Etching (DRIE) for a load case where $F_i + F_e = 100mN$. According to eq. (1) this requires $F_L \geq 100mN$. The design is constrained by a maximum design stress $\sigma_{max} = 200MPa$ and available area $A_{max} = 10mm^2$. Fabrication limitations set an additional constraint on the minimum distance $w_{gap} \geq 180\mu m$ between components.

Reported friction coefficient values for silicon-silicon contact vary between 0.2-0.7 [16, 17]. To ensure locking in all cases, μ is assumed to be 0.2
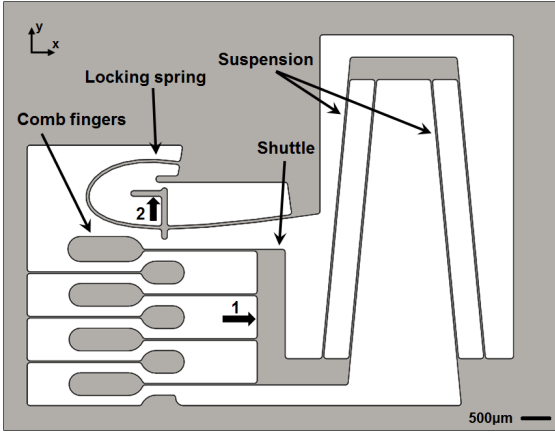
Fig. 4. Locking system design in unlocked state showing the locking spring and 7 comb fingers suspended via shuttle, suspension and base. Actuation points for different measurements are represented by the numbered arrows

Fig. 5. Measurement setup configuration used to determine the prototype stiffness and locking force
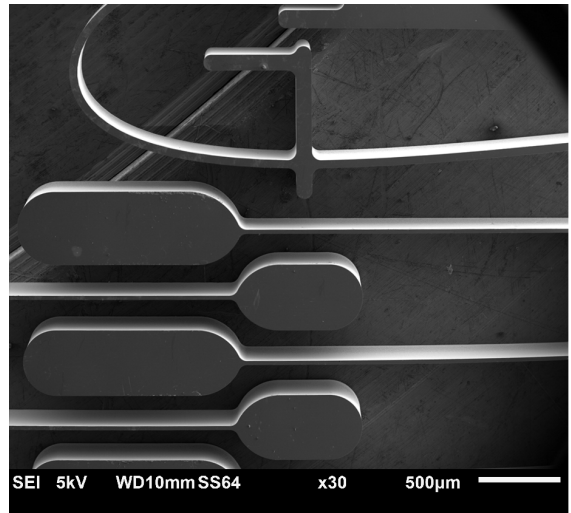
Fig. 6. Skewed top-view SEM image of the locking spring and comb fingers in unlocked state

resulting in $F_s \geq 0.5N$ (eq. (2)).

The optimization process yields a spring with maximum objective values $F_s = 0.069N$ and $\delta_s = 49.9\mu m$ while both the stress and area constraint are active. According to eq. (6) this requires $n_\mu = 8$ which is accomplished by adding 7 comb fingers in line with F_s.

The final design (fig. 4) shows the 7 comb fingers and locking spring. A suspension and shuttle are added to the right set of comb fingers to prevent these from dropping out of the design after production and allow testing.

E. Testing

Multiple tests are performed to confirm the dimensions, evaluate the stiffness characteristics of the locking spring and suspension, and to determine the total locking force.
Prototype dimensions are measured via a scanning electron microscope (SEM). Stiffness characteristics of the prototype are measured using a *Futek LSB200 20gr Miniature S-Beam Load Cell* in combination with a *Physik Instrumente M-406.2DG Precision Linear Stage* to provide a linear motion. A measurement needle is connected to this sensor to actuate the MEMS prototype (fig. 5).

Measurement data is corrected for the stiffness of this measurement needle $k_n = 0.8478N/mm$.
The suspension stiffness and total locking force are measured by actuating the shuttle at point 1 (fig. 4). Readjusting the system in the opposite direction or unlocking is accomplished by reversing the actuation force at this point. The stiffness of the locking spring is measured by actuating the spring at point 2 (fig. 4). This point can also be used for unlocking.

III. RESULTS

A. Locking Spring

The resulting design before and after locking is shown in fig. 6 and fig. 7.

The right set of comb fingers is attached to a shuttle which is suspended via a suspension on the right with $k_i = 0.0052 \pm 6.92e^{-5}N/mm$.

SEM imaging shows a spring thickness of $46.31\mu m$. Prestress displacement is measured to be $\delta_s = 41\mu m$.

Force deflection measurements in x- and y-direction of the spring are presented in fig. 8 and fig. 9 and are compared to the FEA using the measured dimensions.

Fig. 7. Locking system in locked state. The locking spring is prestressed via comb fingers in line below which are attached to the shuttle and suspension with stiffness k_i

Fig. 10. Measurements results of forward locking movement showing a locking force $F_L = 147mN$

Fig. 8. Locking spring measurement results in x-direction showing a 4.6% deviation from the FEM

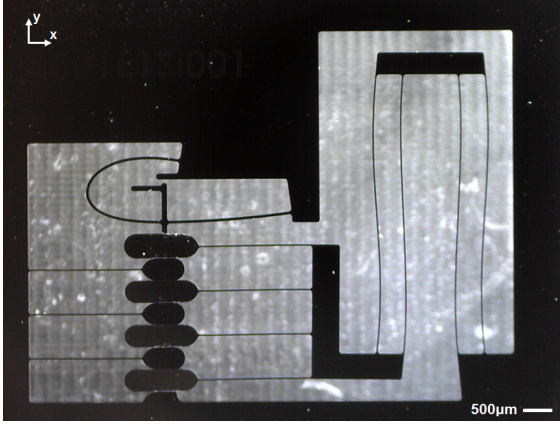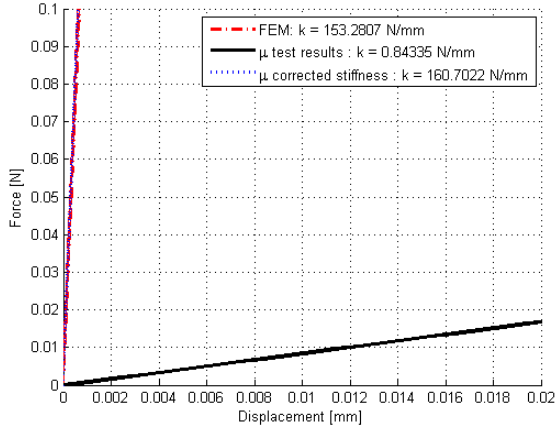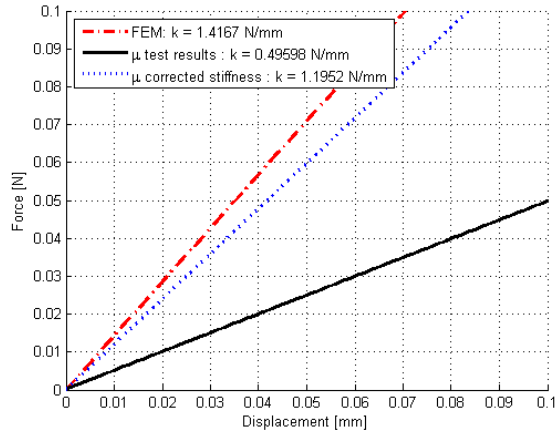Fig. 9. Locking spring measurement results in y-direction showing a 15.9% deviation from the FEM

Measurement results in x-direction show $k'_{s,x} = 0.8434 \pm 0.0041N/mm$. After correcting for the

measurement needle, using a linear fit ($r = 0.997$), this results in $k_{s,x} = 160.70N/mm$ which is a 4.6% deviation from the FEA.

Measurement results in y-direction show $k'_{s,y} = 0.4953 \pm 0.0005N/mm$. After correcting for the measurement needle, using a linear fit ($r = 0.999$), this results in $k_{s,y} = 1.195N/mm$ which is a 15.9% deviation from the FEA.

B. Locking Force

Using eq. (6), where $F_s = k_{s,y}\delta_s$, the theoretical minimum locking force is obtained as:

$$F_L \geq 78mN \tag{8}$$

The real locking force can be derived from the measurement results of a forward locking movement (fig. 10).

Section A-B shows the initial displacement of the shuttle with $k_i = 0.0052N/mm$ until contact occurs between the spring contact tip and upper comb finger. Region B-C shows the prestressing of the spring. The total locking force is equal to:

$$F_L = F_C - F_B - k_i(x_C - x_B) = 147mN \tag{9}$$

In the region C-D the prestress displacement, and therefore locking force, is constant and again only k_i is measured.

A second measurement is performed to confirm the locking force by measuring the initial force to displace the spring in y-direction when the locking mechanism is in locked state. The initial force is measured at $0.052N$ showing a 6% deviation from the normal force based on the measurement as $F_s = 1.195 \cdot 41e^{-3} = 0.049N$.

IV. Discussion

The spring stiffness in y-direction shows a large offset with the FEA results. Main reason for this offset, besides a measurement error, is the out-of-plane variation in spring thickness. The etching process is known to give a trapezoidal cross section with approximately $1\mu m$ offset between top and bottom. The measurement is performed on the thicker top surface. Since stiffness scales to the power 3 with thickness, a $1\mu m$ offset can already account for 7% of the stiffness variation which is close to the offset found during the measurement.

The normal force providing the locking force is calculated based on perfect alignment of the comb fingers, meaning the comb fingers do not influence or contribute to the total locking force, and SEM measurements of the comb finger tip thicknesses between spring contact tip and base. First, the summation of measurement errors of $1\mu m$ per edge could result in an $16\mu m/41\mu m = 39\%$ offset in δ_s, causing an equivalent offset in spring force. Second, measurement footage showed a misalignment in y-direction of the comb fingers up to $10\mu m$. As a result the comb fingers are deflected causing an increase in normal force since these will act as additional spring in parallel with the main spring. A worst case scenario is investigated where all comb fingers are deflected with this maximum error. The resulting normal force is $< 2.5\%$ of the total normal force delivered by the spring, being almost negligible. This also justifies the normal force measurement by only actuating the spring instead of all comb fingers and spring combined which is not possible in the current test setup.

The spring contact is assumed to act as an additional friction contact point. For a regular spring this would be invalid since its stiffness in x-direction could be low. However due to the geometry of the spring used, a high stiffness in the locking direction is obtained (fig. 8) and the spring does act as an additional friction contact point.

The volumetric efficiency of the current design is limited by the minimum required gap distance w_{gap}. Replacing the relatively thick comb finger tips with minimum thickness fingers could decrease the required area for comb fingers with a factor 19 for the current design. One could also choose to flip the direction of the comb fingers such that the left and right set of comb fingers are etched besides each other (fig. 3) instead of the current intermingled layout (fig. 6). The size of the design will increase in y-direction but the size in x-direction will decrease. A second benefit of such a layout is the orientation of the comb fingers which will be loaded in tension when locked compared to the compressed state in the current design.

V. Conclusion

A compliant continuous-locking micro mechanism using a spring force in line with multiple friction contact points is proposed, designed and successfully tested. Adding friction contact points via a comb finger structure has shown to be an easy applicable and volumetric efficient method to increase the overall locking force. Spring design is accomplished using an optimization procedure generating a spring behavior that is both stiff enough to deliver the required normal force but not too sensitive to fabrication errors. Normal force and fabrication error sensitivity are predetermined parameters of the optimization algorithm.

A case study using DRIE showed locking spring characteristics comparable with FEM results, except for a 16% offset in y-stiffness resulting in a lower normal and therefore locking force. However, this decrease in locking force is compensated by a higher friction coefficient yielding a locking force $F_L = 147mN$ which is larger than the required $F_{L,designed} = 100mN$.

References

[1] Q. Ma and A. Berlin. Apparatus for adjusting the resonance frequency of a microelectromechanical (mems) resonator using tensile/compressive strain and applications thereof, 2005.

[2] J. K. Luo, Y. Zhu, Y. Q. Fu, A. J. Flewitt, S. M. Spearing, J. M. Miao, and W. I. Milne. Development of thermal actuators with multi-locking positions. *Journal of Physics: Conference Series*, 34(1):794, 2006.

[3] Kyu-Yeon Park, Chong-Won Lee, Hyun-Suk Jang, Yongsoo Oh, and Byeoungju Ha. Capacitive type surface-micromachined silicon accelerometer with stiffness tuning capability. *Sensors and Actuators A: Physical*, 73(12):109–116, 1999.

[4] E. S. Leland and P.K. Wright. Resonance tuning of piezoelectric vibration energy scavenging generators using compressive axial preload. *Smart Materials and Structures*, 15(5):1413, 2006.

[5] H. Tanigawa, S. Makita, and K. Suzuki. Silicon fishbone-shaped mems resonator with digitally variable resonant-frequency tuning. *IEEJ Transactions on Electrical and Electronic Engineering*, 5(2):164–170, 2010.

[6] W. H. Zhang and J. E. Y. Leea. Frequency tuning in a mems resonator via an integral crossbar heater. *Procedia Engineering*, 47(0): 949–952, 2012.

[7] S. G. Adams, F. M. Bertsch, K. A. Shaw, P. G. Hartwell, Noel C. MacDonald, and F. C. Moon. Capacitance based tunable micromechanical resonators. In *Solid-State Sensors and Actuators, 1995 and Eurosensors IX.. Transducers '95. The 8th International Conference on*, volume 1, pages 438–441, 1995.

[8] V. R. Challa, M. G. Prasad, Y. Shi, and F. T. Fisher. A vibration energy harvesting device with bidirectional resonance frequency tunability. *Smart Materials and Structures*, 17(1): 015035, 2008.

[9] T. Reissman, E. M. Wolff, and E. Garcia. Piezoelectric resonance shifting using tunable nonlinear stiffness. In *Active and Passive Smart Structures and Integrated Systems 2009*, volume 7288, pages 72880G–72880G–12, 2009.

[10] Y. Chiu, C. S. Wu, W. Z. Huang, and J. W. Wu. Assembly of micro-3-d components on soi wafers using novel su-8 locking mechanisms and vertical one-push operation. *IEEE Journal on Selected Topics in Quantum Electronics*, 15 (5):1338–1343, 2009.

[11] Tuomikoski Santeri and Franssila Sami. Wafer-level bonding of mems structures with su-8 epoxy photoresist. *Physica Scripta*, 2004(T114): 223, 2004.

[12] Q. X. Zhang, Y. Du, C. W. Tan, J. Zhang, M. B. Yu, G. Q. Lo, and D. L. Kwong. A mems platform for 2-d fine-positioning and locking of optical ball-lens in silicon photonics packaging. In *Photonics Global Conference (PGC), 2010*, pages 1–5, 2010.

[13] R. A. M. Receveur, C. R. Marxer, R. Woering, V. C. M. H. Larik, and N. F. de Rooij. Laterally moving bistable mems dc switch for biomedical applications. *Microelectromechanical Systems, Journal of*, 14(5):1089–1098, 2005.

[14] D. Dellaert and J. Doutreloigne. Design and characterization of a thermally actuated latching mems switch for telecommunication applications. *Journal of Micromechanics and Microengineering*, 24(7):075022, 2014.

[15] V. A. Henneken, W. P. Sassen, W. van der Vlist, W. H. A. Wien, M. Tichem, and P. M. Sarro. Two-dimensional fiber positioning and clamping device for product-internal microassembly. *Microelectromechanical Systems, Journal of*, 17 (3):724–734, 2008.

[16] K. Deng and W. H. Ko. A study of static friction between silicon and silicon compounds. *Journal of Micromechanics and Microengineering*, 2(1): 14, 1992.

[17] S. Suzuki, T. Matsuura, M. Uchizawa, S. Yura, H. Shibata, and H. Fujita. Friction and wear studies on lubricants and materials applicable to mems. In *Micro Electro Mechanical Systems, 1991, MEMS '91, Proceedings. An Investigation of Micro Structures, Sensors, Actuators, Machines and Robots. IEEE*, pages 143–147, 1991.

II

LITERATURE REVIEW

Tuning Frequency on Micro-Scale

S. van Bracht, N. Tolou and J.L. Herder

Faculty of Mechanical, Maritime and Materials Engineering

Delft University of Technology, Delft, The Netherlands

Abstract—This review presents an overview of frequency tuning mechanism on micro-scale for the the purpose of fabrication error adjustment for oscillating micro systems. A great variety of frequency tuning mechanism do exist, relying on different tuning principles with different properties. This article presents a classification method based on the fundamental principles used to describe a resonating system; mass, damping and stiffness. Literature is organized according to this classification presenting an overview of frequency tuning mechanisms available. Listed tuning properties such as the application moment of tuning, tuning range, working scale, reversibility and actuation principle of the tuning operation allow the reader to choose a frequency tuning method for their specific system requirements.

Index Terms—Frequency, tuning, MEMS, micro

I. Introduction

THERE is an increasing demand in smaller, lighter, more precise and cheaper devices. A technology that is extremely suitable for these kind of devices are Micro-Electro-Mechanical Systems(MEMS). MEMS are structures made using micro-machining techniques and vary in size between less than one micron up to a few millimeter.

Fabrication imperfections do limit product dimensions and affect performance. An example is the production of micromachined vibrational gyroscopes. These are produced using different production techniques such as wafer-to-wafer bonding, surface micromachining, and high-aspect ratio micromachining. Each of these techniques involve multiple processing steps with different tolerances, all contributing to a total fabrication error (Shkel et al., 1999). This production offset will finally result in a gyroscope with deviating frequency and lower accuracy.

One solution would be to eliminate the fabrication error which could be considered practically impossible or too expensive. A second approach would be to correct this error using a frequency tuning mechanism. This mechanism could also compensate for changing material behavior in different environments, making it versatile and widely applicable mechanism.

Multiple solutions to tune frequency do already exist, but these do not necessarily translate into a solution on small or MEMS scale due to limitations in precision or availability of specific elements on that scale. Some examples found in literature are changing the joint stiffness of an robotic arm via an electromotor (Wolf and Hirzinger, 2008), adjusting the pressure in fluidic circuit to control the output stiffness (Zoppi, 2013), regulating the length of a lever arm to change ratio and therefore output stiffness (Jafari et al., 2013) or simply by applying a tensile or compressive force on an elastic member to change its effective stiffness and therefore frequency (Leland, 2006). Another obvious option would be adding mass to lower a structure's frequency.

Presented solutions have different design purposes and therefore show a large variation in working principles and properties while the main objective, tuning frequency, is the same. Therefore the aim of this research is to present an overview of frequency tuning mechanisms on micro-scale including their properties for the purpose of fabrication error adjustment.

A method is defined to search literature for existing tuning mechanisms and a classification method is presented to organize and compare these findings in Section II. Different tuning mechanisms found in literature, and how these mechanisms are structured in the presented classification method is shown in Section III. Section IV discusses these results and implications of these findings. A conclusion is presented in Section V.

II. Methods

A search method is proposed using different search engines and different search terms. In order to compare literature found a classification system is presented.

A. Classification

First consideration is determining when the structure requires tuning. If the structure has a one-time offset, a single tuning step before operation would suffice to tune the device. However, if the offset is building up or varying over time, tuning during operation is required. This difference in timing determines the need for continuous presence of a frequency tuning stage and possible actuation and is therefore listed as the first level of classification.

The application moment of frequency tuning makes a clear distinction between tuning method designs

but does not clarify how the frequency is actually adjusted. In order to find the fundamental principles of frequency adjustment, the governing equation for an oscillating system is presented in (1).

$$m\ddot{x} + c\dot{x} + kx = F(t) \qquad (1)$$

system parameters mass m, viscous damping c, and stiffness k can be found with the forcing function F representing external input forces over time. These system parameters provide different principles to change the frequency response of a system and are therefore adopted as a second classification level. Since this review is interested in changing the system output given an external input, changing the forcing function, and therefore input frequency, is not considered.

To illustrate the effect of each system parameter on the system frequency, the equation for a damped harmonic oscillator is presented in (2). Damping forces in this model are assumed to be directly proportional to velocity and in opposite direction.

$$\omega_0 = \sqrt{\frac{k}{m}} \qquad \gamma = \frac{c}{2m} \qquad \omega_1 = \sqrt{\omega_0^2 - \gamma^2} \qquad (2)$$

with ω_0 the undamped natural frequency, γ the damping coefficient and ω_1 the damped frequency. Different options per system parameter are discussed below:

Mass: Changing frequency via mass can be accomplished by either adding or removing mass but also by moving the mass. According to (2) increasing the mass will lower the frequency.

Damping: Damping can be found in many forms like coulomb damping (mechanical), resistance (electrical) or absorption (optical). This review only considers mechanical and electrical damping. Increasing the damping (coefficient) will result in a lower frequency.

Stiffness: Considering the axial stiffness (3) or spring rate of a clamped cantilever beam (4) one can identify different parameters influencing the stiffness. Area A, length L, and moment of inertia I are clearly all dimension related whereas the Young's modulus E is a material property.

$$k = \frac{EA}{L} \qquad (3) \qquad\qquad k = \frac{3EI}{L^3} \qquad (4)$$

An alternative method is changing the stiffness directly by tensioning or buckling the structure, both imply some sort of preload. According to (2) the frequency will increase when the stiffness increases.

A schematic representation of this classification can now be presented in Table I where level 1 and 2 can be used in any combination while level 3 is a

TABLE I
SCHEMATIC REPRESENTATION OF DIFFERENT CLASSIFICATION LEVELS FOR TUNING FREQUENCY

Level 1 Tuning method	Level 2 Parameter	Level 3 Property
Before operation	Mass	Add
		Remove
		Move
	Damping	Mechanical
		Electrical
During operation	Stiffness	Dimensions
		Material
		Preload

unique subgroup to on level 2.

Tuning methods found are listed according to this classification scheme to find governing principles, similarities, differences or possible missing elements. For an objective comparison additional system properties are reported and evaluated such as the relative size of the tuning range around the nominal tuning frequency, the scale on which the tuning mechanism is used, the range of the tuning mechanism which is either continuous or discrete and whether the tuning step is reversible or not. Finally the required actuation force to apply the tuning step is listed.

To identify a tuning mechanism applicable for fabrication error adjustment different requirements can be distinguished:

1) The tuning mechanism should be capable of correcting all size fabrication errors, i.e. a sufficient tuning range.

2) When energy supply is limited or absent a tuning mechanism should consume little to no energy. Thus power availability and power consumption are important criteria.

3) The tuning actuation force should not interfere with the structural component, e.g. a magnetic actuation force between ferromagnetic structural components.

It is to the reader to decide whether these requirements apply to their specific application and deserve consideration.

B. Search method

Different keywords are defined to find relevant literature. To organize these keywords, synonyms or closely related keywords are grouped in a set as can be seen in Appendix A. These keywords are

combined with keywords from different sets but also with keyword within their own set. The resulting articles also present new keywords which are added to the keyword list.

The literature search is conducted using these keywords in multiple search engines to provide a large diversity of results. *Derwent Innovation Index* and *Googlescolar* are used to find journal articles, conference proceedings and patents, *Scopus* is used to find journal articles and conference proceedings and *Espacenet* is used to find patents. Although there is some overlap in results between search engines, all present unique results as well.

To extend the literature search, the citations in the articles found are also checked and used if relevant. This is repeated for one iteration.

III. RESULTS

The resulting classification scheme is presented in Table II and frequency tuning principles are listed per tuning parameter below.

A. Mass

Tuning before operation

Add: Multiple methods do exist to add mass to an oscillating system and obtain a permanent change in resonance frequency. Depending on the resonating beam and added material, different results are obtained in terms of tuning range but in all cases the frequency is only one-way adjustable.

The frequency sensitivity of a relative low density material deposition such as polysilicon on a resonating beam (Joachim and Liwei, 2002) can be found to be lower than a focused ion beam platinum deposition on a polysilicon cantilever beam (Enderling et al., 2007)(Figure 1).

A method with even higher frequency sensitivity is Pulsed Laser Deposition using gold on a resonating shuttle(Chiao and Lin, 2003)(Figure 2). Donor material is suspended above the resonating shuttle, a laser is used to remove material from this donor depositing it on the resonating shuttle increasing its weight and lowering its frequency.

Preferred technique can be decided on the accuracy of the deposition method and amount of tuning required.

Move: Moving mass will change the center of gravity of the system adjusting the resonance frequency. Wu et al. (2008) used this principle in a prototype at macro scale with a steel screw as adjustable mass (Figure 3). Tuning range of this solution is relatively large but cannot directly be translated to micro scale. Especially fixating a free
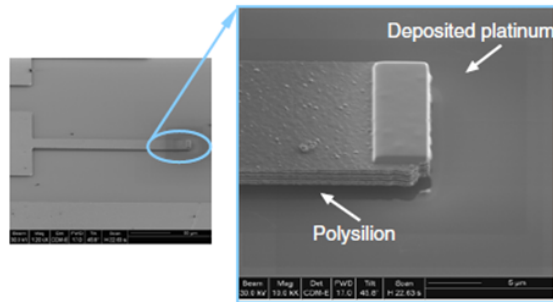

Fig. 1. Polysilicon cantilever beam with 1 μm thick deposited platinum at tip on a 13 μm x 5 μm surface (Enderling et al., 2007)
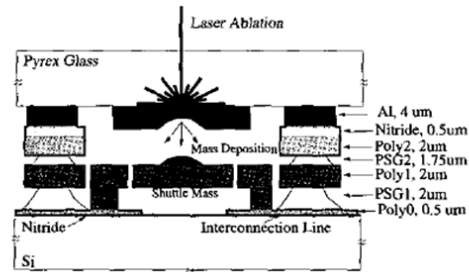

Fig. 2. Frequency tuning by mass addition via Pulsed Laser Ablation (Chiao and Lin, 2003)
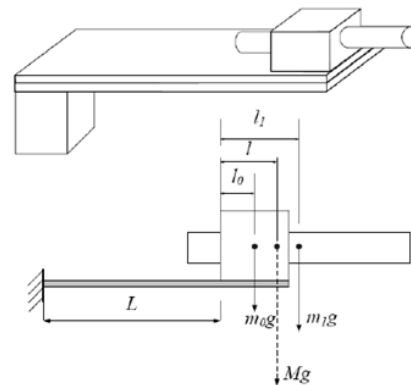

Fig. 3. Schematic of resonating beam with gravity center movable mass (Wu et al., 2008)

mass after adjusting could prove difficult.

Tuning during operation

Move: Miller et al. (2013) presented a passively self-tuning resonator using a mass free to slide along a fixed-fixed beam to self-tune (Figure 4). Self-tuning is only possible within a small preset operating regime resulting in a limited tuning range.

It is shown that the system in not sensitive to size scale or material used. Scaling down is therefore limited by manufacturing and material capabilities. Note that this solution does not require any form of

TABLE II
OVERVIEW OF FREQUENCY TUNING MECHANISMS FOUND IN LITERATURE

| Level 1 Tuning Method	Level 2 Tuning Parameter	Level 3 Tuning Property	References	Reported frequency tuning range [%]	Nominal frequency [Hz]	Working scale	Tuning range	Reversible	Actuation Principle
Before operation	Mass	Add	Joachim and Liwei (2002)	+0,7 to 2	86600	micro	continuous	no	-
			Chiao and Lin (2003)	-1,2	12450	micro	discrete	no	-
			Enderling et al. (2007)	-15,5	66,96	micro	continuous	no	-
		Move	Wu et al. (2008)	-18,5 to +9,9	162	macro	continuous	yes	-
	Stiffness	Dimensions	Tanaka et al. (1995)	-5	13731	micro	continuous	no	-
			Joachim and Liwei (2002)	+0,7 to 2	86600	micro	continuous	no	-
			Syms and Moore (1999)	-5	≈650	micro	continuous	no	-
		Material	Kun et al. (1997)	2,7	313781	micro	continuous	no	Thermal
		Preload	Challa et al. (2008)	20	26	macro	continuous	yes	Magnetic
			Reissman et al. (2009)	6	-	macro	continuous	yes	Magnetic
			Leland and Wright (2006)	-24	250	macro	continuous	yes	-
			Gonzalez Rodriguez et al. (2011)	-	-	macro	continuous	yes	-
			Ma and Berlin (2005)	-	-	micro/macro	discrete	yes	Electrostatic
			Tanigawa et al. (2010)	-	-	micro	discrete	no	Electrostatic
			Dehghan Niri and Salamone (2012)	+60Hz	-	macro	continuous	no	-
During operation	Mass	Move	Miller er al. (2013)	4,3 to 28,6	45 to 140	macro	continuous	yes	-
	Damping	Electrical	Wu et al. (2006)	1,6	93	macro	discrete	yes	-
			Cammarano et al. (2010)	-	-	macro	continuous	yes	-
			Badel et al. (2006)	+0,43	56.06	macro	continuous	yes	-
	Stiffness	Material	Nguyen and Howe (1993)	-1	66500	micro	continuous	yes	Thermal
			Zhang and Leea (2012)	-1,1	39200	micro	continuous	yes	Thermal
			Remtema and Lin (2001)	6,5	31000	micro	continuous	yes	Thermal
			Zoppi (2013)	-	-	macro	continuous	yes	Pressure
		Preload	Wolf and Hirzinger (2008)	-	-	macro	continuous	yes	Electromagnetic
			Cabuz et al. (1994)	-14Hz	-	micro	continuous	yes	Electrostatic
			Adams et al. (1995)	7,7 to 146	25000	micro	continuous	yes	Electrostatic
			Yao and MacDonald (1995)	6	1e6	micro	continuous	yes	Electrostatic
			Park et al. (1999)	-539	5120	micro	continuous	yes	Electrostatic
			Clark and Wang (2005)	-	-	micro	continuous	yes	Piezoelectric
			Azizi et al. (2013)	-	-	micro	continuous	yes	Piezoelectric
			Syms (1998)	-25 to +50	1560	micro	continuous	yes	Thermal
			Lee et al. (2009)	+10,7	1,698e6	micro	continuous	yes	Thermal
			Remtema and Lin (2001)	6,5	31000	micro	continuous	yes	Thermal
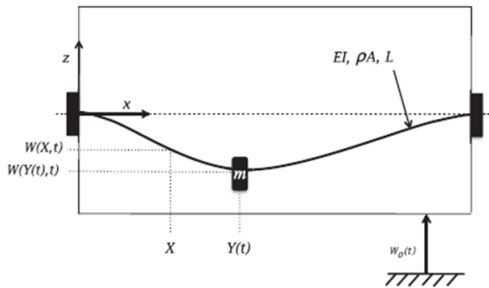
Fig. 4. Schematic of the beammass resonator system. The fixed-fixed beam is secured to a reference frame which is subjected to input vibrations. The mass is free to slide along the beam and has a moment of inertia about the y-axis. (Miller et al., 2013)

energy to obtain tuned behavior.

B. Damping

Tuning during operation

Electrical: Wu et al. (2006) reported a clamped piezoelectric bimorph. The upper layer of the cantilever beam consists of piezoelectric material used for frequency tuning while the lower layer is used to harvest vibration energy. The resonant frequency of the system can be shifted by switching in different capacitive loads. A microcontroller samples the external frequency and adjusts the capacitive load accordingly.

Cammarano et al. (2010) presented a vibration-based energy harvester where the reactive component of an electrical load is used to tune the harvester system.

Badel et al. (2006) used semi-active damping as vibration control using so called synchronized switch damping (SSD). The new semi-passive techniques offer self-adaptation compared with standard passive piezoelectric damping. Piezoelectric elements are switched between open- and short-circuit which finally results in energy dissipation. Different SSD techniques are discussed but the resulting resonance frequency is similar for all versions, namely (5) where the influence of damping C on the resonance frequency is clearly visible.

$$\omega_0 = \sqrt{\frac{K + \alpha^2/C}{M}} \tag{5}$$

with α a force factor of the force applied by piezoelectric elements.

The tuning range via damping is very small but could prove sufficient for fabrication error compensation. Application of tuning via damping on micro scale should be investigated, since examples found and reported are applied at macro scale and translation of the required electrical components to micro scale is unknown.

C. Stiffness

Tuning before operation

Dimension: Syms and Moore (1999) lowered the stiffness of a microactuator by local material removal(Figure 5) using focused ion beam (FIB) machining.
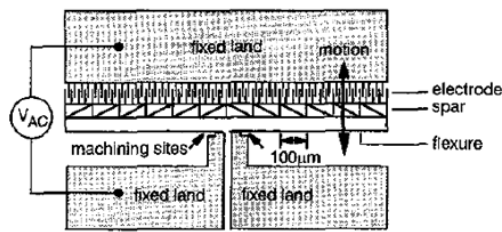
Fig. 5. Comb-drive electrostatic microactuator with FIB machining at indicated sites. (Syms and Moore, 1999)
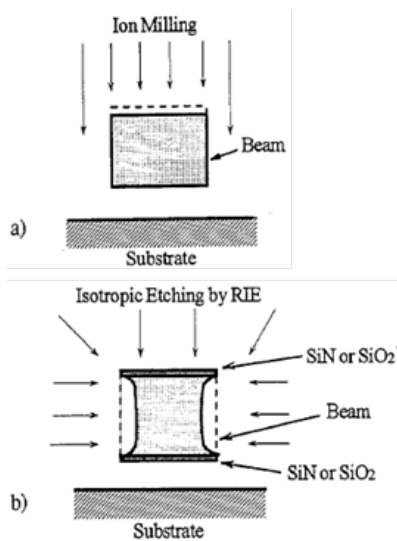

Fig. 7. Schematic of a compressively loaded piezoelectric bimorph vibration energy scavenger (Leland, 2006)

Fig. 6. (a) Ion milling to reduce beam height and (b) RIE to reduce beam width (Tanaka et al., 1995)

Fig. 8. Various exciting electrode configuration: (a) central electrode, (b) cis-electrode, and (c) trans-electrode (Tanigawa et al., 2010)

Tanaka et al. (1995) also modified beam dimension to change the lateral and vertical beam stiffness by ion-milling for beam height or reactive ion etching (RIE) for beam width as shown in Figure 6.

Both techniques are only capable of removing material and therefore only one-way tuning. During design it is advised to over-dimension critical flexures to allow tuning by material removal, when beams are already too thin these techniques are not applicable.

Note that applying milling techniques could damage surrounding elements. A mask to protect critical elements should be considered.

The polysilicon deposition reported before by Joachim and Liwei (2002) did not only function as a mass addition but also increased the stiffness. It is shown that a material deposition close to the root of the single beam results in a large change in the k/m ratio, meaning a large change in frequency.

Material: Kun et al. (1997) altered the resonance frequency of their structure by filament annealing. A current was send through a micromechanical resonator, raising the temperature high enough to anneal
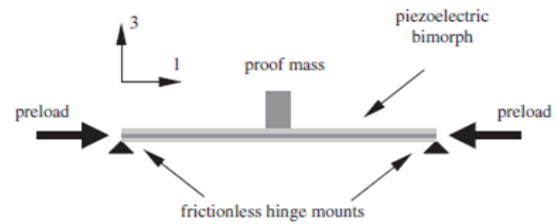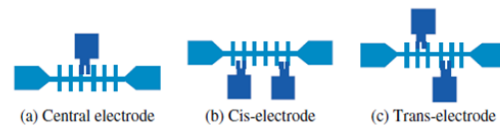
it. Although Kun et al. (1997) concluded this to be a convenient post-fabrication technique, the high sensitivity to structure and process variations will make a consistent outcome difficult to control.

Preload: Different methods do exist to apply a preload on a structure but in principle all methods use an actuation force to apply a tensile or compressive force on a structure. The direction of this force does vary. A simple case demonstrating this principle is reported by Leland (2006) where a piezoelectric bimorph is compressively loaded using a micrometer screw gauge (Figure 7).

Tanigawa et al. (2010) used an electrostatic force induced by a voltage on electrodes. Different sets of exciting electrodes on a fishbone-shaped resonator are used. By exciting the electrodes an electrostatic force is exerted on the cross-beams generating a moment on the main beam resulting in in-plane vibrations. Using different electrode configurations as in Figure 8 results in different output frequencies. This method requires preliminary info regarding the required frequencies since only specific frequencies can be excited due to the limit amount of electrodes.

A different method using an discrete tuning range are the methods patented by Ma and Berlin (2005). By vertically displacing a ratcheting shaft via electrostatically actuated comb like fingers a beam is buckled. A second similar method is presented but now with fully rotational ratcheting wheel. Also a stepped wedge is suggested to tension a beam (Figure 9). A different tuning setting will result in a different preload, hence changing the frequency.

The discrete steps could limit the amount of fine tuning since only preset errors can be corrected, especially for small corrections this would be disadvantageous. However the tuning step as result of
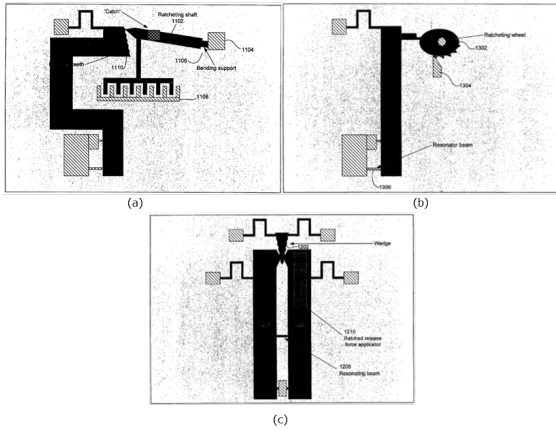
Fig. 9. (a) Ratcheting shaft to buckle a beam, (b) ratcheting wheel to buckle a beam, and (c) Wedge to tension a beam (Ma and Berlin, 2005)
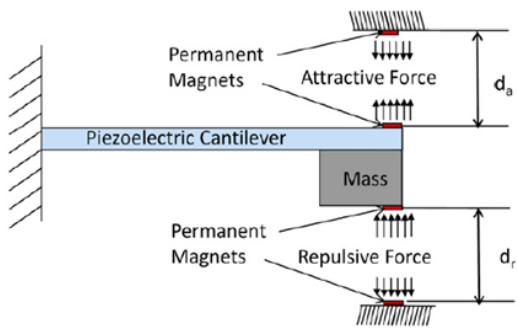

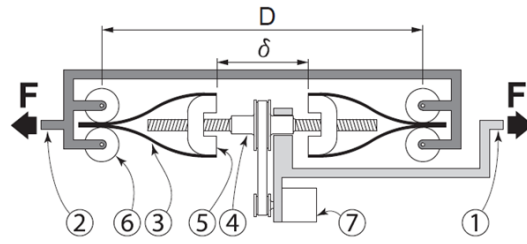Fig. 10. Schematic of the tunable resonating beam (Challa et al., 2008)

Fig. 11. Leaf spring stiffness adjustable resonator (Gonzalez Rodriguez et al., 2011)
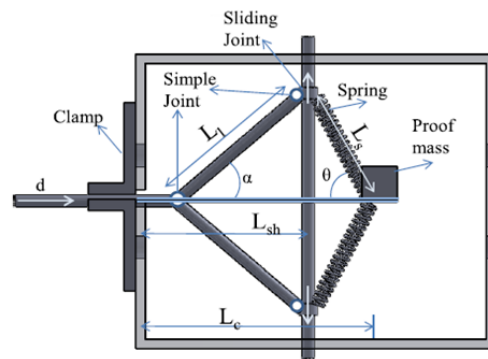
Fig. 12. Tunable energy harvesting beam via adjustable springs (Dehghan Niri and Salamone, 2012)

a specific tuning force will be more accurate. For example in the case of Ma and Berlin (2005) multiple local equilibria do exist, given a certain tuning force with small deviation, the tuning step will be equal since there is a local energy minimum due to the design geometry.

Both Challa et al. (2008) and Reissman et al. (2009) reported a tuneable resonating beam using permanent magnets to stiffen the beam respectively in axial or transverse direction. Magnetic material is placed at the tip end, a permanent magnet placed at a distant from this tip causes a magnetic tuning force (Figure 10). Changing this distance will change the tuning force and therefore resonance frequency. Advantage of magnetic tuning is the lack of contact and it does not suffer from hysteresis. Although these solutions are tested at macro scale, a transition to micro scale seems to be possible using micromagnetics.

A macro scale tuning method is presented by Gonzalez Rodriguez et al. (2011) as shown in Figure 11. The global stiffness of the device can be adjusted by modifying the shape, and therefore preload,

of leaf springs. C-shaped element 5 can be shifted along a spindle changing distance δ, the leaf spring shape, and global stiffness. Prestress in this solution is applied via a rotational input and auxiliary C-shaped element with physical contact on the spring beams.

Dehghan Niri and Salamone (2012) also made use of an auxiliary structure (linear springs on a sliding joint as inFigure 12). Modifying the position of the mounting point changes both the angle and force exerted by the auxiliary device, influencing the resonating beam stiffness and frequency.

Although Gonzalez Rodriguez et al. (2011) and Dehghan Niri and Salamone (2012) proposed tuning structures at macro scale, they present unique solutions by not using a direct force but a force on an auxiliary structure which transmits this force in a different direction and/or in multiple directions. Whether these specific solutions are suitable for use at micro scale is debatable, especially with mechanical springs, but the method is worth mentioning.

Tuning during operation

Material: An often reported technique is heating a structure to change the Young's modulus of the material. Both Remtema and Lin (2001) and Zhang and Leea (2012) used a DC current to resistively heat elements in their structure. The generated
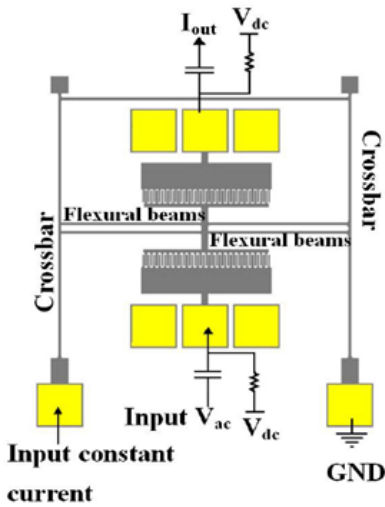
Fig. 13. Schematic of the MEMS resonator with crossbar heaters to lower the resonance frequency (Zhang and Leea, 2012)
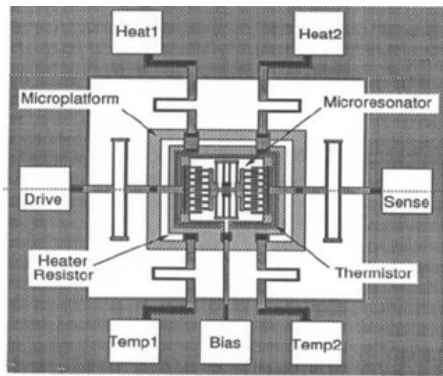

Fig. 14. Schematic of the micro-over control system with microplatform, microresonator and heaters (Nguyen and Howe, 1993)
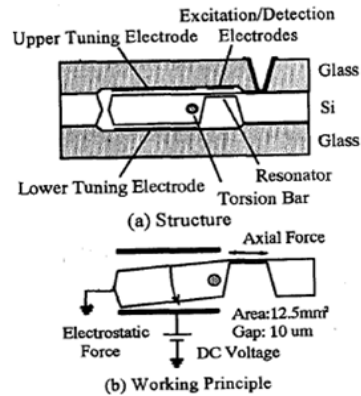

Fig. 15. Schematic of the resonance frequency tuning device by an electrostatically induced axial force (Cabuz et al., 1994)
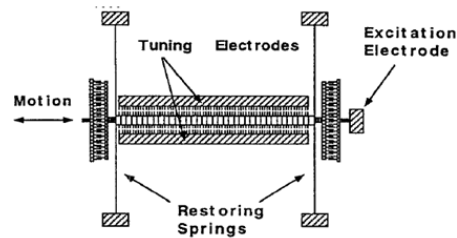

Fig. 16. Schematic of the tunable resonator with straight finger type electrodes (Adams et al., 1995)

heat results in material softening due to the negative temperature coefficient. Figure 13 shows a design where crossbars provide a restoring force on the flexural beams, softening these crossbars by heating lowers this restoring force, reducing the frequency.

Bandwidth with thermal tuning is limited and power consumption is relative high although thermal isolation of heated elements have improved efficiency of these structures.

Nguyen and Howe (1993) showed a microresonator with integrated micro-oven to adjust the operating frequency and compensate for temperature variations(Figure 14). Heating was accomplished via heating resistors on the thermally isolated platform, minimizing power consumption.

Preload: Similar to tuning before operation, solutions to adjust the stiffness via preload are based on a tensile or compressive load. Yao and MacDonald (1995) presented a resonating cantilever beam which is tuned via a DC tuning electrode exerting an electrostatic force on the beam. This principle is exactly the same as the preload via permanent magnets(Figure 10), except the tuning force which can now be varied during the process by changing the voltage on the electrodes.

Cabuz et al. (1994) used a movable support which could rotated around a torsion bar as an electrostatic force is exerted via tuning electrodes(Figure 15). Depending on the rotation direction a tensile or compressive stress is induced in the resonator beam.

Different electrode geometries and configurations are also reported. Adams et al. (1995) showed straight finger type electrodes to stiffen a structure and alter the resonance frequency (Figure 16) . Park et al. (1999) used this principle but introduced a branched finger type with improved functionality (Figure 17).

Large variations in performance do exist between electrostatically actuated tuning mechanisms in both nominal frequency as tuning range and a

An alternative to electrodes is tuning via piezoelectric actuators which are often used to induce axial forces on a beam. Advantages of piezoelectrics are the high output force with low power consumption and the potential of two-side shifting of the resonance frequency. This principle is also used by Azizi et al.
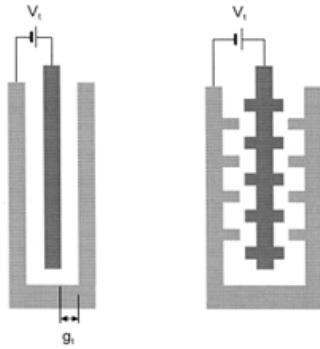
Fig. 17. Electrodes for stiffness tuning with straight and branched finger type (Park et al., 1999)
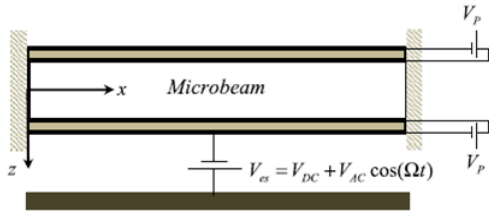

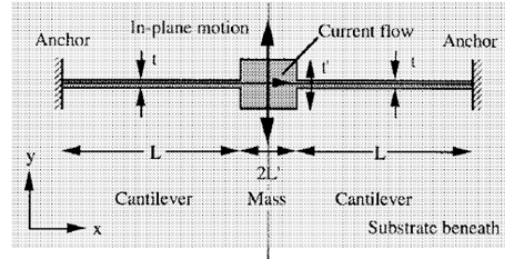Fig. 18. Clamped-clamped piezoelectrically sandwiched microbeam (Azizi et al., 2013)

Fig. 19. Schematic with clamped-clamped cantilever beam with electrothermal heating (Syms, 1998)
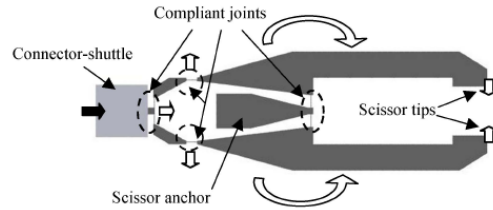
Fig. 20. Motion of thermally actuated scissor mechanism (Lee et al., 2009)

(2013) who presented a clamped-clamped piezoelectric microbeam sandwiched with a two piezoelectric layers(Figure 18). By changing the strength and polarity of the piezoelectric actuation the primary resonance frequency is tuned.

A similar concept with a clamped piezoelectrically sandwiched cantilever beam resonator was also reported by Clark and Wang (2005). One active piezoelectric layer is used to cause vibrations and detected this frequency. The second passive layer tunes the frequency.

Remtema and Lin (2001) resistively heated a beam to change the Young's modulus as discussed before. A second effect of this resistive heating is a thermal induced expansion. In the design a straight-beam is placed in a constrained environment, heating will induce a compressive stress lowering the resonance frequency.

Syms (1998) also used thermal induced forces in a clamped-clamped cantilever beam(Figure 19), again resulting in compressive stress. An opposite effect by convective cooling is also discussed.

A new method to use a thermally induced force is presented by Lee et al. (2009). The displacement of a thermal actuator is used to close a scissor mechanism via compliant hinges, mechanically stiffening a torsional spring(Figure 20).

Thermally actuated principles in general are more difficult to control. Besides higher power consumption, the energy dissipation throughout the structure is difficult to predict and often an additional sensor is required to measure the frequency response given a thermal input, increasing the system complexity.

IV. DISCUSSION

From the results it can be seen that frequency tuning during operation always requires a tuning mechanism and often a feedback loop to control the system. These components are not necessarily required for tuning before operation. These additional components increase the system complexity, volume and power consumption. Note that if the frequency tuning mechanism for tuning before operation cannot be removed, it will remain on the final design decreasing the space-efficiency of the overall structure.

If frequency tuning before operation is preferred one should not fully discard methods used during operation. When a locking mechanism is developed and used in combination with a during operation tuning mechanism, the resulting mechanism could function as a before operation tuning solution. This property is also embedded in the solution by Ma and Berlin (2005): the geometry of the preloading element is such that it is locked within certain force bounds.

Table II shows that few solutions with low ($<$ 100Hz) nominal frequencies do exist. Interesting is that tuning via damping is only focused in this lower frequency region. Tuning via damping in these papers is used to adjust the frequency of energy harvesters which are especially interested in these lower frequencies explaining this focus.

No solutions are found where stiffness is changed via dimensions during operation. This would imply

adding or removing mass on a resonating system which can be considered highly unpractical.

Also no damping solutions before operation are found since all solutions do incorporate a feedback loop to adjust damping during operation. In some cases it is possible to convert a during operation into a before operation method, e.g. Wu et al. (2006) where it is possible to select a capacitive load before operation, however the effect of this capacitive load on the frequency must be very well known otherwise accuracy of this frequency tuning method will be low.

When deciding between a mass or stiffness oriented solution it is recommended to make a comparative calculation to determine whether it is more efficient to tune stiffness of mass. For their design Syms and Moore (1999) calculated a ratio of sensitivity between stiffness k and mass m as (6):

$$R = \eta_k/\eta_n = -3A/(LNb) \qquad (6)$$

with area A, flexure length L, number of cuts N, and breadth b.

It shows that tuning mass is more effective if $A/(LNb) > 1/3$ which is the case for relatively high mass and relatively short flexures. This calculation also explains why no solutions were found where mass is removed solely to lower mass since it is rather focused on reducing the stiffness.

It would also be interesting to know the linearity of the tuning range but this data is only available in a few cases and therefore not reported.

Reported results and this classification method only considered viscous damping as in (1) while non-viscous damping could also be present. In this case a better approximation would be the displacement related hysteretic damping model as (7) or a combination of the viscous and hysteretic damping model as in the fractional damping model according to (8).

$$m\ddot{x} + k(1 + i\eta)x = F(t) \qquad (7)$$

with η the hysteretic damping coefficient

$$m\ddot{x} + A\frac{d^r x}{dt^r}i + kx = F(t) \qquad (8)$$

with A the general damping coefficient and r between 0 (hysteretic) and 1 (viscous).

The introduced classification system assumes unique solution types per end group while in practice the solution space will look like Figure 22. An example is Groothuis et al. (2012) using a lever arm with moving pivot point as in Figure 21. Moving this pivot point changes the effect of the mass but also the transmission ratio between input and output resulting in a stiffness change. This solution is therefore a combination between mass and stiffness

(a) Moving the elastic elements.

(b) Moving the application point of the output force F.
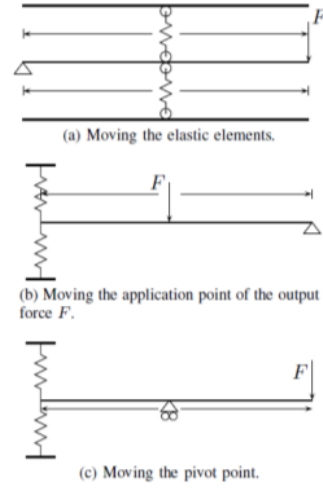
(c) Moving the pivot point.

Fig. 21. Single solution affecting multiple tuning parameters and properties (Groothuis et al., 2012)
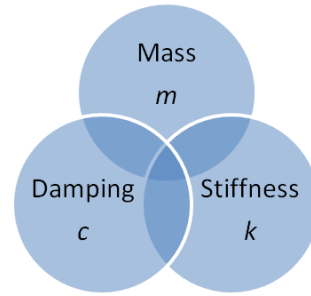
Fig. 22. Schematic overview of the solution space

and does not belong in one group. Same reasoning holds for the polysilicon deposition presented by Joachim and Liwei (2002) which adds mass and increases the stiffness. These methods are placed in both groups.

Due to the choice of search keywords, the scope on larger scale tuning structures is limited and it is possible these will not be reviewed although they could provide a scalable solution.

Interesting remark is the difference in working scale between stiffness adjustable solution via preload before and during operation. All solutions found during operation are used at micro scale but require actuation. Almost all solutions before operation work at macro scale and the only solution tested at micro scale does require continuous power. No passive, micro-scale, preload solution before operation is found. A locking mechanism on the existing during operation solutions, as discussed before, would yield multiple new solution on micro-scale in this branch of the classification scheme.

V. Conclusion

A classification method to organize literature on tuning frequency on micro-scale is presented. First, literature is structured based on the application moment of the frequency tuning step, which can be either before or during operation. Second, system parameters mass, damping and stiffness are used to organize literature within these groups. Finally, subcategories per system parameter separate literature into unique end groups. An overview of frequency tuning mechanisms is presented according to this classification scheme and relevant working principles and properties are discussed.

When a solution to adjust for fabrication error on micro scale is required a before operation tuning method is preferred. If the error is systematic, a single correction will suffice and a continuous correction would only increase the system complexity and power consumption decreasing the reliability of the system. To precisely balance the mechanism fabrication error a continuous tuning range is preferred. Using these criteria solutions for different tuning ranges can be distinguished:

When the fabrication error is small and only solutions already at micro-scale are considered a frequency adjustment is best accomplished with a mass addition or via a stiffness change by dimensions or material change. Depending on the required nominal frequency a specific solution can now be identified.

When the fabrication error is large and only solutions already at micro-scale are considered, a frequency adjustment can only be accomplished via a mass addition.

Appendix A

TABLE III
Search keywords overview

Set	Keywords
Tuning	Tuning, variable, changing, adapting, regulating, adjusting, higher, lower, increasing, decreasing, reducing, compensating, calibration, precision, correcting, trimming
Tuning method	Frequency, stiffness, damping, mass
Size	Micro Electro Mechanical Systems, MEMS, micro, small
Range	Continuous, discrete, step, interval, small, large, fine
Alternative principles	Pretension, fabrication error, tolerances, manual, automatic, static, dynamic

References

Adams, S. G., Bertsch, F. M., Shaw, K. A., Hartwell, P. G., MacDonald, N. C., and Moon, F. C. Capacitance based tunable micromechanical resonators. In *Solid-State Sensors and Actuators, 1995 and Eurosensors IX.. Transducers '95. The 8th International Conference on*, volume 1, pages 438–441, 1995.

Azizi, S., Ghazavi, M. R., Rezazadeh, G., Ahmadian, I., and Cetinkaya, C. Tuning the primary resonances of a micro resonator, using piezoelectric actuation. *Nonlinear Dynamics*, pages 1–14, 2013.

Badel, A., Sebald, G., Guyomar, D., Lallart, M., Lefeuvre, E., Richard, C., and Qiu, J. Piezoelectric vibration control by synchronized switching on adaptive voltage sources: Towards wideband semi-active damping. *The Journal of the Acoustical Society of America*, 119(5):2815–2825, 2006.

Cabuz, C., Fukatsu, K., Hashimoto, H., Shoji, S., Kurabayashi, T., Minami, K., and Esashi, M. Fine frequency tuning in resonant sensors. In *Micro Electro Mechanical Systems, 1994, MEMS '94, Proceedings, IEEE Workshop on*, pages 245–250, 1994.

Cammarano, A., Burrow, S. G., Barton, D. A. W., Carrella, A., and Clare, L. R. Tuning a resonant energy harvester using a generalized electrical load. *Smart Materials and Structures*, 19(5): 055003, 2010.

Challa, V. R., Prasad, M., Shi, Y., and Fisher, F. T. A vibration energy harvesting device with bidirectional resonance frequency tunability. *Smart Materials and Structures*, 17(1):015035, 2008.

Chiao, M. and Lin, L. Post-packaging tuning of microresonators by pulsed laser deposition. In *TRANSDUCERS, Solid-State Sensors, Actuators and Microsystems, 12th International Conference on, 2003*, volume 2, pages 1820–1823 vol.2, 2003.

Clark, W. and Wang, Q. Tunable piezoelectric micromechanical resonator, 2005.

Dehghan Niri, E. and Salamone, S. A passively tunable mechanism for a dual bimorph energy harvester with variable tip stiffness and axial load. *Smart Materials and Structures*, 21(12):125025, 2012.

Enderling, S., Hedley, J., Jiang, L., Cheung, R., Zorman, C., Mehregany, M., and Walton, A. Characterization of frequency tuning using focused ion beam platinum deposition. *Journal of Micromechanics and Microengineering*, 17(2):213, 2007.

Gonzalez Rodriguez, A., Chacn, J. M., Donoso, A., and Gonzalez Rodriguez, A. G. Design of an adjustable-stiffness spring: Mathematical modeling and simulation, fabrication and experimental validation. *Mechanism and Machine Theory*, 46(12): 1970–1979, 2011.

Groothuis, S. S., Rusticelli, G., Zucchelli, A., Stramigioli, S., and Carloni, R. The vsaut-ii: A novel rotational variable stiffness actuator. In *Robotics*

and Automation (ICRA), 2012 IEEE International Conference on*, pages 3355–3360, 2012.

Jafari, A., Tsagarakis, N. G., and Caldwell, D. G. A novel intrinsically energy efficient actuator with adjustable stiffness (awas). *IEEE/ASME Transactions on Mechatronics*, 18(1):355–365, 2013.

Joachim, D. and Liwei, L. Selective polysilicon deposition for frequency tuning of mems resonators. In *Micro Electro Mechanical Systems, 2002. The Fifteenth IEEE International Conference on*, pages 727–730, 2002.

Kun, W., Ark-Chew, W., Wan-Thai, H., and Nguyen, C. T. C. Frequency trimming and q-factor enhancement of micromechanical resonators via localized filament annealing. In *Solid State Sensors and Actuators, 1997. TRANSDUCERS '97 Chicago., 1997 International Conference on*, volume 1, pages 109–112 vol.1, 1997.

Lee, J., Park, S., Eun, Y., Jeong, B., and Kim, J. Resonant frequency tuning of torsional microscanner by mechanical restriction using mems actuator. In *Micro Electro Mechanical Systems, 2009. MEMS 2009. IEEE 22nd International Conference on*, pages 164–167, 2009.

Leland, R. P. Adaptive control of a mems gyroscope using lyapunov methods. *Control Systems Technology, IEEE Transactions on*, 14(2):278–283, 2006.

Ma, Q. and Berlin, A. Apparatus for adjusting the resonance frequency of a microelectromechanical (mems) resonator using tensile/compressive strain and applications thereof, 2005.

Miller, L. M., Pillatsch, P., Halvorsen, E., Wright, P. K., Yeatman, E. M., and Holmes, A. S. Experimental passive self-tuning behavior of a beam resonator with sliding proof mass. *Journal of Sound and Vibration*, 332(26):7142–7152, 2013.

Nguyen, C. T. C. and Howe, R. T. Microresonator frequency control and stabilization using an integrated micro oven. In *7th International Conference on Solid-State Sensor and Actuators*, volume 20, pages 1040–1043, 1993.

Park, K.-Y., Lee, C.-W., Jang, H.-S., Oh, Y., and Ha, B. Capacitive type surface-micromachined silicon accelerometer with stiffness tuning capability. *Sensors and Actuators A: Physical*, 73(12):109–116, 1999.

Reissman, T., Wolff, E. M., and Garcia, E. Piezoelectric resonance shifting using tunable nonlinear stiffness. In *Active and Passive Smart Structures and Integrated Systems 2009*, volume 7288, pages 72880G–72880G–12, 2009.

Remtema, T. and Lin, L. Active frequency tuning for micro resonators by localized thermal stressing effects. *Sensors and Actuators A: Physical*, 91(3): 326–332, 2001.

Shkel, A. M., Howe, R. T., and Horowitz, R. Model-ing and simulation of micromachined gyroscopes in the presence of imperfection. In *Int. Conf. On Modelling and Simulation of Microsystems*, pages 605–608, 1999.

Syms, R. R. A. Electrothermal frequency tuning of folded and coupled vibrating micromechanical resonators. *Microelectromechanical Systems, Journal of*, 7(2):164–171, 1998.

Syms, R. R. A. and Moore, D. F. Focused ion beam tuning of in-plane vibrating micromechanical resonators. *Electronics Letters*, 35(15):1277–1278, 1999.

Tanaka, K., Mochida, Y., Sugimoto, M., Moriya, K., Hasegawa, T., Atsuchi, K., and Ohwada, K. A micromachined vibrating gyroscope. *Sensors and Actuators A: Physical*, 50(12):111–115, 1995.

Tanigawa, H., Makita, S., and Suzuki, K. Silicon fishbone-shaped mems resonator with digitally variable resonant-frequency tuning. *IEEJ Transactions on Electrical and Electronic Engineering*, 5 (2):164–170, 2010.

Wolf, S. and Hirzinger, G. A new variable stiffness design: Matching requirements of the next robot generation. In *Robotics and Automation, 2008. ICRA 2008. IEEE International Conference on*, pages 1741–1746, 2008.

Wu, W.-J., Chen, Y.-Y., Lee, B.-S., He, J.-J., and Peng, Y.-T. Tunable resonant frequency power harvesting devices. volume 6169, pages 61690A–61690A–8, 2006.

Wu, X., Lin, J., Kato, S., Zhang, K., Ren, T., and Liu, L. A frequency adjustable vibration energy harvester. In *Proceedings of PowerMEMS 2008+ microEMS2008*, pages 245–248, 2008.

Yao, J. J. and MacDonald, N. C. A micromachined, single-crystal silicon, tunable resonator. *Journal of Micromechanics and Microengineering*, 5(3):257–264, 1995.

Zhang, W. and Leea, J. E. Y. Frequency tuning in a mems resonator via an integral crossbar heater. *Procedia Engineering*, 47(0):949–952, 2012.

Zoppi, M. Method for adapting stiffness in a variable stiffness actuator, 2013.

III

TECHNICAL REPORT

2

INITIAL CASE STUDY

At the start of this study a small case study is introduced based on a real life application. This application cannot be disclosed for confidentially reasons. The general case for this case study considers a planar, monolithic micro-oscillator resonating at a certain frequency. Goal of this case study is to adjust this frequency to a desired, fixed value.

2.1. SPECIFICATIONS

The oscillator has the maximum dimensions of a circle with $D = 30mm$. Typical flexure beam dimensions within this design are width $w = 25\mu m$, height $h = 500\mu m$ and a varying beam length L (fig. 2.1).
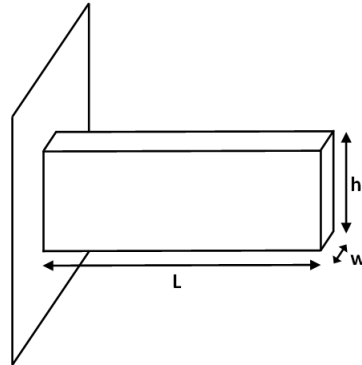

Figure 2.1: Cantilever beam for in-plane oscillation

The desired oscillating frequency $\omega = 25Hz$ and stiffness is known to be $k = 1N/m$. Using the formula for the fundamental frequency eq. (2.1) the device mass can be calculated as $m = 4.0528e^{-5}kg$.

$$\omega_n = \sqrt{\frac{k}{m}} \tag{2.1}$$

The beam is assumed to be in air at ambient pressure $P_{air} = 10^5 Pa$ at $T = 293K$. This results in air density $\rho_{air} = 1.20kg/m^3$ and viscosity $\mu_{air} = 18.3e^{-6}Pa\ s$.

2.2. INITIAL REQUIREMENTS

For production, operation and maintenance reasons multiple requirements are given which need to be fulfilled in order to create a useful product:

- The micro-oscillator is a commercial product and only allows one initial tuning step before operational use. At $t = 0$ sufficient energy is available for tuning. For $t > 0$ energy is limited and as little energy as possible should be consumed for frequency tuning.

- To allow maintenance and readjustments the tuning step should be reversible.

- The tuning range should be established based on the maximum frequency offset due to fabrication errors.

- The added tuning stage should not interfere with the structural components of the mechanical oscillator other than a frequency change, i.e. no magnetic parts, magnetic actuation or temperature influences.

3

FABRICATION ERROR ANALYSIS

Due to fabrication errors the real operating frequency differs from the designed operating frequency. The goal of this project is to tune the frequency such that it is as designed. In order to know how much tuning is required, the frequency offset due to fabrication errors needs to be determined. This frequency offset is the result of a different beam stiffness due to varying beam thickness.

When an beam is oscillating, the beam stiffness is described by eq. (3.1).

$$k = \frac{3EI}{L} \tag{3.1}$$

with second moment of inertia

$$I = \frac{hw^3}{12} \tag{3.2}$$

Equation (3.2) shows that beam width w has a large influence on the frequency.

Per fabrication process the beam shape is roughly known. In one process the beam is known to be trapezoid-shaped with a beam width offset $\delta w = 0.1 \mu m$ / $h = 100 \mu m$. Assuming a beam with $w_{top} = 25 \mu m$ at the top and $h = 500 \mu m$ yielding $w_{bottom} = 25.5 \mu m$ (fig. 3.1).

The offset in natural frequency per beam thickness variation is plotted in fig. 3.2 for the trapezoidal-shaped beam and a beam with increased width over the entire height.

This plot shows that the expected fabrication results in a natural frequency of maximal 25.4Hz. From this it can be concluded that the required tuning step should be able to tune 0.4 Hz. This corresponds to a tuning range of $\approx 1.6^{\%}$. If the beam height is lowered or fabrication specifications improve this value will decrease
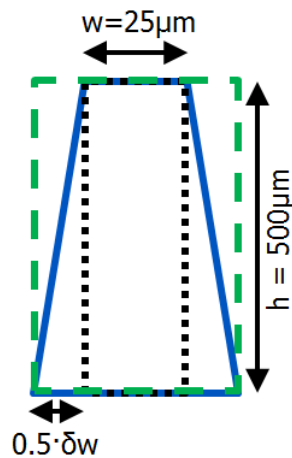

Figure 3.1: Original beam (black dashed), Trapezoidal beam (blue solid), Thicker beam (green dashed)
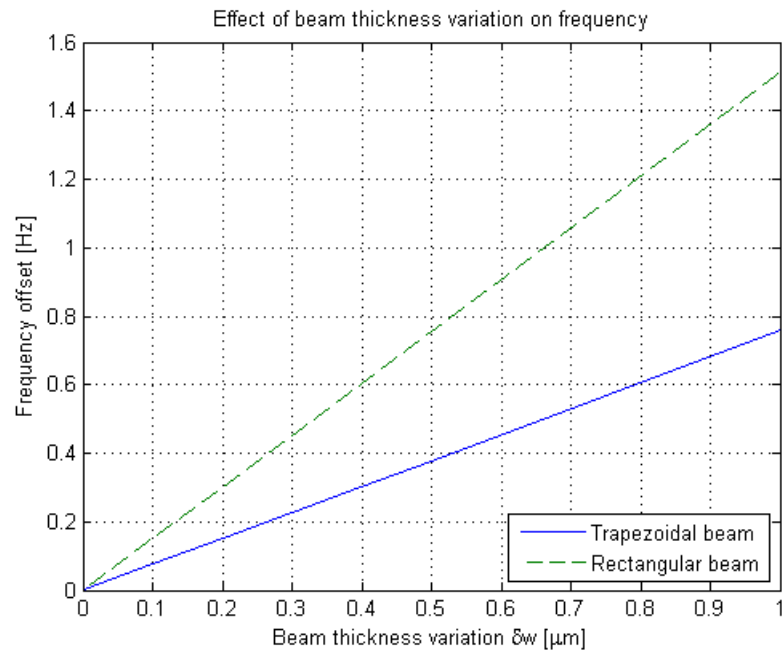
Figure 3.2: Change in natural frequency due to beam thickness or shape variation

linear to these variables. A second possibility would be to design for this specific beam shape. When the offset is more or less known, this can be incorporated in the initial design , resulting in a smaller fabrication error.

4

FREQUENCY TUNING: MASS

4.1. TUNING VIA MASS

The influence of mass on the natural frequency of a system clearly shown in eq. (2.1). Adding an additional mass to the original structure will lower the natural frequency. How much the frequency is changed depends on the amount of mass added and can be calculated by subtracting the natural frequency for the original structure with the natural frequency of the original structure plus additional mass.
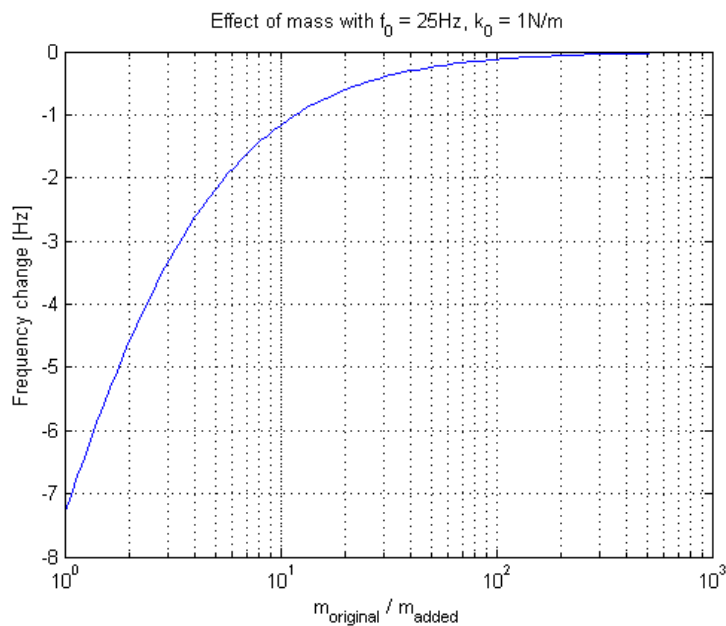

Figure 4.1: Effect of mass on the natural frequency of a structure

Figure 4.1 shows this frequency change $\delta\omega_n$ due to the amount of mass added w.r.t. the original mass. For a high $m_{original}/m_{added}$, the added mass is relative low w.r.t. the original mass and a small frequency change is found, lowering this factor, i.e. increasing the added mass will result in a larger change in frequency.

Looking at the region where $\delta\omega_n = 0.4Hz$ is accomplished (fig. 4.2), it can be seen that $m_{original}/m_{added} \approx 30$.

Since $m_{original} = 4.053e^{-5}kg$, m_{added} should be $\approx 1.351e^{-6}kg$.

4.2. FEASIBILITY STUDY - MASS

An easy applicable solution on small scale would be a mass deposition. In the literature research multiple deposition techniques are identified which can be used to estimate the feasibility of a mass addition. Key characteristics in this analysis are the density of the deposited material and the possible material deposition.
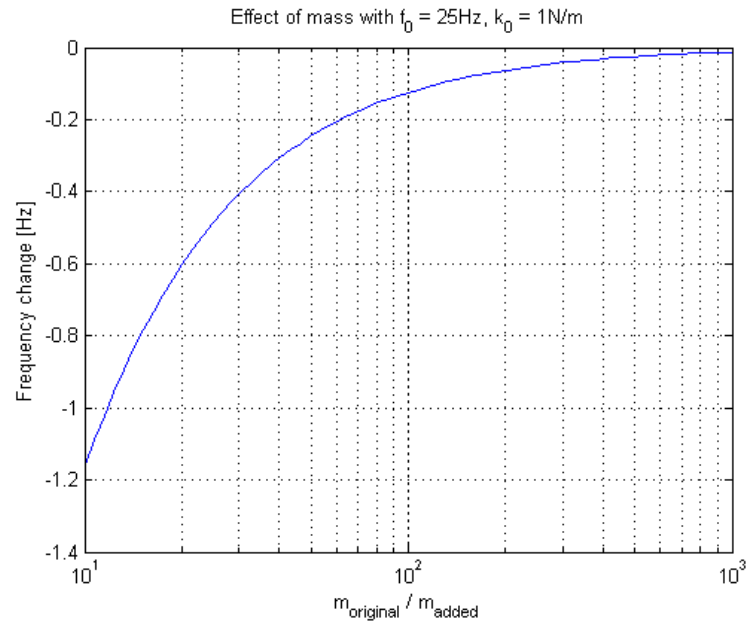
Figure 4.2: Effect of mass on the natural frequency of a structure - area of interest

Table 4.1: Required deposition area for for different deposition techniques

Material	Density [kg/m^3]	Deposition thickness [μm]	Required volume [μm^3]	Required deposition area [mm^2]
Polysilicon	$2.71e^3$	0.3	$4.99e^8$	$16.63e^2$
Platinum	$21.45e^3$	1.2	$6.30e^7$	52.5

Using these values a required deposition area can be calculated. Two deposition techniques are evaluated and deposition characteristics are as reported in literature:

1. Polysilicon deposition. Reported by Joachim and Liwei [7].

2. Platinum deposition. Reported by Enderling et al. [4].

Different deposition techniques or settings are also possible but these values provide sufficient data for an initial estimation.

From table 4.1 it can be seen that a polysilicon deposition requires to much area which is not available since $A_{max} = \pi(\frac{d}{2})^2 = 804mm^2$. A platinum deposition would require $\approx 6.5\%$ of the maximum available area requiring a significantly large oscillating mass which it can be removed from.

Instead of adding, it is also possible to remove this amount of mass. This will reverse the tuning direction. In this case the graphs shown will be mirrored around $x = 0$. Since the structure in the case structure is planar and monolithic (single material), all additional effective mass should be added within the functional structure. When considering a silicon structure an area of $1.16mm^2$ (table 4.2) should be removed from the resonating mass which is $\approx 0.14\%$ of the maximum available area.

From these results it can be concluded there is a possibility to tune frequency by adding or removing mass. One serious issue that has not yet been addressed is the effect of this mass addition or removal on the out of

Table 4.2: Required removal area

Material	Density [kg/m^3]	Removal thickness [μm]	Required volume [μm^3]	Required removal area [mm^2]
Silicon	$2.33e^3$	500	$5.80e^8$	1.16

plane stiffness of the structure. Often micro-oscillators are suspended on small beams. Adding or removing mass from these beams or from a mass suspended at these beams could have serious effects of the resonator performance.

Both adding or removing mass in the methods shown above are irreversible processes, once the frequency tuning step via mass change is applied, it cannot be undone. The tuning step required needs to be reversible. Therefore frequency tuning via mass change is not a feasible solution for this case study.

5

FREQUENCY TUNING: DAMPING

An analysis is performed to check whether it is possible to tune frequency via damping. The proposed damping methods should therefore be able to change damping such that the frequency is changed with 0.4Hz as concluded in chapter 3.

5.1. INCLUDE DAMPING

When damping is introduced to a system the oscillating frequency is influenced and a damped frequency can be determined as in eq. (5.1).

$$\omega_d = \omega_n \sqrt{1 - \zeta^2} \tag{5.1}$$

with damping ratio eq. (5.2):

$$\zeta = \frac{c}{2\sqrt{km}} \tag{5.2}$$

Only underdamped systems need to be considered i.e. $0 \leq \zeta < 1$. By varying damping factor c while ζ is within these bounds the change in frequency ($\omega_n - \omega_d$) can be plotted (fig. 5.1).

This graph shows that when the system is critically damped ($\zeta = 1$) when $c = 0.0127 kg/s$ and the oscillation is immediately damped i.e. frequency change = 25Hz.

Since the fabrication error requires tuning up to 0.4 Hz, only a small section of the graph shown is interesting (fig. 5.2). From this graph it can be seen that damping up to $c = 1e^{-3} kg/s$ is required. Methods used to create damping should therefore be capable of introducing this amount of damping.

5.2. FEASIBILITY STUDY - DAMPING

Different forms of damping can be distinguished. Due to scaling effects, for small or MEMS structures gas damping is usually orders of magnitude higher than structural damping. Forms of damping investigated are 1) air drag, 2) squeeze film damping and 3) slide film damping. To compare the effects the effective beam length in the total device is estimated at $L = 20mm$.

5.2.1. AIR DRAG

When a beam is oscillating in free air it makes contact with free air particles causing air drag. Sumali and Carne [12] present different air drag damping models on a micro-scaled cantilever beam in air. Some of these models are used in the case study to obtain an initial air drag damping estimate.

Christian [3] gave an expression for the damping coefficient per unit length based on Anderson's particle velocity distribution to derive the pressure difference between leading and trailing faced by the momentum change with mass of one effective molecule $m_m = 5.6e^{-26}$ and Boltzmann's constant $k_b = 1.38e^{-23}$ (eq. (5.3)).

$$C^{Christian} = 4h\sqrt{\frac{2m_m}{\pi k_b T}}P \tag{5.3}$$
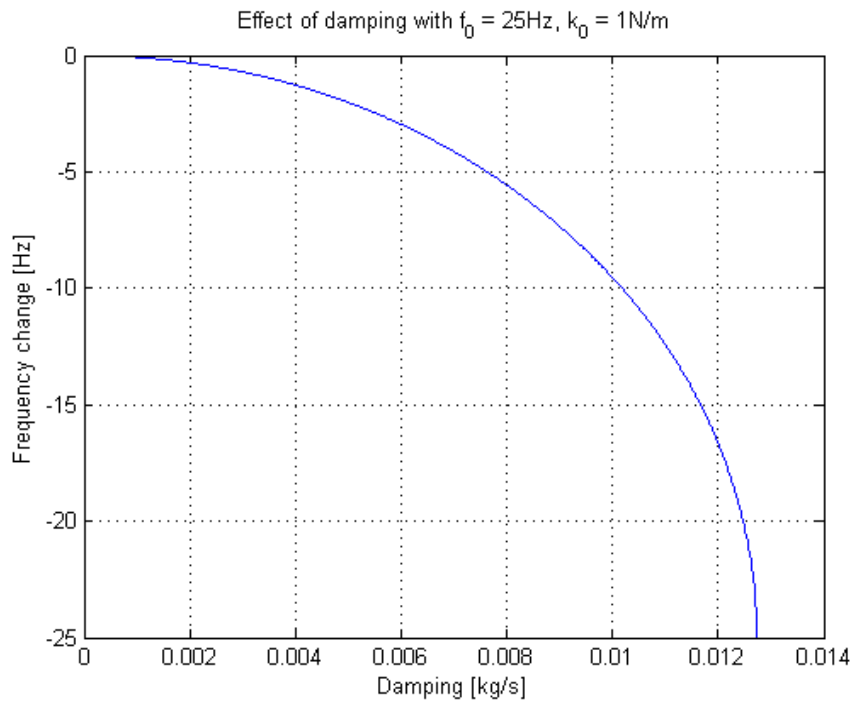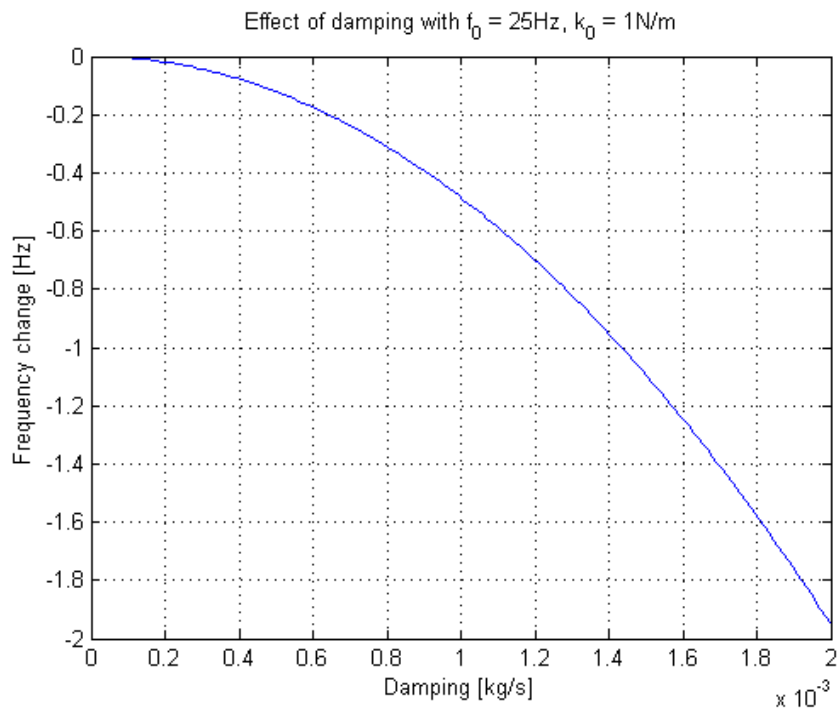
Figure 5.1: Effect of damping on oscillating frequency

Figure 5.2: Effect of damping on oscillating frequency - area of interest

Table 5.1: Air drag damping coefficient

Model	c [kg/ms]	c [kg/s]	δf [Hz]
Kokubun	$3.47e^{-4}$	$6.93e^{-6}$	$-3.65e^{-6}$

Kokubun et al. [9] used Stokes' law to derive a damping coefficient which is translated to a damping coefficient per unit length by Hosaka et al. [6].

$$C^{Hosaka} = 3\pi\mu + \frac{3}{4}\pi h \sqrt{2\mu\rho\omega} \tag{5.4}$$

Results are listed in table 5.1

From this result it can be concluded that damping via air drag does not provide enough damping to tune the structure.

5.2.2. SQUEEZE FILM DAMPING

Squeeze film damping occurs when a structure has a relative movent orthogonal to a second structure. An example would be a beam resonating orthogonal to a fixed wall (fig. 5.3).
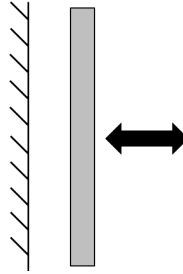

Figure 5.3: Squeeze film damping: beam resonating orthogonal to fixed wall

An central parameter in squeeze film damping is the non-dimensional squeeze film number σ:

$$\sigma = \frac{12\mu L^2 \omega}{Pd^2} \tag{5.5}$$

with gap distance $d = 40e^{-6}$. In the case study this distance is determined as the smallest distance reasonably possible in the desired fabrication process. For small squeeze numbers ($\sigma << 0.2$ (Starr [11])) the medium is squeezed without compression, hence the fluid stiffness can be neglected. A similar analysis is described using a cut-off frequency f_c:

$$f_c = \frac{\mu}{2\pi\rho d^2} = 1.52kHz >> 25Hz \tag{5.6}$$

For $f << f_c$ a constant damping coefficient can be assumed and stiffness effects are neglected. For $f >> f_c$ a constant stiffness coefficient can be assumed and damping effects are neglected. Both analysis indicate clearly that stiffening effects can be neglected and the damping coefficient is constant in the operating regime.

Multiple approximations do exist to estimate this damping coefficient (Andrews et al. [1], Novack [10]) but most commonly used is the coefficient of viscous damping force for strip plates derived by Griffin et al. [5] defined as:

$$c_{Grifin} = \frac{\mu L h^3}{d^3} = 0.71e^{-3}kg/s \tag{5.7}$$

This value is close to the desired $c = 1e^{-3}$ so based on literature squeeze film damping seems to provide sufficient damping. This formula points out that for this case study both beam height h as film thickness d scale to the power three while dynamic viscosity μ and beam length L only scale linear.

ANSYS MODEL

To validate this number an ANSYS model is created as a plate moving orthogonal to a fixed object(fig. 5.4)(Appendix A.1). Squeeze film damping is simulated using FLUID136 elements which are designed for this specific behavior. This element is based on the Reynolds squeeze film theory assuming a continuous flow regime which is accomplished when gap thickness $d << 100 * L_m$ (L_m =mean free path) of the medium particles. The mean free path of air particles at ambient pressure $L_{m\_air} = 64nm << 100 * 40 \mu m$ so this assumption is verified.

Knudsen number Kn is used to check the validity of continuum theory and should be less than 0.01 which is also verified:

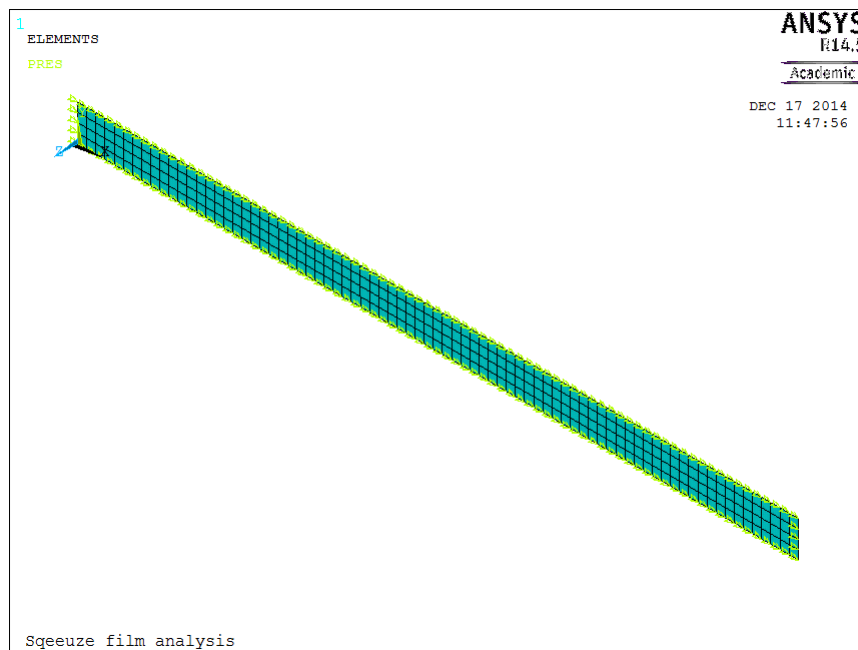$$Kn = \frac{L_m}{d} = 1.6e^{-3} < 0.01 \tag{5.8}$$

Figure 5.4: ANSYS model of squeeze film damping plate

Model validation   First the correctness of the model is verified using Xiongxing et al. [13]. This study simulates the squeeze damping effects of two parallel plates with $L = 100 \mu m$, $h = 60 \mu m$, $w = 5 \mu m$ and $s = 4 \mu m$. Using the same dimensions and testing frequencies as presented in this study the ANSYS model is executed and damping and stiffness coefficients per frequency are calculated. These results are also compared with the theoretical estimation by Griffin et al. [5].

Figure 5.5 shows that results for both damping as stiffness are very similar for the ANSYS model and Xiongxing et al. [13]. The small discrepancy can be explained by an unreported value of dynamic viscosity μ which is therefore estimated. $c_{Griffin}$ shows a larger offset but is still in the same order of magnitude. From these results it is concluded the model yields comparable results.

Analysis on case study   A static analysis is now used to determine the damping effects for low operating frequencies where stiffening effects are negligible, which should be the case as discussed before. Next a harmonic analysis is used to determine fluid stiffening and damping effects at higher frequencies to find out that stiffening effects are indeed negligible.

Figure 5.6 shows the damping coefficient as a function of total length L. Error between $c_{Griffin}$ and ANSYS at the length of interest is also very small.

When the film thickness can be decreased even more due to an improved or different manufacturing process a large change in damping and therefore tuning capacity is seen (fig. 5.7).
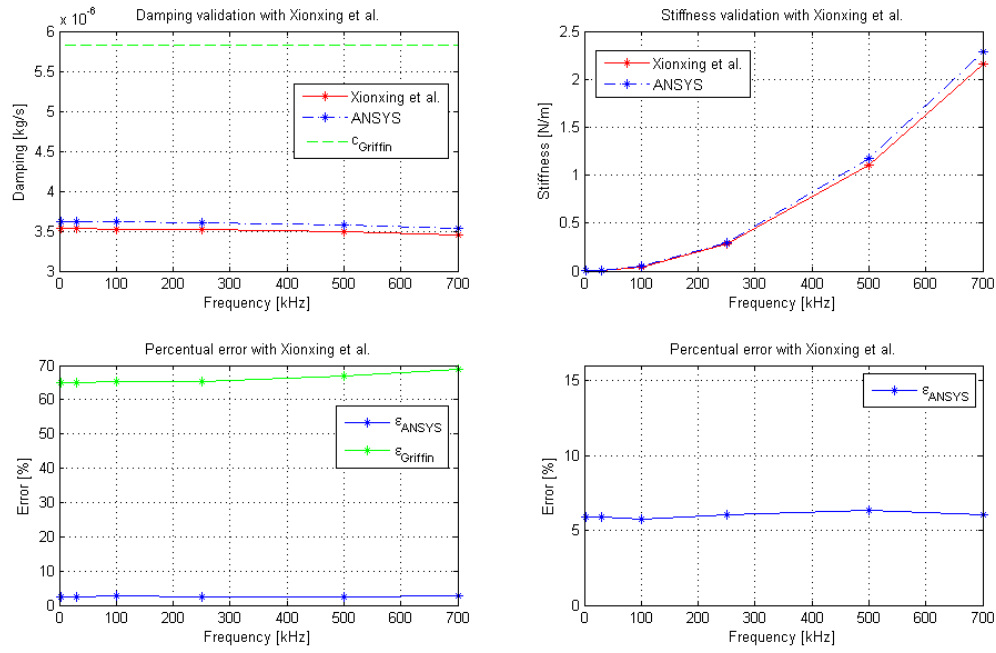
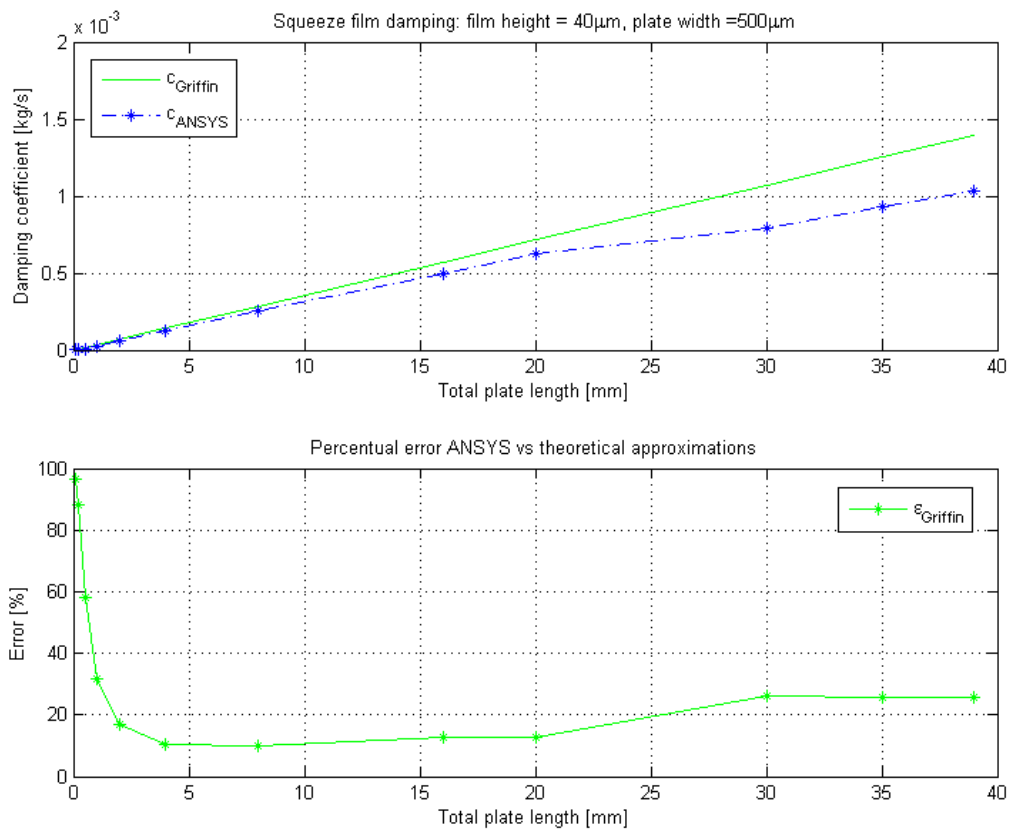Figure 5.5: Comparison of ANSYS model, Xiongxing et al. [13] and Griffin et al. [5]

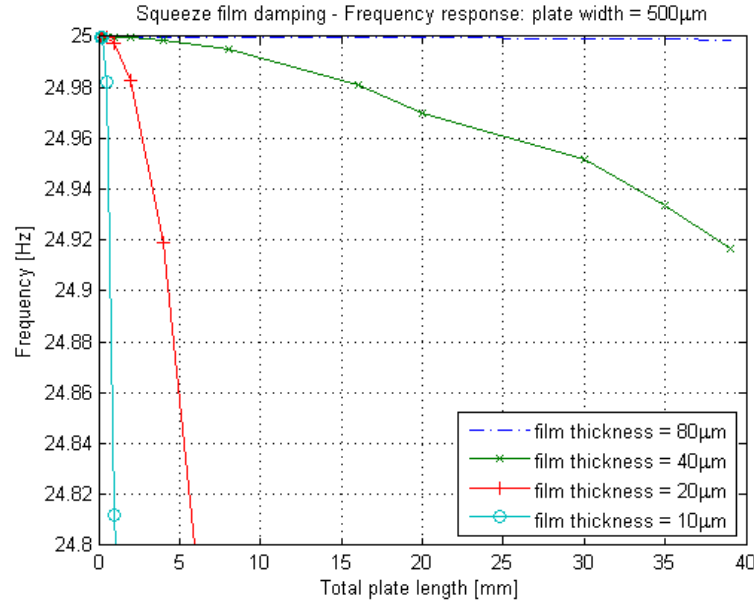Figure 5.6: Squeeze film damping in case study

Figure 5.7: Squeeze film damping for different film thickness

From this analysis it can be concluded that, provided sufficient beam length, it is possible to tune frequency using squeeze film damping. Depending on the amount of tuning required and tuning method developed different sensitivities can be obtained by changing a specific parameter.

5.2.3. SLIDE FILM DAMPING

Slide film damping happens when a structure has a relative movent parallel to a second structure. Shear stress τ over the gap will result in a damping force. An example would be a beam resonating parallel to a fixed plate (fig. 5.8).
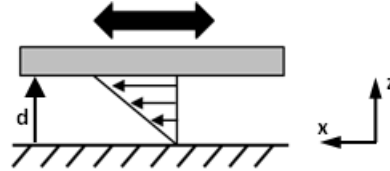

Figure 5.8: Slide film damping: beam resonating parallel to fixed plate

Depending on the plate velocity(frequency) a different fluid velocity profile over the gap develops, changing the slide film damping characteristics. For low frequencies this velocity gradient is constant across the fluid gap and Couette flow can be assumed. In cases of high frequencies Stokes flow is applied which assumes a non-constant velocity gradient (fig. 5.9).

Cut-off frequency $f_c = 1.51 kHz$ as used before gives the transition between both regimes. Since 25Hz is well below f_c, Couette flow is assumed. Kirby [8] also indicates the influence of start up effects which can be neglected if $\omega << \frac{\mu}{\rho R^2}$ with R the fluid half depth. Since $\omega << 38.13 kHz$ start up effects can be neglected.

The slide film damping can now be derived using:

$$\tau = \mu \frac{d v_x(z)}{dz} \tag{5.9}$$

$$v_x(z=0) = 0 \qquad v_x(z=d) = v \qquad \rightarrow \qquad v_x(z) = \frac{z}{d} v_x \tag{5.10}$$

Combining both yields eq. (5.11):
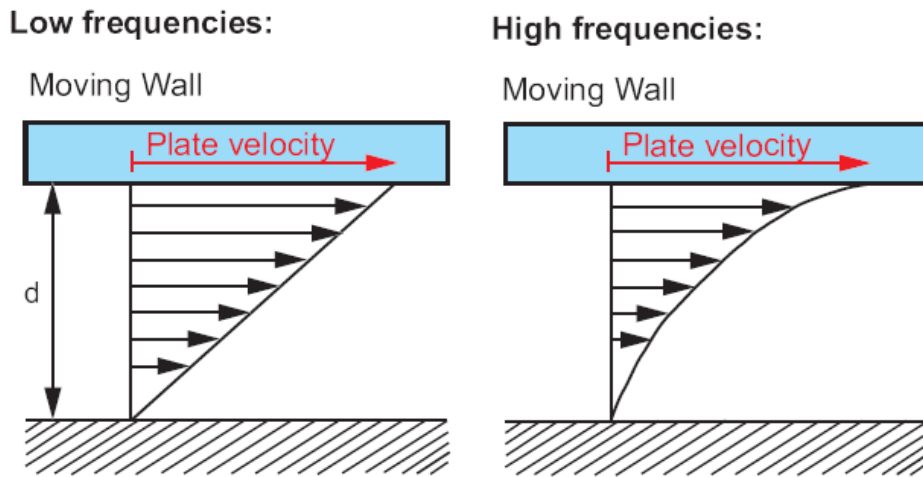
Figure 5.9: Velocity gradients across the fluid gap for low and high frequencies

$$\tau = \frac{\mu}{d} v_x \tag{5.11}$$

and since

$$F_{damping} = \tau A = \frac{\mu A}{d} v_x \tag{5.12}$$

the slide film damping coefficient is established as $c_{slide} = \frac{\mu A}{d}$ with A the slide surface area.

Analysis on case study   Applying this on the case study results in $c_{slide} = 4.58e^{-6}$. This value seems to be too small to be applicable. However due to the planar layout of the case study the entire top and bottom surface can be used, greatly increasing the surface area ($A_{max} = 2 * \pi(\frac{d}{2})^2$). A possible reduction in gap would also help making slide film damping a feasible option as can be seen in fig. 5.10 showing the change in frequency due to slide film damping for different film thicknesses.

Figure 5.10: Slide film damping for different film thicknesses

5.2.4. ENERGY LOSS
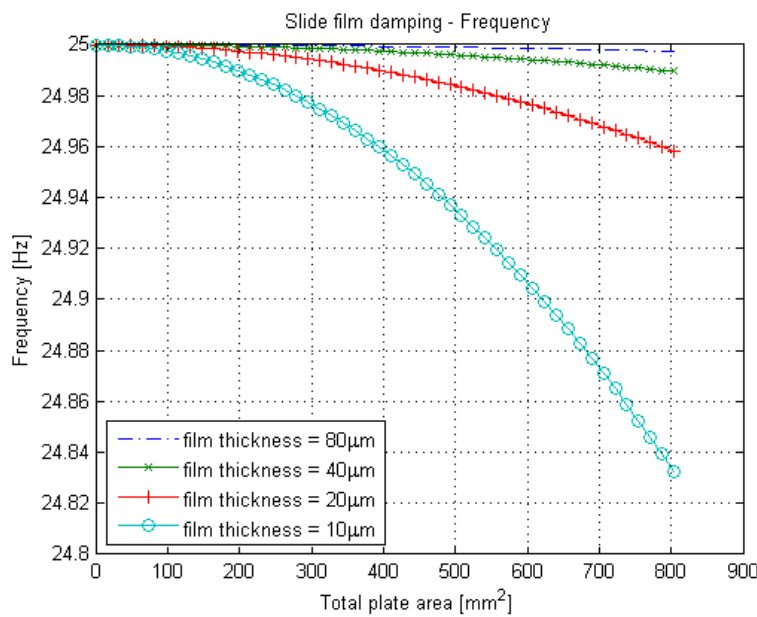
Usually it is preferred to avoid damping since it is a source of energy loss, however when this loss is small or sufficient energy is available, damping could be used. To know how much energy loss is expected, the curve describing the amplitude of an underdamped system is considered(fig. 5.11).
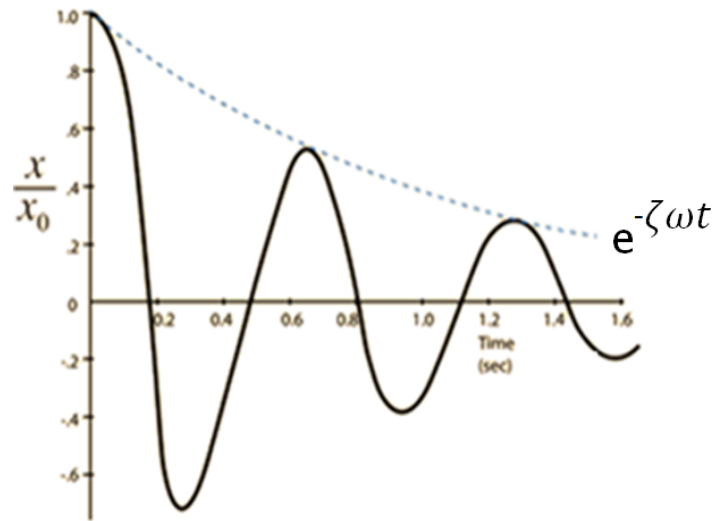
Figure 5.11: Amplitude decay of underdamped system over time

This system amplitude is described by $e^{-\zeta\omega t}$. The difference in amplitude between the first and second peak squared is the energy loss per cycle, i.e. $E_{loss} = 1 - (e^{-\zeta\omega t})^2$. Varying the damping in E_{loss} will give the amount of energy lost per cycle for different frequency tuning values(fig. 5.12).
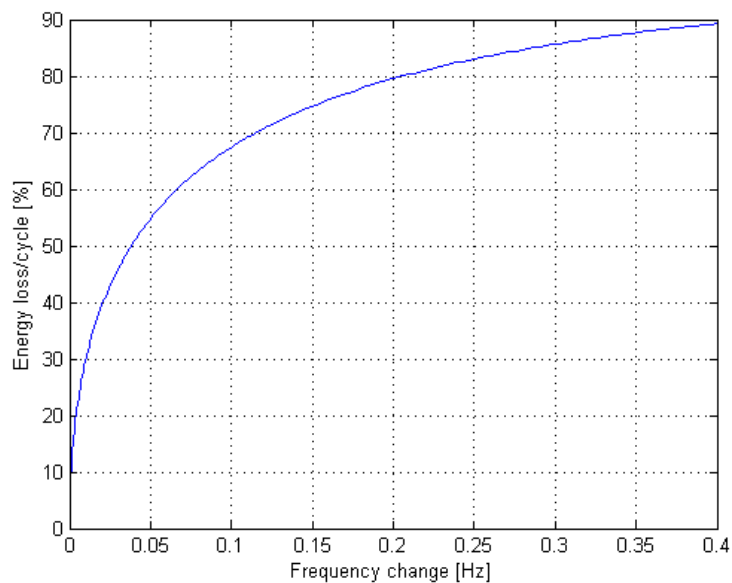
Figure 5.12: Energy loss per cycle using damping

From this graph it immediately becomes clear that damping is not a feasible solution when power is limited. To obtain the desired amount of tuning(0.4Hz) $\approx$ 90% of the total system energy is dissipated per cycle. When a system is oscillating at 25Hz it would be fully damped within a few oscillations.

Since energy efficiency is a criterion in the case study, damping is not a feasible solution to tune frequency.

6

FREQUENCY TUNING: STIFFNESS

6.1. TUNING VIA STIFFNESS

Using again eq. (2.1) the influence of stiffness on the natural frequency of a system is calculated. Figure 6.1 shows a positive relation between frequency change $\delta\omega_n$ and stiffness where:

- $\delta\omega_n < 0$ for $k_{tuned}/k_0 < 1$

- $\delta\omega_n = 0$ for $k_{tuned}/k_0 = 1$

- $\delta\omega_n > 0$ for $k_{tuned}/k_0 > 1$

Figure 6.1: Effect of stiffness on the natural frequency of a structure

Zooming in at area of interest an almost linear relation between frequency change $\delta\omega_n$ and stiffness is found which is almost symmetric w.r.t. $k_{tuned}/k_0 = 1$.

Figure 6.2 shows that $0.969 < k_{tuned}/k_0 < 1.033$ meaning $0.969 N/m < k_{tuned} < 1.033 N/m$ to provide a tuning range agreeing with the requirement.
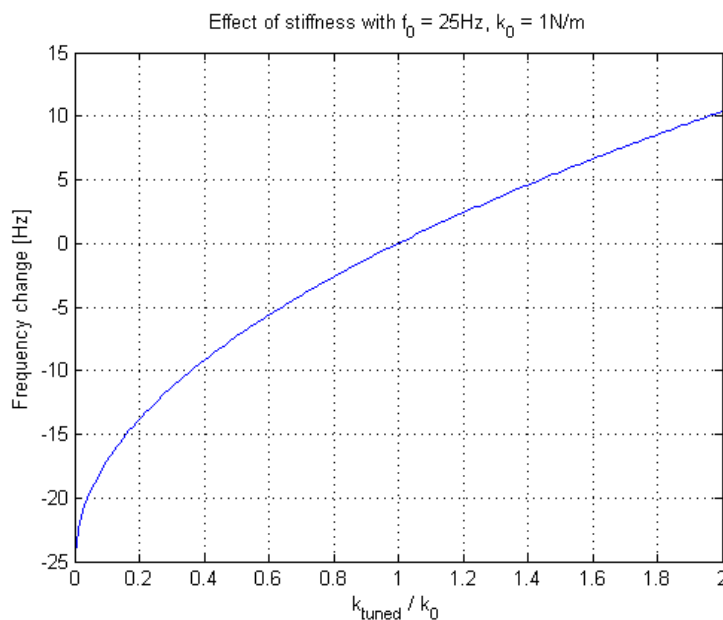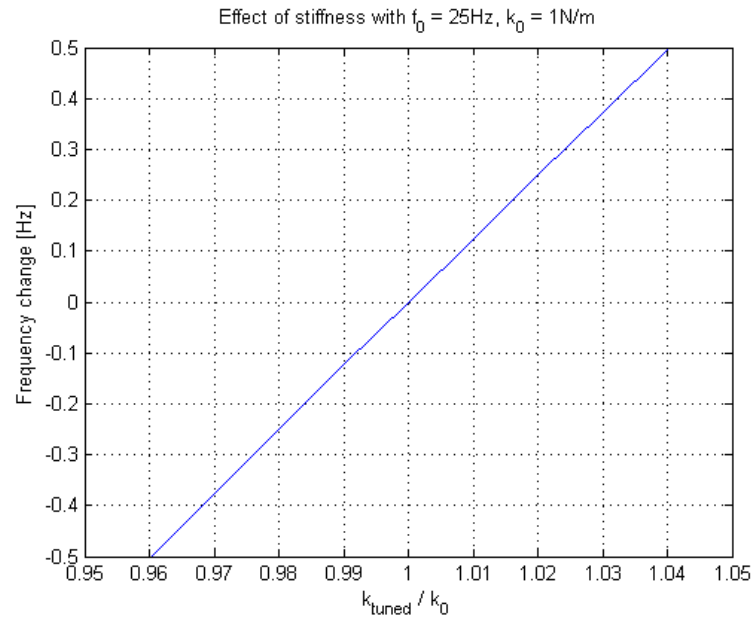
Figure 6.2: Effect of stiffness on the natural frequency of a structure - area of interest

6.2. FEASIBILITY STUDY - STIFFNESS

Changing the frequency by adapting the stiffness can be accomplished by buckling the structure(fig. 6.3) resulting in a lower stiffness or by pulling the structure resulting in a higher stiffness and changing the frequencies accordingly.
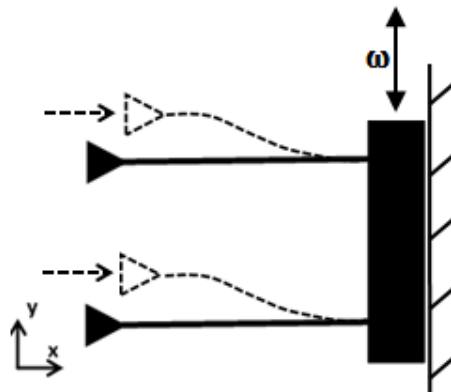
Figure 6.3: Changing frequency by lowering structure stiffness

In the intended application multiple suspension beams do exist which can be buckled or pulled. Since these suspensions can be designed for negative, zero and positive stiffness with varying values it is also possible to design a suspension such that a certain amount of stress on a beam results in the right amount of softening/stiffening for the required tuning range and resolution.

It is therefore concluded that frequency should be tuned via a stiffness change. This system should contain a suspension that can be modified by an input motion/force in the desired tuning range.

<div align="right">

7

</div>

SYSTEM FUNCTIONS

The goal is to design a mechanism capable of high resolution tuning within a specified range before operation. An actuation stage with sufficient displacement and force range is required. To obtain a certain range an amplifier might be used or a combination of a large range coarse tuner and a small range fine tuner. After tuning the tuning step should be robust to shocks implying a locking method either incorporated in the displacement stage or via a additional system.

7.1. ACTUATION

Different types of actuators do exist. Due to the working scale the ones of interest are actuators for MEMS. In a review by Bell et al. (2005) [2] MEMS actuators are observed on their performance. Four types of actuators, which cover the largest part of MEMS actuators are considered and also adopted in this overview; electrostatic, piezoelectric, thermal and magnetic.

7.1.1. ELECTROSTATIC

Electrostatic actuators use the attraction force between oppositely charged conductors. Displacement values up to $200\mu m$ and a force range of $10^{-6}N - 10^{-3}N$ can be found [2].

Coulomb's law is also used to get a first guess whether the required force output is met using such an actuator (eq. (7.1)).

$$F_{electrostatic} = \frac{A\varepsilon_0\varepsilon_r}{2d^2}(\triangle V)^2 \tag{7.1}$$

with permetivitty $\varepsilon_0 = 8.854e^{-12}\ C^2/Nm^2$, relative permetivitty $\varepsilon_r = 1$, plate distance d, voltage V and plate area $A = h \cdot L$. For characteristics values in the case study the electrostatic force can be calculated as a function of the effective capacitor plate length L (fig. 7.1).

The required actuation force is $70mN$ which is 20 times larger than the maximum value found in fig. 7.1. No feasible change in parameter of combination of parameters can result in such an increase. Therefore it can be concluded that, based on the force output, this actuator is not directly applicable. A force amplification stage however might be a solution to this problem at the cost of a stroke reduction.

7.1.2. PIEZOELECTRIC

Piezoelectric elements get there displacement due to strain induced by an electric field. Displacement values with a maximum between $10^{-7}m$ and $10^{-3}m$ and a force range with a maximum between $10^{-5}N$ and $10^{-3}N$ can be found [2].

A piezoelectric element typically achieves a nominal displacement around 0.1 to 0.15% of the actuator length. Therefore a maximum movement distance of 800 μm results in an actuator length of at least $\frac{800\cdot100}{0.15} \approx 533mm$ which is not a feasible solution for the entire displacement stroke within the current dimensional requirements. It can still be used as fine tuning on a less accurate but larger displacement actuator (coarse tuning). A second option is to use an amplifier to increase the range at the cost of resolution loss. A typical amplification rate is around 20 times which implies an actuator of $533/20 \approx 27mm$ which is still factors to high.

Electrostatic actuator force parallel plates
h= 400 [μm], V = 300 [V], d = 50 [μm]
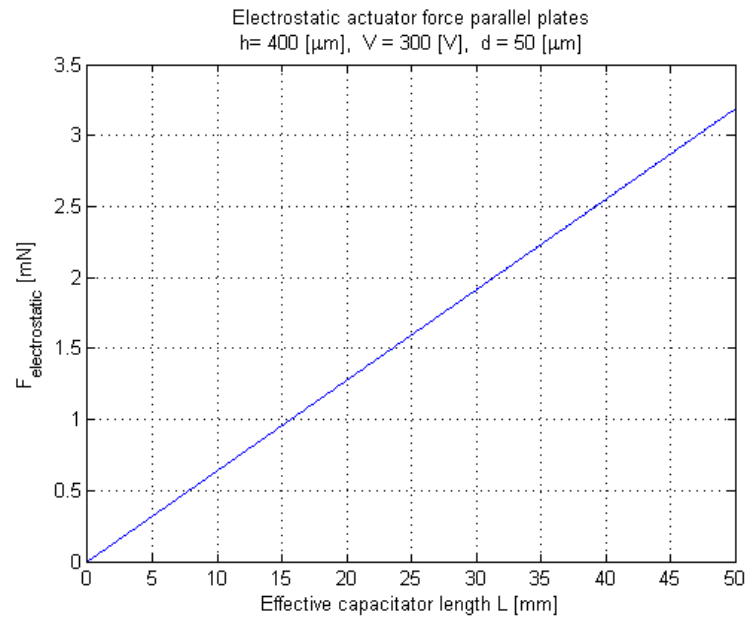
Figure 7.1: Required capacitor length for specific actuator force

7.1.3. THERMAL

Thermal actuators rely on the thermal expansion of structural elements to cause a displacement. Depending on the design configuration and material, and therefore different thermal expansion coefficient, different displacements can be achieved.

A calculation is used to estimate the maximum achievable stroke for a thermal expansion actuator. The beam is assumed to freely rotate at its endings. In a monolithic design this rotation will be caused by bending in the beam and will therefore be smaller. This calculation therefore gives displacement value for an ideal situation. A small initial angle is applied to the beams to escape the singular position and set the movement direction (fig. 7.2).

Figure 7.2: Simple thermal expansion beam model

The linear thermal expansion for silicon $\alpha = 2.56e^{-6}/K$, an initial beam angle $\gamma = 2\,\text{deg}$ and a temperature difference $\delta T = 400K$ is applied.

Using the following sequences of equations the maximum x-displacement can be determined as a function of the initial beam length L.

$$
\begin{aligned}
x_0 &= L_0 \sin\gamma \qquad y_c = L_0 \cos\gamma \\
\delta L &= \alpha \triangle T L_0 \\
x_\alpha &= \sqrt{(L_0 + \delta L)^2 - y_c^2} \\
\delta x &= x_\alpha - x_0
\end{aligned}
$$

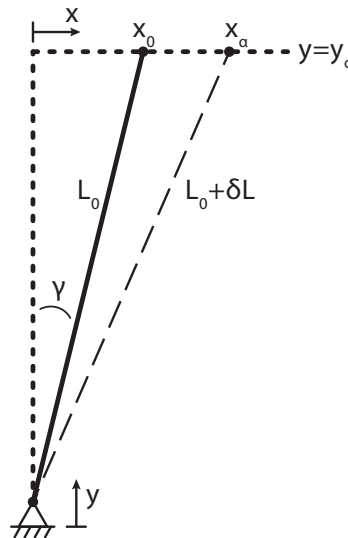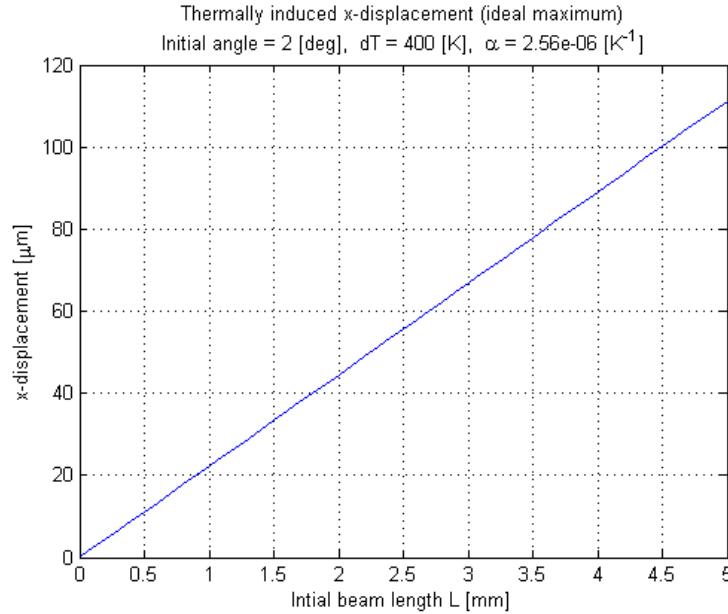Figure 7.3: Theoretical maximum x-displacement of an thermal actuation beam

7.3 shows that an initial beam length of $5mm$, results in a maximum x-displacement of $\approx 110\mu m$ which is well below the requirement.

Based on this result it can be concluded that a thermal actuator is not directly applicable as actuation stage. A thermal actuator in combination with an amplification or coarse-tuning stage might still be possible.

7.1.4. MAGNETIC

Displacement in a magnetic actuator is caused due to interaction among various magnetic elements: permanent magnets, external magnetic fields, magnetizable material, and current-carrying conduct. Displacement values with a maximum between $10^{-5}m$ and $10^{-3}m$ and a force range with a maximum between $10^{-7}N$ and $10^{-4}N$ can be found [2].

Surrounding elements in the micro oscillator are highly sensitive to magnetism and should not be affected by a magnetic actuator. Therefore a magnetic field is not allowed to exceed a certain amount of tesla T and/or the surroundings should be shielded for this magnetic fields implying a more complicated and expensive system.

7.1.5. SUMMARY: ACTUATION

Results above show that neither one of the actuation principles can fulfill both the displacement as force requirement. From this it can be concluded that an improvement or addition to the current or a different actuation principle is required. Examples could be the addition of an amplification stage or a larger range coarse tuning stage as initial tuning step in combination with a smaller fine tuning stage.

A second issue that should be considered is the space-efficiency of the actuation stage. It has been shown that an 'on-board' actuation stage requires almost all available space while the actuation stage is only required once during initial tuning and not during operation. Based on the volumetric efficiency it is therefore preferred to have an external actuation stage that is only connected during initial tuning. This also allows for a standard (not custom designed) actuation stage where only the connection with the tuneable device is considered.

7.2. Locking

After tuning the tuning-shuttle is not allowed to change position during operation under internal or external disturbances. A method is required to lock the device against these disturbances. A schematic representation of the current system is presented (fig. 7.4). As stated in the requirements the lock should allow release and re-locking up to at least *20* times to allow re-tuning.
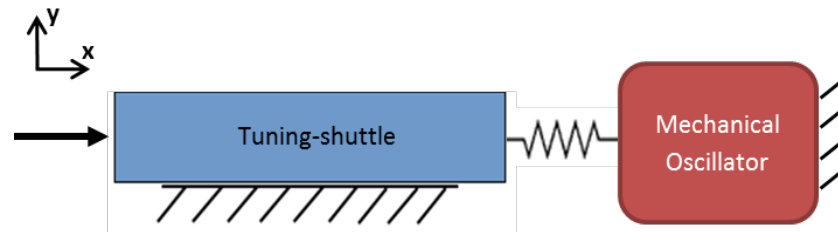

Figure 7.4: Schematic representation of locking structure

7.2.1. Locking classification

Different locking methods are identified covering the spectrum of locking techniques:

- Geometry: The geometry of the locking mechanism results in a shape lock that prevents the mechanism from moving provided the shape lock is maintained and no mechanical failure occurs.

- Friction: Two surfaces are pressed together and resulting friction force locks the mechanism.

- Adhesion/ bonding: Locking between two relative moving surfaces by bonding materials due too interaction between these layers. Interaction might occur via additional substance.

These methods categorize solutions based on their working principle but do not provide direct insight in key-properties of these solutions. A different classification is proposed based on a hierarchic-structure where unique methods are defined which can fulfill the main function 'Locking'. For these methods different solutions principles are established. Finally means (working solutions) that fulfill this solution are listed (table 7.1). This classification provides both insight in the key-properties of the working solutions as it guarantees overview of the entire solution-space since sub-categories are unique and exclusive subsets in the solution-space. Depending on the application more means to fulfill the solution could be determined but for this case study they are limited to means that work in monolithic structures, on micro scale without energy consumption during operation.

The main function is, as listed in the first column, locking the tuning shuttle after tuning/ positioning. This can be accomplished by either continuously positioning the device ensuring any target position can be reached or by discrete positioning where positioning accuracy is determined by the incremental nature of the locking solution. In practice continuous positioning is also discrete due to the resolution of the actuator but the resolution of the locking device is known to be dominant and therefore limiting.

Discrete position locking   Discrete position locking can be accomplished by using the rigidity of materials to provide a certain behavior such as interlocking teeth to prevent movement. The second option is when a material is not rigid i.e., a compliance lock where the deformation of a material is used to provide a locking force or geometry.

The fabrication resolution used in the case study is lower than the required tuning resolution excluding all discrete position locking solutions. For a large 'resolution to tuning range ratio' one could argue to use a Vernier-mechanism but since this case study clearly has a very small 'resolution to tuning range ratio' this is not possible leaving only continuous position locking solutions a feasible option.

Continuous position locking   Continuous position locking can be accomplished by introducing a reaction force that counter-acts the internal and external forces. Since this is a 2D situation, only solutions are a force in x- and y-direction and a moment about the z-axis (out-of-plane). For these solutions specific means can be found as listed in the fourth column.

Table 7.1: Locking method classification

Function	Method	Solution	Means
Lock tuning-shuttle	Continuous position locking	Fx	Magnetic (permanent)
			Direct bonding
			Adhesive bonding
			Eutectic bonding
			Plasma-activated bonding
			Soldering (metal/thermoplast)
			Stiction
		Fy	Pretension
			Mass
			Magnetic (permanent)
		Mz	Fx and/or Fy + moment arm
	Discrete position locking	Rigid lock	Interlocking teeth
			Singularity
		Compliance lock	Bistable beam switch
			Snap buckle

All main forces that can disturb the tuning position have a dominant vector in x-direction so the most efficient way to counteract these forces would be via a force Fx in x-direction. Several wafer bonding techniques are listed, however these techniques are designed to permanently bond two objects making re-tuning impossible. One could consider incinerating the bonding layer but this requires high temperatures ($>200°C$) affecting the entire structure and new bonding material must again be added to allow re-locking. Stiction forces could provide a locking force but only lock sufficient on very small scale. The use of magnets is not preferred due to the flux-sensitive nature of surrounding elements. A second option is to use a force Fy in y-direction with a resulting force in x-direction. Again a magnetic force could be used, but as previously stated this is not desired. A mass can also be used to generate a passive force in y-direction but is dependent on the orientation of the structure and will therefore only work if the structure is positioned and operated in one specific plane. Pretension on an elastic member will also generate a force in y-direction which will be transferred via friction. A third option would be to introduce a moment on the system but in practice this will result in a force applied via Fx and/or Fy in combination with a moment arm.

In conclusion continuous position locking is the preferred method to lock the tuning shuttle for this specific case study. When applying all requirements to the different means, only pretension is a feasible candidate to generate sufficient locking force in all orientations and is therefore selected for further investigation.

<div align="right">

8

</div>

PRETENSION LOCKING

Pretension in a planar, monolithic structure is accomplished by deforming an elastic member with a stiffness. As result of this deformation displacement input a force will be exerted by the deformed elastic element. This force can be used to clamp(lock) the tuning shuttle. The schematic representation of the locking structure can be extended with a 'pretension-beam' represented by a spring (fig. 8.1).
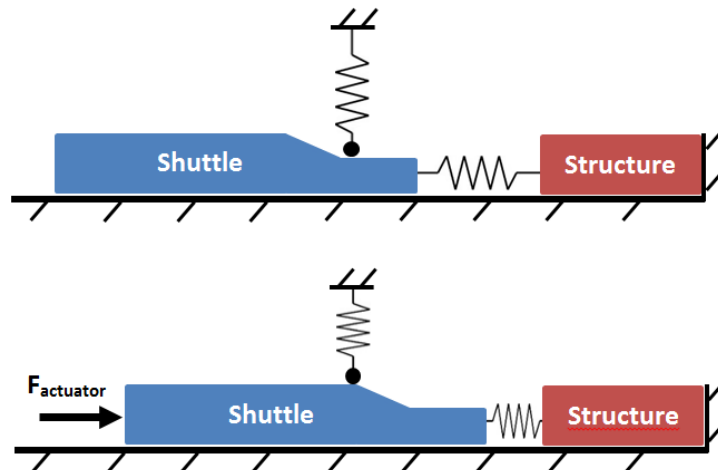

Figure 8.1: Schematic representation of locking structure via pretension

After fabrication there is no prestress in the pretension-beam. An initial prestress displacement on this element is therefore required to ensure the locking force is high enough in the desired region. Figure 8.2 shows the required behavior of this pretension-beam with initial position and locking force **A**. Region **A** to **B** represents the coarse tuning region, region **B** to **C** the fine tuning region where the relative distance between pretension-beam and tuning-shuttle is 0 (contact) and the locking force is high enough to lock the tuning shuttle. These are the basic requirements the pretension-beam must fulfill to guarantee sufficient locking force in the required region.

Given three points **A**, **B** and **C** with the requirement of contact and locking between **B** and **C** and the ability for re-tuning, a limited amount of motion paths for the pretension-beam can be determined (fig. 8.3).

In this schematic contact is assumed for all points co-linear with **A**, **B** and **C** and the locking force is assumed sufficient in case of contact between **B** and **C**. Re-tuning is guaranteed when region **B**-**C** can be repetitively reached at any desired point. Note that re-tunability requires repetitive motion between **B** and **C** but repetitive motion between **A** and **C** or **A** and **B** is not required!

Example Option 7: there is no contact and locking force at point **A** between pretension-beam and tuning-shuttle. In this state the coarse tuning is performed resulting in contact with sufficient locking force at point **B**. The physical motion between **A** and **B** can be anything between 'contact just after **A** with sufficient locking
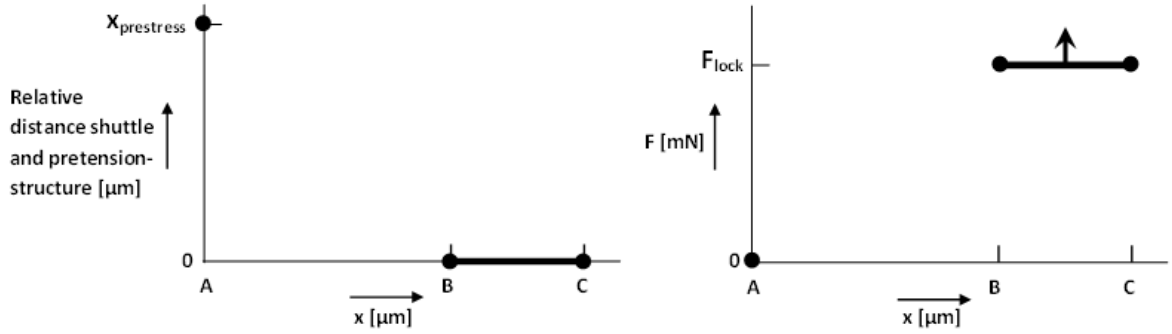
Figure 8.2: Required pretension-beam position (left) and locking force (right)

force' to 'no contact (so no locking force) until **B**'. From **B** to **C** the pretension-beam can be fine-tuned provided the tuning force is higher than locking force $F_{lock} \cdot \mu$. After **C** the locking force is (partially) released and via a cyclic movement the pretension-beam moves back to **B** to allow re-tuning.

8.1. LOCKING MOTION PATH EVALUATION

Option 1-5 can be eliminated since they are in contact and provide sufficient locking force right after fabrication which is impossible for monolithic devices.

While option 6, 7, 9 and 10 all possess a cyclic motion, option 8 does not. This means that, given the motion is possible, the first set can be achieved using a single actuator while option 8 always needs at least two i.e., 1) for positioning and 2) for the instance of applying the locking force. This is a possibility but more difficult compared to a single actuator and therefore not preferred.

Option 7,9 and 10 can be distinguished from option 6 by the nature of re-tuning. Option 6 does not require an additional motion for unlocking en re-locking while 7, 9 and 10 all require an additional motion where the locking force is released before re-tuning. Advantage of option 6 is no additional motion paths and therefore suspension elements need to be added greatly simplifying the locking system. Disadvantage is that the amount of pretension-beam geometries is limited since the pretension-beam must be able to coop with re-tuning while the locking force is maintained resulting in large shear forces in the beam. It can be said that option 6 only allows symmetric pretension-beam geometries or geometries that can deal with the shear stresses as a result of the back and forth sliding while option 7, 9 and 10 allow highly asymmetric pretension-beam geometries. This phenomena is illustrated in fig. 8.4.

When the tuning-shuttle is moving to the right, the pretension-beam(black) will slightly move up(red) allowing the tuning shuttle the move with low force which can be seen as positive feedback. Moving the tuning shuttle to the left will result in bending of the pretension-beam(green) requiring higher force which is equivalent to negative feedback. This negative feedback could be a useful feature to increase the locking force when the counter-force increases. However the bending stress could exceed the yield-stress when the tuning-shuttle moves too far.

8.2. SPRING REQUIREMENTS

The tuning-shuttle is displaced in x-direction using an actuator until the desired or tuned x-position is reached. Displacement of this shuttle will result in a counter force on the shuttle due to the deformation of elastic members connected to this shuttle. To ensure the shuttle position is maintained after removal of the actuator force $F_{lock} \geq F_{counterforce}$ where $F_{lock} = \mu \cdot F_N$ with F_N the normal force on the shuttle in y-direction resulting in a x-force via friction with friction coefficient μ.

Normal F_N is acquired by deforming a spring structure which can be described by eq. (8.1) with spring stiffness k and spring deformation δ.

$$F_N = F_{spring} = k \cdot \delta \tag{8.1}$$

Knowing that $F_{counterforce} \leq 100mN$ and $\mu \geq 0.1$ it can be found that $F_N \geq 1N$. Now it is possible to determine the required spring stiffness k for different spring deformation or prestress distances (fig. 8.5).
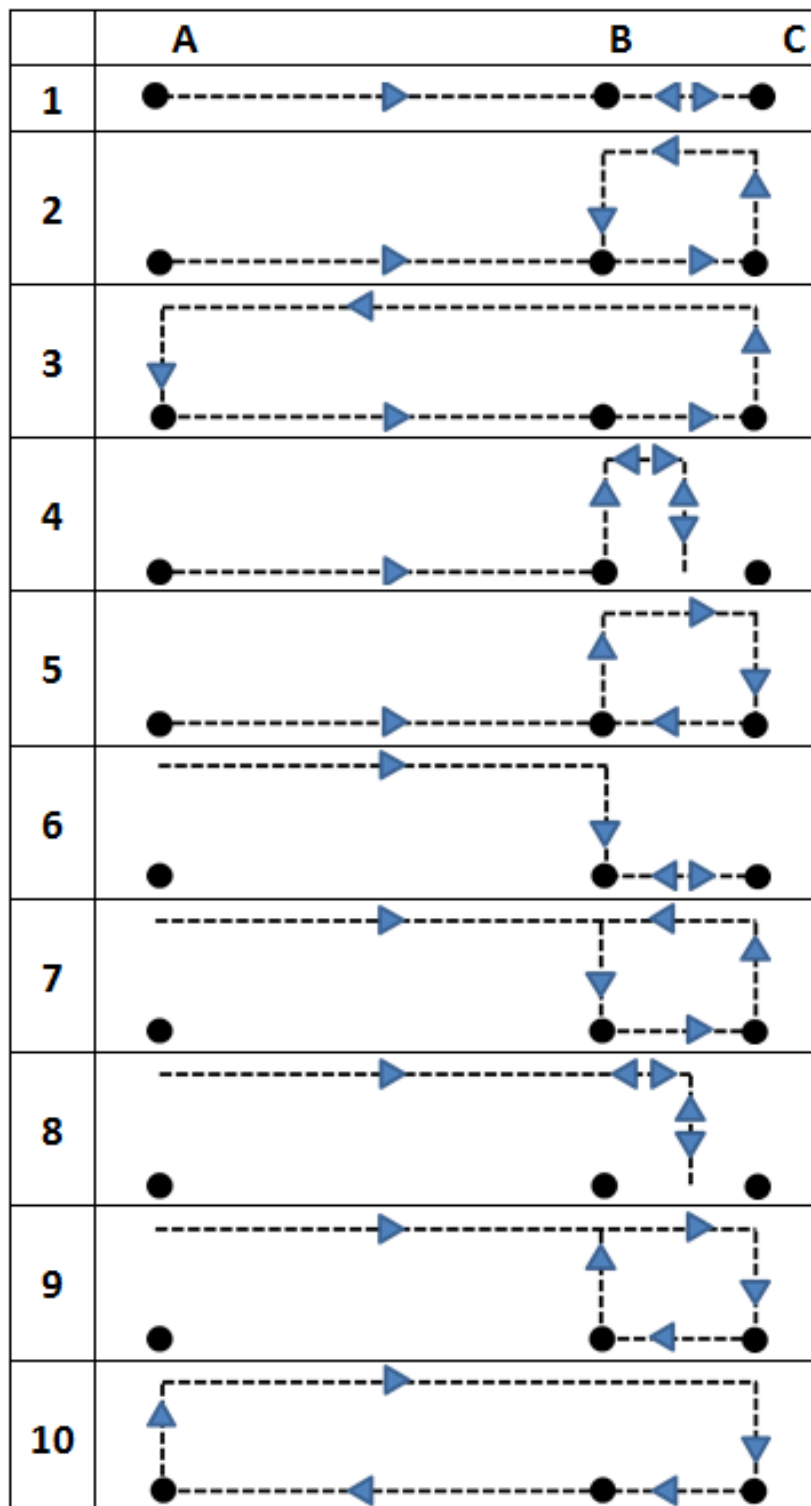
Figure 8.3: Possible motion trajectories between **A**,**B** and **C** with locking between **B** and **C**
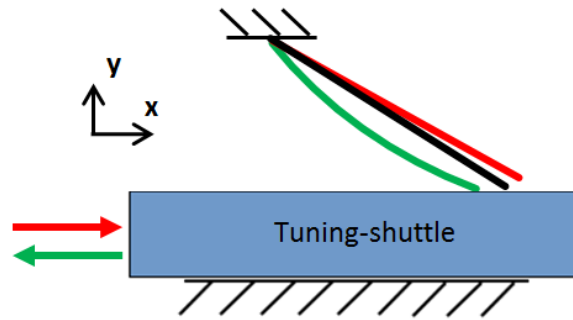
Figure 8.4: Asymmetric pretension-beam locking
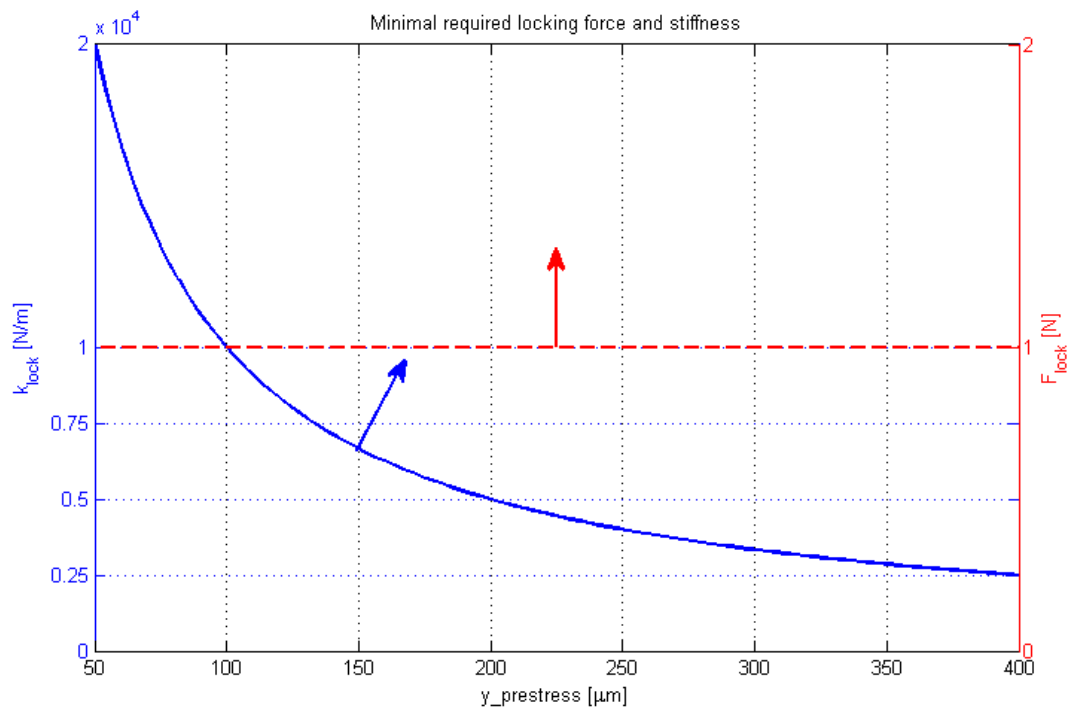

Figure 8.5: Required spring stiffness and output force

<div align="right">

9

</div>

SPRING DESIGN

Geometry of the spring with stiffness k is free within design constraints such as the maximum stress due to deformation δ and maximum area A, or fabrication constraints such as minimum beam thickness or minimum separation between different elements.

Different spring shapes are evaluated and optimized towards and spring design that delivers the required locking force with a lower limit to the deformation δ subjected to the design and fabrication constraints. Different shapes are created using a 5-control points Bézier curve.

MATLAB is used to create a spring geometry which is evaluated using ANSYS to determine the force-deflection behavior and stress induced by this deflection. A genetic optimization algorithm uses these outputs to optimize the spring design.

9.1. OPTIMIZATION

An optimization algorithm is used to vary design variables and find a suitable solution that does not violate the design constraints. The finite element package ANSYS is used to evaluate different spring geometries. Occasionally ANSYS does not converge resulting in a non-smooth irregular solution-plane. Such a solution space is difficult to optimize using a gradient-based optimizer. Therefore the non-gradient based, genetic algorithm is used which creates an initial population of candidate solutions. The fitness of these individuals is evaluated and the fitter individuals are stochastically selected, modified and crossed with different individuals during different generations leading to a fitter solution. When the change in fitness (objective) value is lower than a certain threshold or a certain amount of generations is reached the optimization is completed.

9.1.1. OBJECTIVE

The objective of this optimization is to find a spring geometry that delivers the required force with a maximum prestress displacement to lower the sensitivity to fabrication errors. Designs with a higher force and larger prestress displacement are favored and obtain a higher objective value.

A general version $fa = -f1 - f2$ of the objectives for the locking force and prestress displacement is plotted in fig. 9.1. Locking force is ranked using objective $f1$ and prestress displacement using $f2$. It can be seen that the objective values have a high gradient until a desired value is reached, after this desired value the gradient decreases.

Example: Assume $F_{lock} > 1N$ and $y\_prestress < 50\mu m$. The required locking force is already satisfied while the required prestress displacement is not. Although the objective value will still increase by increasing the locking force, it is more efficient to increase the prestress displacement since this gradient is higher.

Finaly summing these values results in the overall objective value(fig. 9.2).

After testing it turned out this objective function preferred to maximize either $f1$ or $f2$. Since these objectives contradict each other maximizing one results in minimizing for the other yielding unusable results. Therefore the objective function is changed to also evaluate the difference between both objectives according to eq. (9.1) resulting in fig. 9.3.

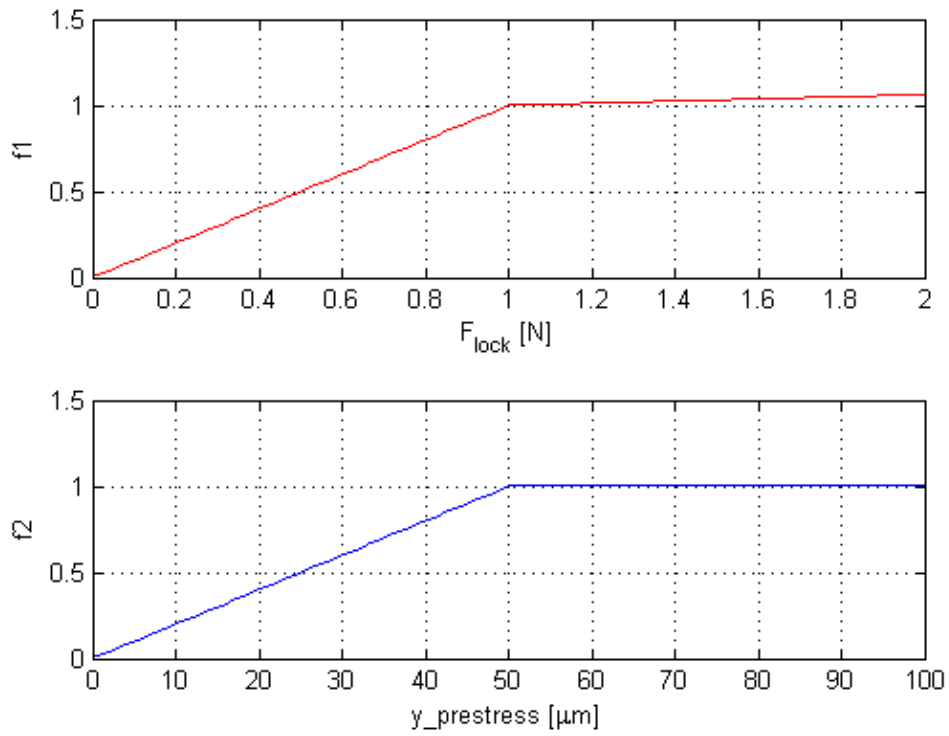$$fb = \left| \frac{\min[f1; f2]}{\max[f1; f2]} \right| \cdot \max[f1; f2] \cdot (-f1 - f2) \tag{9.1}$$

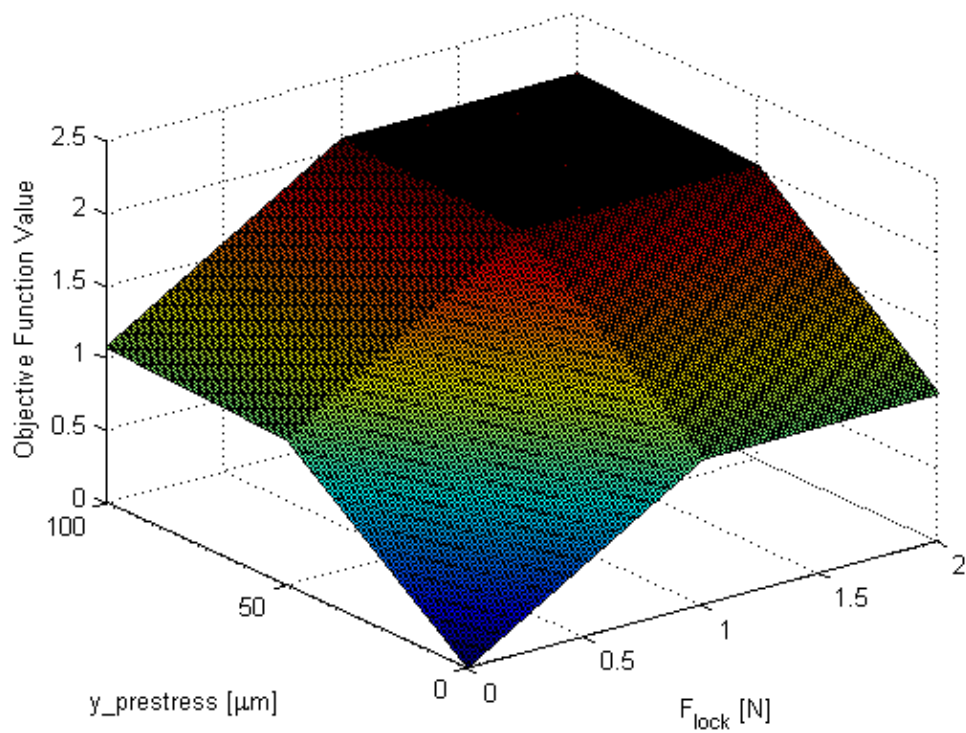Figure 9.1: Objective values for different locking force and prestress displacement

Figure 9.2: Objective function fa
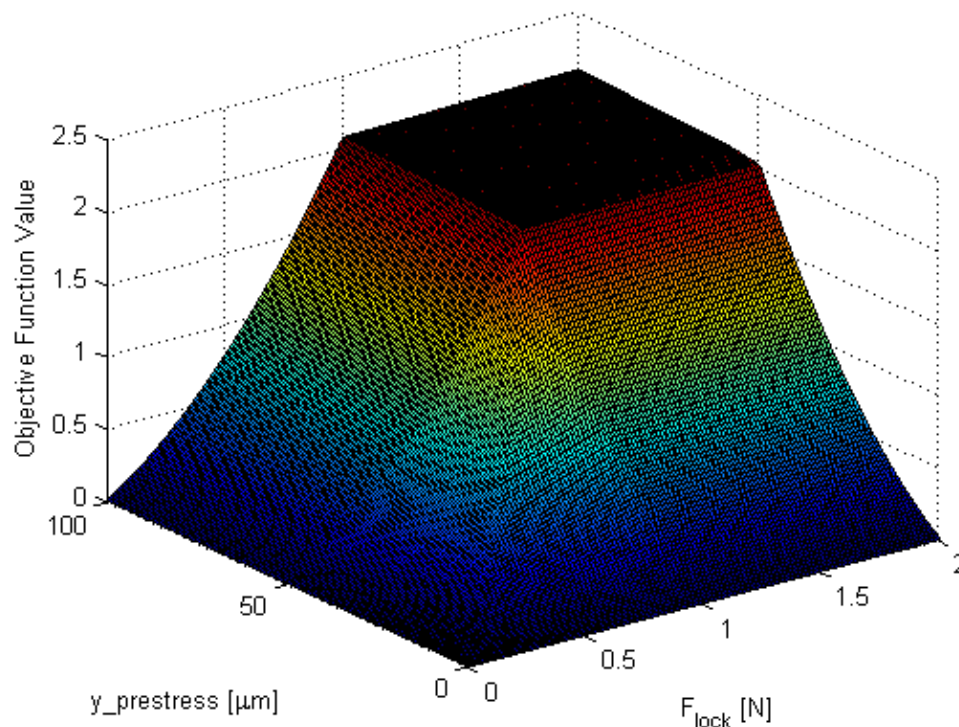
Figure 9.3: Objective function fb

However the gradient for low inputs is very small. To solve this, objective function fa and fb are added resulting in the overall objective function fig. 9.4.

9.1.2. Constraints
Optimization constraints are:

1. Maximum stress in the prestressed spring

2. No intersections in the spring geometry

3. Fabrication

4. Bézier curve control points

5. Spring thickness

These constraints are evaluated in the pre- and post data analysis and influence the final objective value.

1. Maximum stress
The maximum stress in the spring should not exceed 200MPa.

2. Intersections
The possible spring designs are limited to designs without intersection (fig. 9.5). In reality it is off course possible to have cross-connections between spring elements, but this implicates the FEM and is not considered for simplicity reasons.

3. Fabrication
The bezier curve generated by MATLAB is a single spline and possibly with sharp corners. When the material thickness is added around these lines material will overlay in these corners resulting in a triangular inner geometry. The fabrication process sets a minimum distance of $180\mu m$ on the gap between different

Figure 9.4: Objective function

Figure 9.5: Spring design with intersecting elements

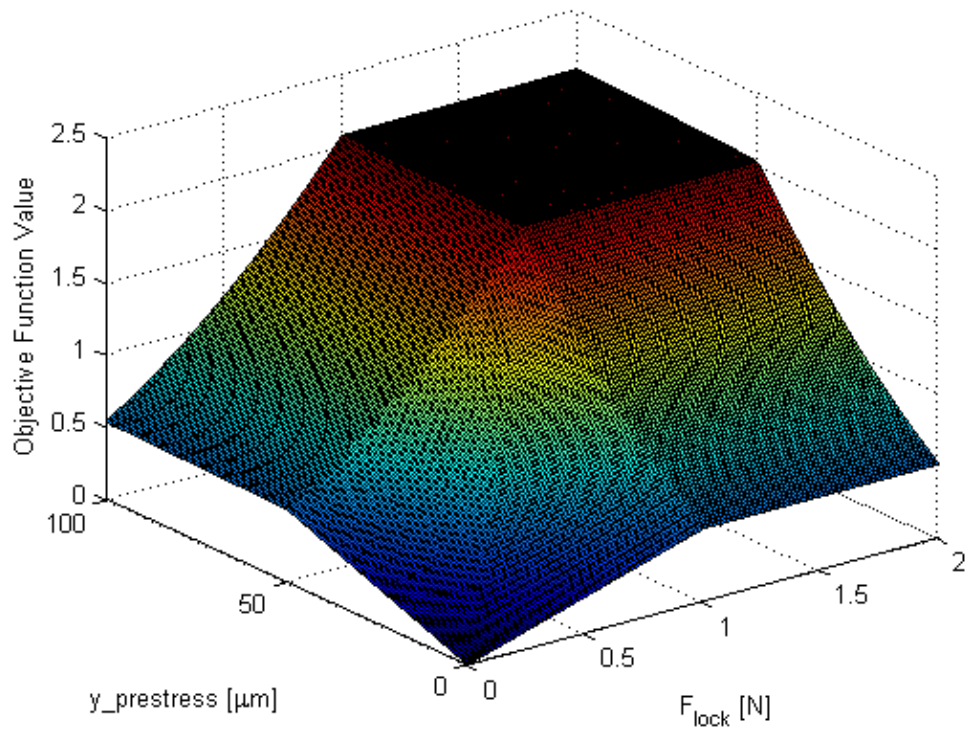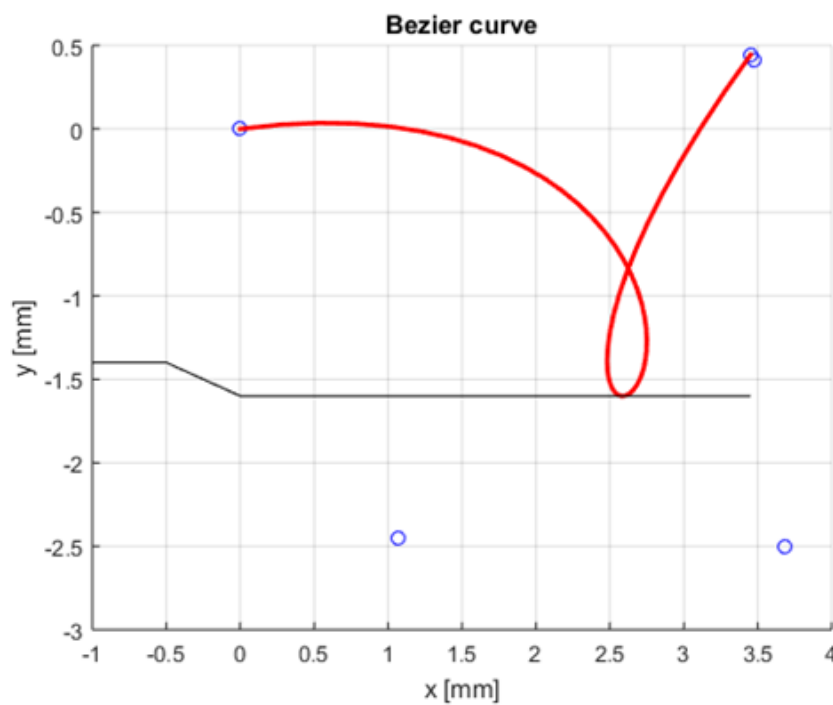material elements. This is equivalent to a minimum curve radius. An example is given in fig. 9.6 where a random geometry is generated visible in red. The minimal element boundaries due to the fabrication process are represented by the blue dashed lines. Due to the small curve radius the boundaries intersect at

$(x, y) = (1.15, 0.61) mm$ resulting in a sharp edge which cannot be produced. Therefore these designs are eliminated.
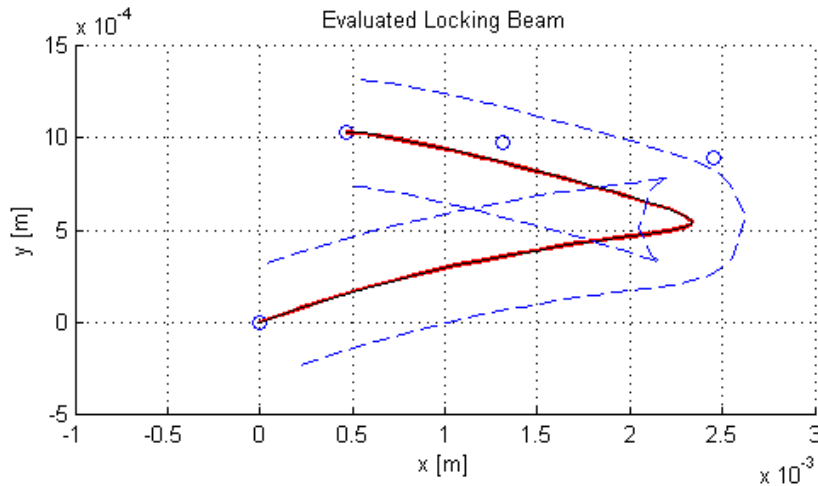

Figure 9.6: Spring design with too small curve radius

4. BÉZIER CURVE CONTROL POINTS

The Bézier curve is created using a certain amount of control points. One could argue that a larger amount of control points is beneficial to create a larger diversity of shapes which is true. However every control point introduces two additional variables for the optimization function slowing it down. Therefore the minimum amount of control points needs to be established that can still create a wide variety of spring shapes. The amount of shapes that can be created with, 2-, 3- and 4-control points is very limited since these represent linear, quadratic en cubic curves. More 'random' curve shapes can be created when using 5- or 6-control point Bézier curves. The amount of intersections (constraint 2) and fabrication violations (constraint 3) however significantly increases when using 6-control points while the amount of additional usable curves is limited. Therefore it is decided to use a 5-control point Bézier curve for spring shape generation.

Besides using a single Bézier curve it could be decided to couple multiple Bézier curves to create a coupled stiffness behavior. This will introduce additional variables and is not considered for simplicity and time reasoning.

5. SPRING THICKNESS

The thickness of the spring is constant over its entire length. It could be desired to stiffen the spring at specific points to change the stress or stiffness behavior. This is not considered in this study.

9.1.3. TOPOLOGY OPTIMIZATION

In close cooperation with Alexandert Verbart a small study is conducted to investigate the possibility of using topology optimization (TO) to create a spring shape. Software design and implementation of this study in this software is done by Alex.

Conventional way of using TO is applying a load case (force vectors) in the design space. Material specifications are inserted in the optimizer and finally the TO tries to maximize the stiffness of the structure or to minimize the mass used depending on the objective. After optimizing a FEM is used to evaluate the optimized structure for the stress constraint. The load case in this problem will result in a trivial solution being a

skewed straight beam that does fulfill the stress constraint. However the compliance of this shape is not sufficient. When looking for a large compliance the stress constraint will most likely be violated. Therefore when using TO to optimize compliant members it is crucial to incorporate stress constraint within the optimizer which is the topic of Alex' dissertation (Topology Optimization with Stress Constraints).

Two different formulations of the objective are tried for a design case(fig. 9.7):
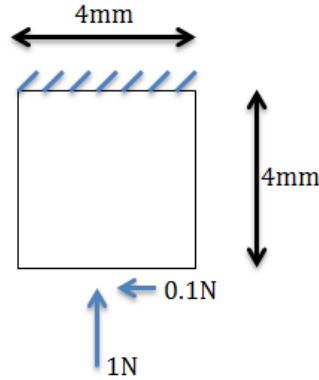
Figure 9.7: Design case and domain for TO

CASE 1

$$\min \left(\frac{C}{C_{max} - 1} \right)^2 \qquad \text{s.t.} \qquad \sigma(x) \leq \sigma_{max} \tag{9.2}$$

with C_{max} the target compliance based on the required locking force and prestress displacement distance. Assume a required locking force of 1N and prestress displacement of $50\mu m$ than results in $C = F \cdot y = 50e^{-6} Nm$. Results of this optimization are presented in fig. 9.8.
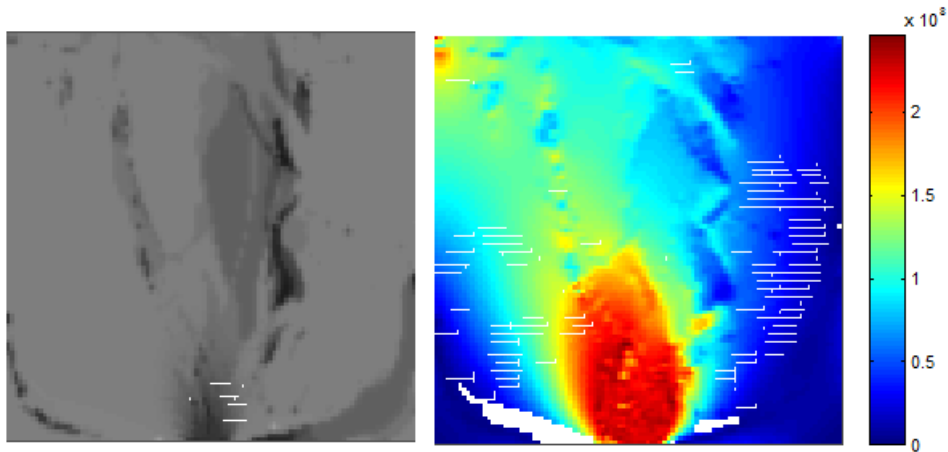
Figure 9.8: Density distribution and Von Mises stress for TO case 1

$$V(\%) = 53.671\% \tag{9.3}$$
$$C = 3.4859e^{-6} \tag{9.4}$$
$$\sigma = 246MPa \tag{9.5}$$

Both the compliance as stress requirements are not met. Also the density distribution shows are large amount of grey matter while a white-black or 0-1 distribution is desired where white is no material and black is 100% material.

In case 2 a penalty method is used while the target compliance is added to the objective function with $p > 0$ as a constant penalty factor. The height of this penalty determines the importance of the compliance value where a higher penalty results in a larger influence of this compliance.

$$\min \quad V(\%) + \left(\frac{C}{C_{max} - 1}\right)^2 \qquad \text{s.t.} \qquad \sigma(x) \leq \sigma_{max} \tag{9.6}$$

Result for $p = 1$ is presented in fig. 9.9:
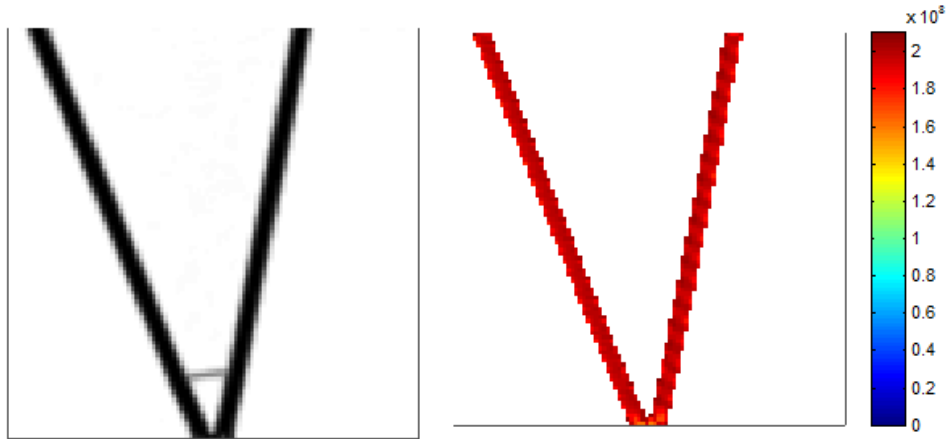
Figure 9.9: Density distribution and Von Mises stress for TO case 2 with $p = 1$

$$V(\%) \quad = \quad 9.629\% \tag{9.7}$$
$$C \quad = \quad 5.1449e^{-6} \tag{9.8}$$
$$\sigma \quad = \quad 210MPa \tag{9.9}$$

It can be seen that the solution converges to a 0-1 distribution that almost fulfills the stress constraint. However the stiffness of the design is 10 times larger than required.

When $p = 1e^3$ the result is as in fig. 9.10:

Figure 9.10: Density distribution and Von Mises stress for TO case 2 with $p = 1e^3$

$$V(\%) \quad = \quad 16.566\% \tag{9.10}$$
$$C \quad = \quad 49.577e^{-6} \tag{9.11}$$
$$\sigma \quad = \quad 1082MPa \tag{9.12}$$

Now it can be seen that the compliance requirement is almost met but the stress constraint is violated. Furthermore the design does not converge to a 0-1 solution.

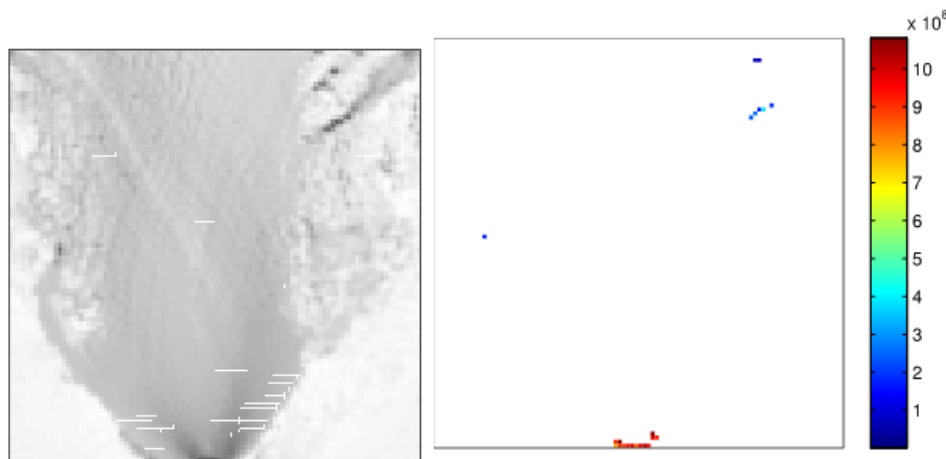This short study shows that is possible to use TO but the optimizer has problems creating a shape that converges to a 0-1 distribution while also solving the conflicting compliance and stress constraints. For this study TO is not further investigated since it requires lots of additional effort to get it functional or to quote Alex: 'Ik denk eerlijk gezegd dat hier een hele master opdracht aan gewijd zou kunnen worden'.

9.2. MODELING

9.2.1. FINITE ELEMENT MODEL

To obtain force, displacement and stress data from the created spring the finite element package ANSYS Mechanical APDL is used. First the spring geometry and thickness created in MATLAB are saved to a text-file (Appendix A.2.1). These variables are then combined with the actual model to be tested. Two different models are used; 1) a contact model with two contacting surfaces and 2) an equivalent contact model where the second surfaces is modeled via reaction forces.

1. CONTACT MODEL

The contact model uses a Pure Langrange Multiplier on contact normal and tangent model to determine the contact characteristics between a contact and target surface(Appendix A.2.2). This model enforces zero penetration and allows a small amount of slip for the contact condition. Contact is controlled via chattering control parameters which determine whether the contact is either 'open' or 'closed'. Different methods such as a 'Penalty Method' or 'Augmented Langrangian' do exist with different contact modeling approach. When considering convergence time and robustness this contact model was favored for this specific design.

The spring is meshed using contact elements and the shuttle is meshed using target elements. Next the shuttle moves right prestressing the spring, resulting in a force in y-direction (fig. 9.11).
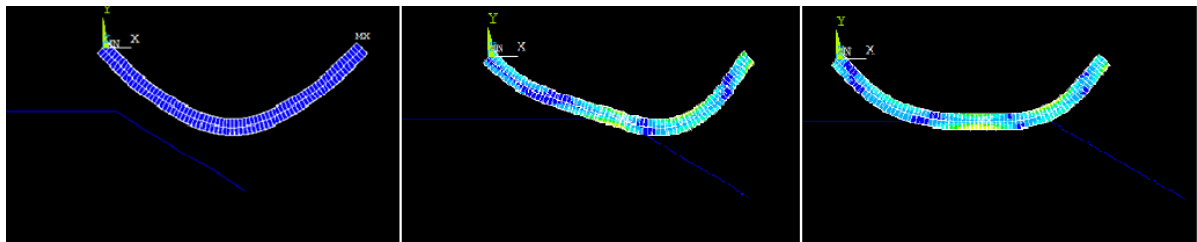
Figure 9.11: Prestressing using a contact model

The model is verified by checking the force equilibrium in y-direction where the prestressing force should be equal to the reaction force in the grounding points of the spring. A second check is the required actuation force to move the shuttle. On the horizontal surface of the shuttle $F_x = -F_y \cdot \mu$ which is also true.

The model showed convergence issues with the sharp corner on the prestressing shuttle as a result of penetration between the contacting nodes. Therefore the corner is rounded, resulting in faster convergence. However solving this model takes approximately 80 seconds on a 2.5GHz Dual Core, 4GB RAM computer which is very expensive. Therefore the contact model is simplified by using an equivalent contact model.

2. EQUIVALENT CONTACT MODEL

The equivalent contact model does not use contact elements but approximates the contact behavior via forces in x- and y-direction on the lowest spring point (Appendix A.2.3). The model assumes that contact happens on a single point on the spring and this point is the same before and after deformation while the contact model can have multiple and changing contact points.

The force in y-direction is used to simulate the prestressing behavior. This normal force will also result in a force in x-direction due to friction with coefficient μ. This model solves within a few seconds and shows results within 1% of the original contact model for the before and after prestressing position.

Note that the assumption of non-changing contact point is valid for this specific case since the geometry is fairly simple and the material is very stiff resulting in trivial deformations. For different materials and different spring geometries this assumption should again be verified.

9.2.2. MATLAB SCRIPT

The script used to run the optimization is presented in Appendix B.1. Before starting the optimization an initial population is determined within the design area that already satisfies the constraints to prevent non-feasible designs being used in the optimization process. The optimization is started in `LockExeOptim` where an initial population, and lower and upper bounds are set for the optimization process. The variables created by the optimizer are used in `LockAnalysis` to create a Bezier curve, checking this curve for intersections and finally sending the spring design to ANSYS with `run_ansys`. The results from ANSYS are then used to determine the objective function value in `LockObjGA_unconstrained` which is used to rank the evaluated spring geometry.

9.3. OPTIMIZED SPRING DESIGN

The final spring design created by optimizing a 5-control point Bézier curve including load case is shown in fig. 9.12.
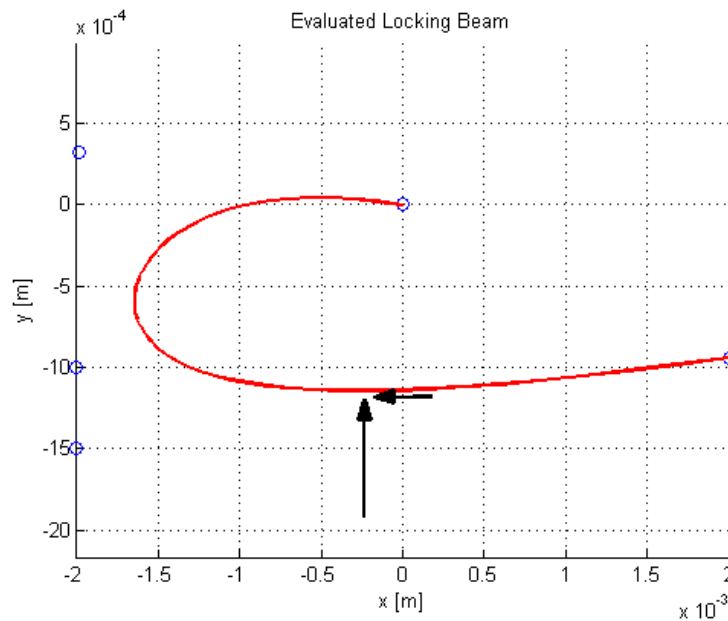
Figure 9.12: Final spring design(red line), Bézier control points (blue circles) and load case (black arrows)

The spring behavior is evaluated using a FEM(fig. 9.13) resulting in the following locking behavior w.r.t. stress and prestress displacement constraint (fig. 9.14).

It can be seen that the maximum locking force $F_{lock} = 0.07N$ for $\sigma_{max} \leq 200MPa$ and $y_{prestress,min} \geq 50\mu m$. Spring thickness $t = 44\mu m$.

It appears that the horizontal(right) part is optimized to counteract the horizontal force without conflicting the compliance constraint. The left part seems to be optimized to deliver the required compliance. Depending on the required stroke this C-shape will grow or shrink. This suspicion is checked by flipping the horizontal force and restarting the optimization. This indeed results in a mirrored version (around the y-axis) of this spring.
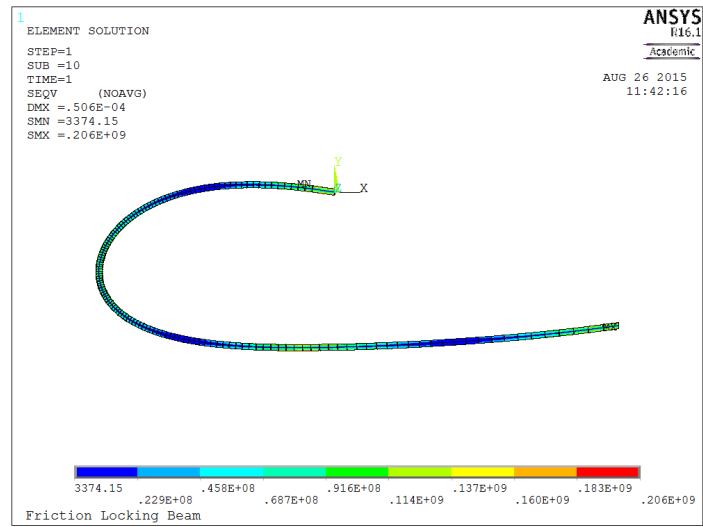
Figure 9.13: FEM evaluation of the spring design
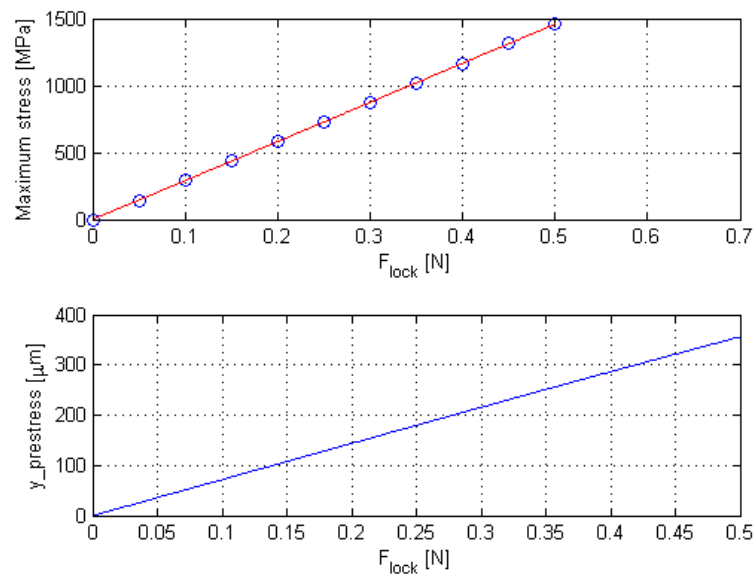
Figure 9.14: Spring specifications

10

LARGE SCALE LOCKING PROTOTYPE

A large scale prototype is created for a proof of principle evaluation in 5mm thick PMMA and cut using a laser cutter (fig. 10.1).
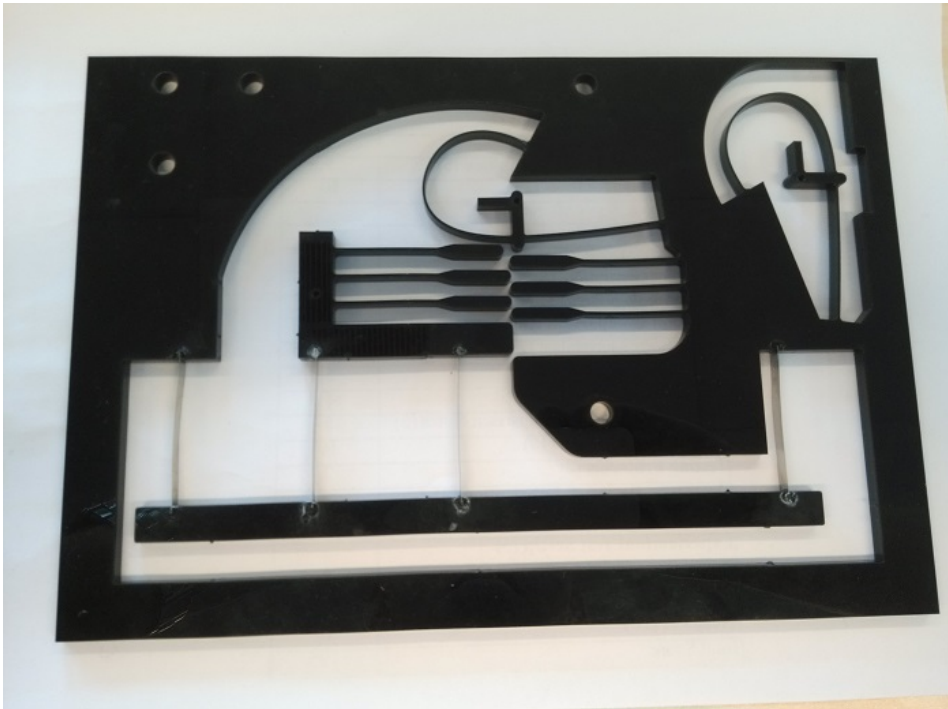
Figure 10.1: Large scale locking prototype

10.1. DESIGN

The optimized spring is scaled with a size factor 20(fig. 10.2). This spring designed for a 2mm prestress displacement resulting in a reaction force of 1N. Multiple cantilever beams are added to increase the locking force as explained in the paper. A straight guidance is added to provide a horizontal input motion for the shuttle. Suspension members of this straight guidance are represented by the thinnest beams in the structure which are produced from stainless steel 1.4310, 0.05mm thickness which are added after cutting the plastic. The thicker straight beams are support structures to ensure alignment of the upper and lower shuttle after laser cutting before the flexures are inserted. Once the flexures are in place and locked using super glue the supports are removed.
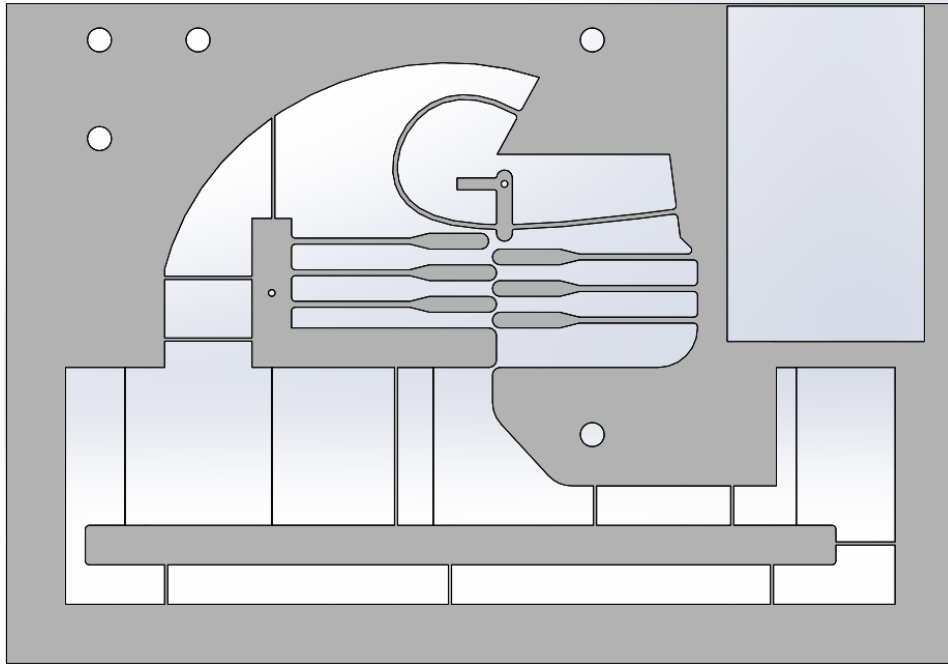
Figure 10.2: CAD design of the large scale locking prototype

10.2. TESTING

Prototype dimensions are measured using a caliper. Stiffness characteristics of all individual members in the structure are measured using a *PI Linear Stage* equipped with a *Futek LSB200 Miniature S-Beam Load Cell* (fig. 10.3).
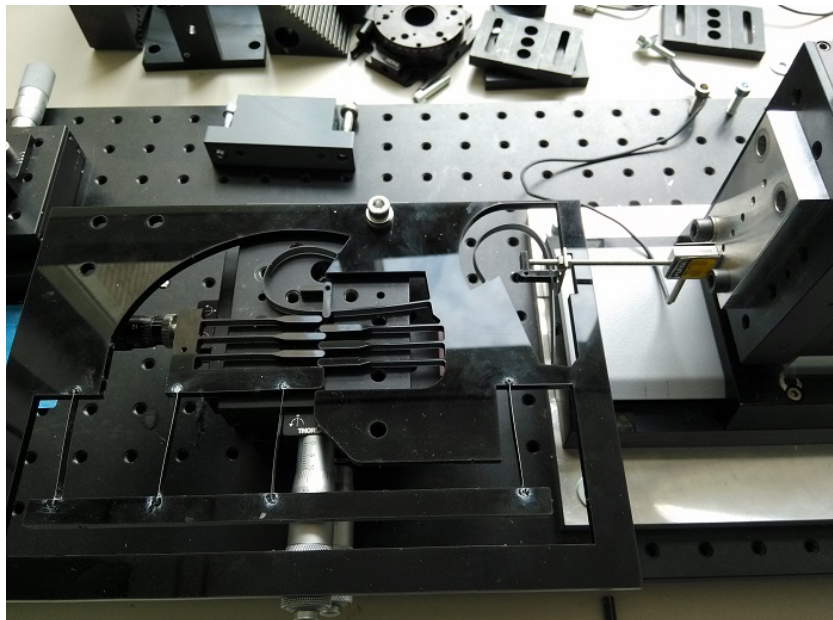
Figure 10.3: Measurement setup for large scale prototype

10.3. RESULTS

Due to very poor laser cutting specifications the final prototype shows large differences w.r.t. the intended dimensions. In general all relevant elements are too small/thin and a laser focus offset results in a different

in-plane thickness with a difference between top and bottom varying between 0.2 and 0.3mm. To improve the comparison measurement results are compared with the measured dimensions instead of the design dimensions.

SPRING

Two spring are incorporated in the prototype. Spring 1 is positioned above the cantilevers with thickness $t \approx 1.03mm$. Spring 2 is a separate spring only used for measuring purposes with $t \approx 0.95mm$. A comparison between the test data and FEM simulation is given in fig. 10.4 and fig. 10.5.
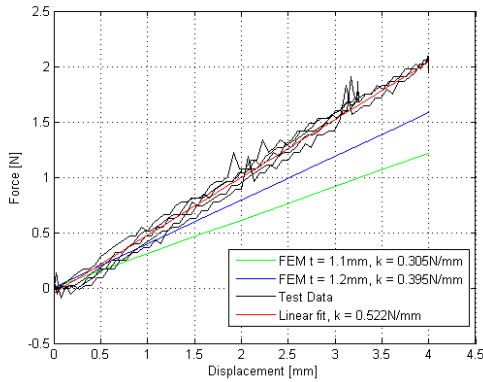
Figure 10.4: Measurement and FEM results spring 1
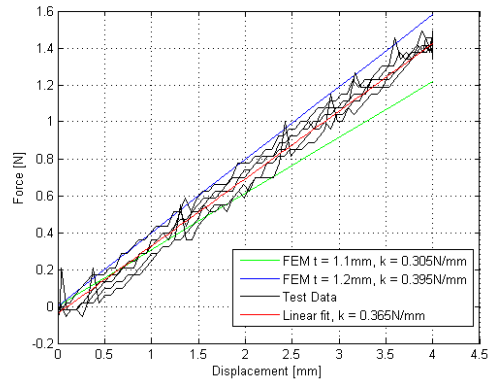
Figure 10.5: Measurement and FEM results spring 2

It can be seen that both springs show a very linear behavior as expected from the model. However a large discrepancy is found in the absolute stiffness values. Reasons for this offset could be: 1) the in-plane thickness variation which could have a large influence in the overall stiffness (power of 3), 2) a heat effect on the material properties, this will especially influence very thin elements such as the spring or 3) different material properties in the original material.

LOWER SHUTTLE

The lower shuttle is the lower moving element in the prototype used for the straight guidance. It is suspended by two, 40mm flexures with stiffness $k = 0.014N/m$. Since these flexures are placed in parallel the measured stiffness should be equal to $2 \cdot k$.
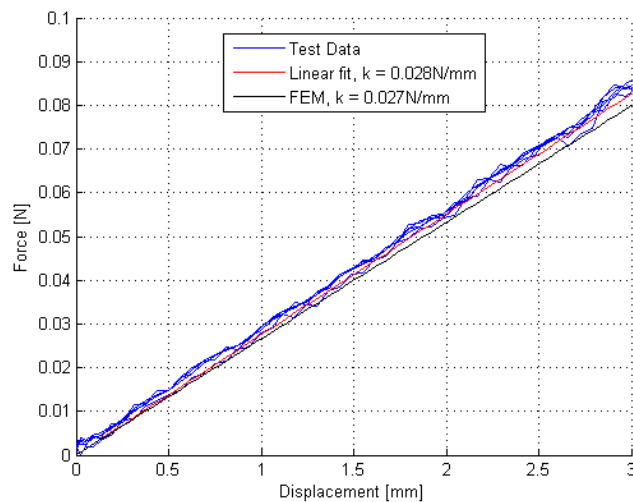
Figure 10.6: Measurement and FEM results lower shuttle

Figure 10.6 shows that the prototype acts as modeled.

Upper Shuttle

Similar two the lower shuttle, the upper shuttle(attached to the left set of cantilevers) should show a stiffness of $2 \cdot k$ which is the case as shown in fig. 10.7.
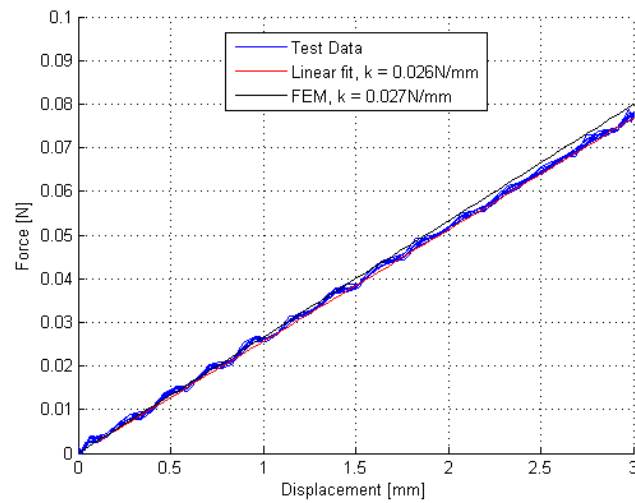
Figure 10.7: Measurement and FEM results upper shuttle

Locking behavior

Finally the overall locking behavior is tested by pushing the upper shuttle (fig. 10.8).
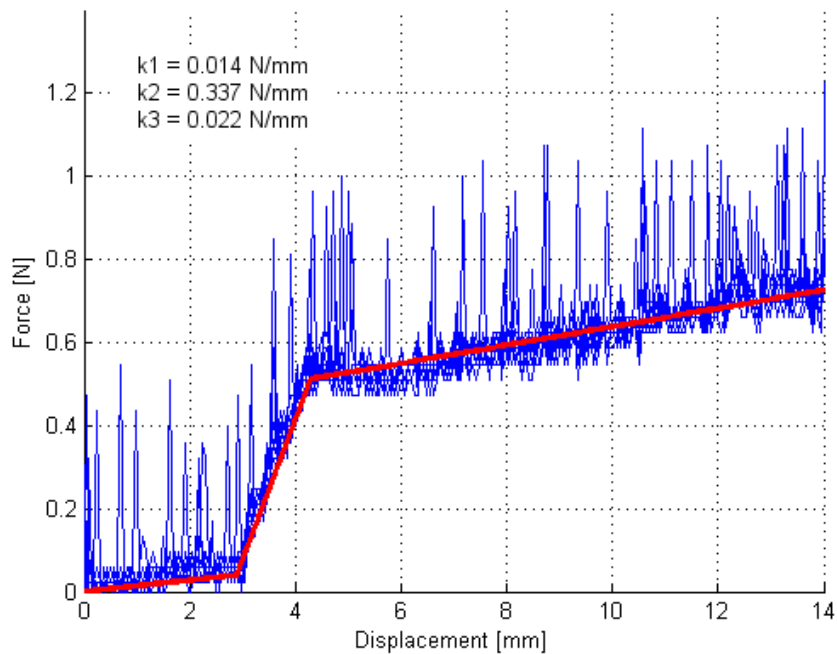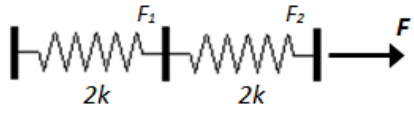
Figure 10.8: Measurement results of the overall locking design

Although the force measurement data is noisy, 3 different sections of the locking stroke can be divided as also quantified by the linear fits:

1. There is no contact yet and the only force required is to overcome the stiffness of the suspension. This

stiffness is composed of two sets of parallel spring in series. The combined stiffness should therefore be $k_{total} = k$ (fig. 10.9).

$$F_1 = F_2 = F$$

$$U = \frac{F^2}{2k}$$

$$U_1 = U_2 = \frac{\frac{F_1^2}{2}}{4k_{\frac{1}{2}}}$$

$$U_{tot} = \frac{F^2}{4}\left(\frac{1}{k_1} + \frac{1}{k_2}\right), \quad k_1 = k_2$$

$$U_{tot} = \frac{F^2}{4}\left(\frac{2}{k}\right) = \frac{F^2}{2}\left(\frac{1}{k}\right)$$

$$k_{tot} = k$$

Figure 10.9: Calculation of overall suspension stiffness

2. The upper cantilever hits the spring which is being preloaded. Ideally the cantilevers should align perfectly and only the spring is preloaded. However the cantilevers do not fit each other perfectly and do not align. Therefore first some bending occurs in the cantilevers to overcome the gap between them. As a result 1mm of the preloading is 'lost'.

3. Once the spring is fully preloaded the locking force should remain constant and only the suspension stiffness should be measured. The results show that additional stiffness is measured besides the suspension stiffness. This can be explained by the misalignment of the cantilevers: instead of a straight sliding surface the beams are under a small angle w.r.t. each other. During displacement the surfaces are forced to align horizontally resulting in more bending in the cantilevers; moreover, additional preload is added to the spring.

The straight guidance used in this prototype removes the DOF in y-direction in neutral position and delivers a high stiffness in y-direction when the shuttles are displaced. When the cantilevers do not align perfectly this suspension greatly reduces the locking force of the device since all locking force is stored in the suspension instead of in a normal force on the fixed world.

10.4. CONCLUSION

The large scale prototype shows that the general principle works. Due to the very poor production resolution no results can be drawn w.r.t. the total locking force. The sensitivity to production tolerances should be taken into account for a real scale prototype, especially for the cantilever beam dimensioning and alignment. Also the DOF limitations of the suspension, which were not the directly within scope of this project, should be considered.

11

MEMS LOCKING PROTOTYPE

A 1:1 scale prototype is designed, produced and evaluated for its locking behavior. The prototype is produced in a $525\mu m$ silicon wafer(table 11.1) via deep reactive ion etching (DRIE). As also mentioned in Chapter 9 there is a minimum required separation distance between different elements in the design and a minimum curve-radius to prevent over-etching and other flaws on these elements.

11.1. DESIGN

The design(fig. 11.1) is build-up around the optimized spring which is discussed in Chapter 9. Other elements are discussed below. The DRIE process used is known to over-etch elements with $5\mu m$ per edge. Therefore all critical edges are over-dimensioned with this exact amount.

1: SPRING CONTACT AND RELEASE ELEMENT

A small lump is added below the spring which is the contact point between the spring and top comb finger. The length is determined such that the minimum spacing between the spring and top cantilever is satisfied. Since this contact point has an arm w.r.t. the spring a small moment will act on the spring when it is pre-stressed. However the rotational stiffness of the spring is so strong this effect is negligible. Above the spring an release lever is added to unlock the device if required. This element should not be necessary since the locking device should be able to function only via a x-actuation but is added for testing purposes. Also note the bump stop above the release lever to prevent extreme displacements of the spring.

2: COMB FINGERS

Comb fingers are added until the desired locking force is acquired. Lowest expected friction coefficient $\mu = 0.2$, the required locking force $F_{lock} = 0.1N$ and the spring can provide a $F_{spring} = 0.069N$. Therefore the required amount of contact points is $\frac{0.1}{0.069 \cdot 0.2} = 7.25 \Longrightarrow 8$, resulting in a minimum locking force of $8 \cdot 0.069 \cdot 0.2 = 110mN$ assuming $\mu_{min} = 0.2$.

The orientation of the comb fingers has flipped compared to the large scale prototype. As a result all comb fingers can be produced in the same x-layer saving space in this direction. This was required due to limited space on the mask used to produce this prototype. Trade of is a higher prototype since a thick comb finger tip end is required to ensure the minimum element separation. Note that the comb fingers will be loaded in compression, instead of tension, once the mechanism is locked. A worst case scenario for a single comb finger is derived as:

Table 11.1: Silicon material properties

E_x	169 GPa	E_y	169 GPa	E_z	130 GPa
v_{xy}	0.064	v_{yz}	0.36	v_{xz}	0.28
G_{xy}	50.9 GPa	G_{yz}	79.6 GPa	G_{xz}	79.6 GPa
ρ	2330 kg/m^3				
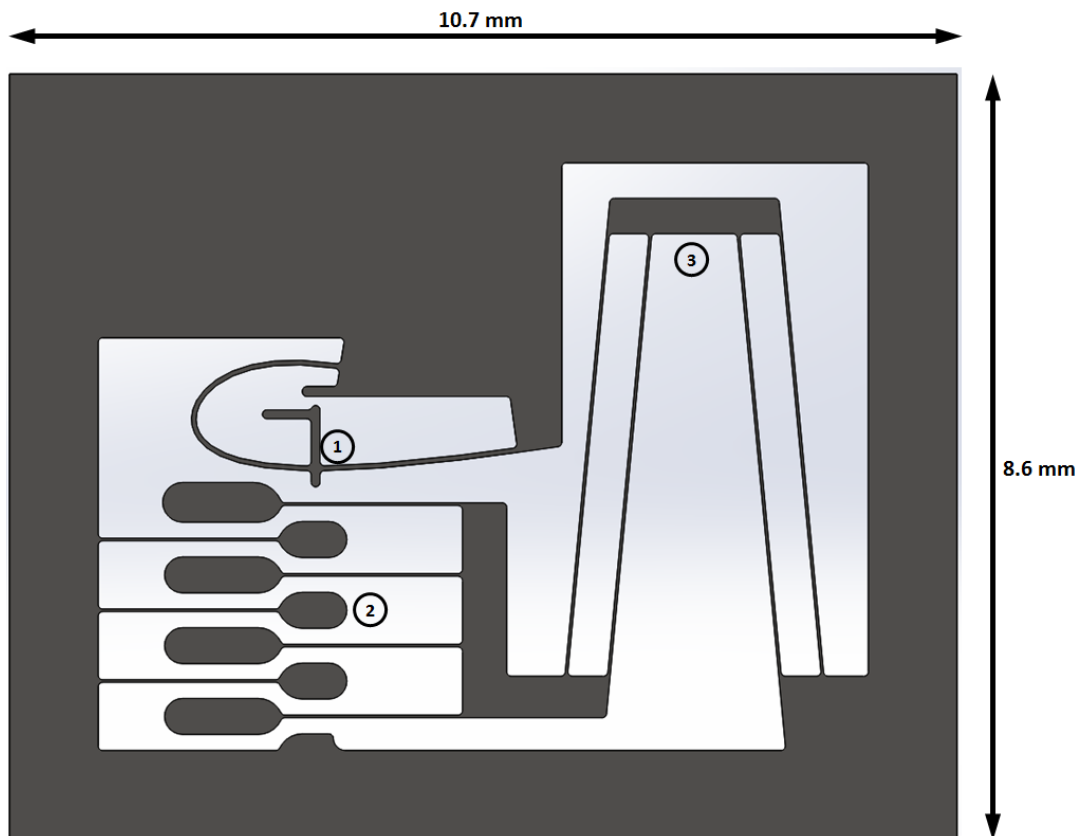
Figure 11.1: CAD design of the MEMS scale locking prototype consisting of a spring (1), comb fingers to increase the amount of friction points (2), and a suspension (3)

- The total load $F_{max} = 100mN$ is ideally distributed over 4 beams resulting in $F_{beam} = 25mN$. Worst case scenario is all load on a single comb finger resulting in $\mathbf{F_{beam,max}} = \mathbf{100mN}$.

- The cantilever beams are designed to align without any deflection. When there is a small production error the beam will not only be loaded in perfect compression but also in bending. The production error is known to be $2\mu m$ per edge resulting in a maximum misalignment error $\delta_{\mathbf{y}} = \mathbf{4\mu m}$ causing a bending moment on the comb finger.

A FEA is performed to check whether the comb fingers do not fail as a result of this combined compression and bending load. A comb finger is fully clamped at the left beam end and the worst case scenario is applied at the right beam end.

The FEM results(fig. 11.2) show that for a worst case scenario the maximum beam stress $\sigma_{beam,max} = 13.7MPa << 200MPa$. Therefore this beam orientation does not violate the stress constraint. A second error resulting in bending of the comb finger could be due to a drift or offset in y-direction of the shuttle resulting in additional bending for the right set of comb fingers. FEA shows that an y-offset of this shuttle up to at least $\approx 185\mu m$ is allowed (fig. 11.3).

Undesired bending of the comb fingers will also result in a reaction force due to this bending. The stiffness of a single comb finger is determined using FEM at $k_{finger} = 0.022N/mm$. An additional force equal to $F_{finger} = \mu \cdot k_{finger} \cdot \delta_{y,finger}$ per comb finger will be contribute to the overall locking force since it acts as a parallel spring.

3: SUSPENSION

Finally a suspension is attached to the right set of comb fingers to prevent this part from falling out the structure after fabrication and provide a horizontal motion. The suspension is connected via an intermediate body. This type of suspension doubles the effective length of the suspension resulting in a lower stiffness meaning less influence on the locking measurement. Second advantage of an intermediate body is cancellation of the parasitic motion in y-direction compared to a non-intermediate body suspension.
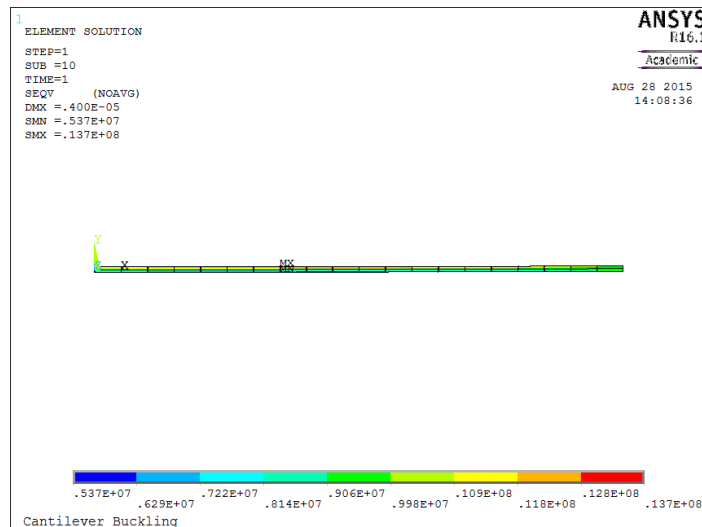
Figure 11.2: FEM analysis for cantilever beam in worst case load scenario
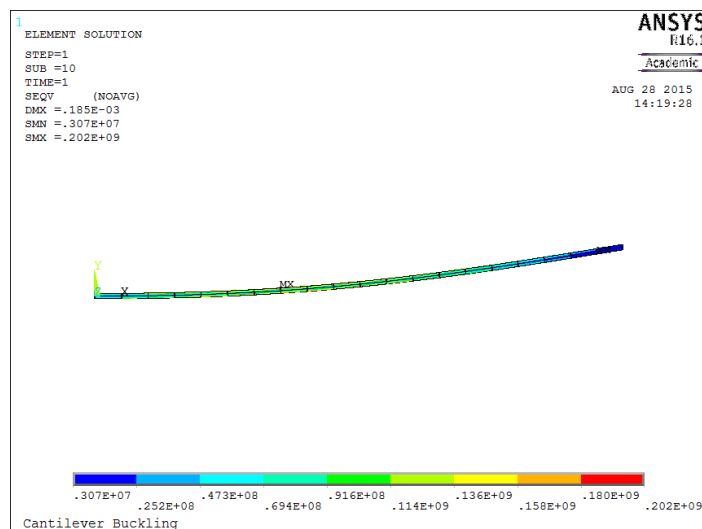
Figure 11.3: FEM analysis for cantilever beam with maximum y-displacement

The suspension is also modeled (Appendix A.3 and fig. 11.4) to determine the force deflection character-istics of the suspension combined with the cantilever beams (fig. 11.4) for the required range of motion with a maximum up to 1.5mm.

The FEA shows a very small rotation in the suspension output to the comb finger carrier. The effect of this rotation on the overall stiffness is analyzed and proven to be negligible (« 1%). Reason for this insensitivity is the high length and low thickness of the cantilever beams which are therefore capable of 'absorbing' the resulting offset.

Now all spring and suspension forces are calculated the hysteresis op loop of the system can be deter-mined assuming $\mu_{min} = 0.2$ (fig. 11.6). Characteristic points in the loop are explained below:

A. After production the locking mechanism is in an undeformed and therefore relaxed state.

B. During the initial movement only the suspension is actuated. Between A and B only the suspension stiffness will be felt.

C. Contact between the upper comb finger and spring cause the spring to prestress.
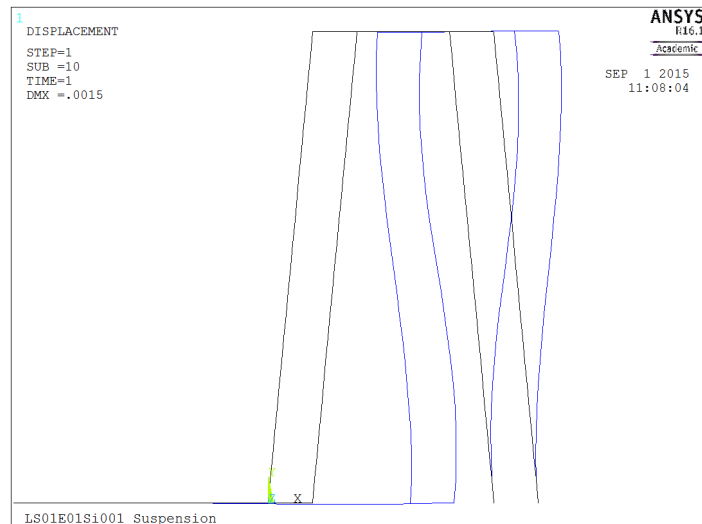
Figure 11.4: FEA prototype suspension in maximum deflected position
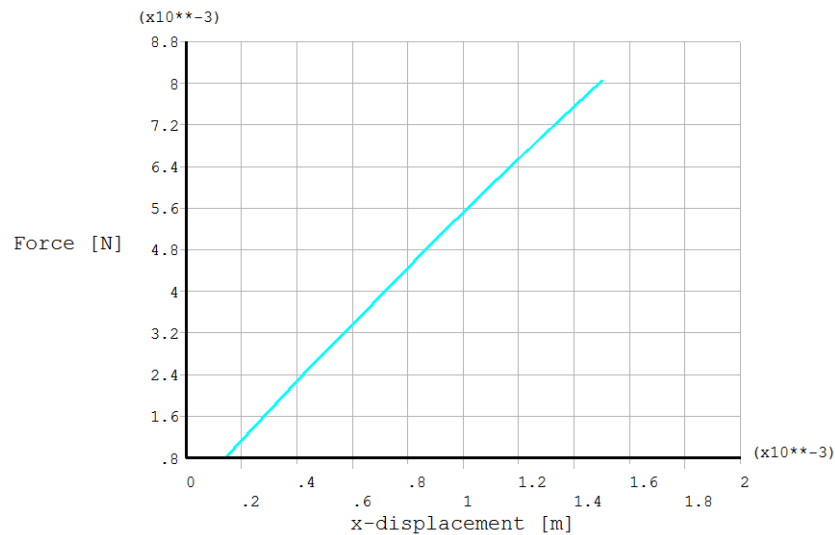
Figure 11.5: Prototype suspension force deflection characteristic

D. After prestressing the spring force and therefore friction force is constant. Only required additional force is to move the suspension until the end of the locking range is reached.

E. For reverse tuning the application force needs to change direction, however since the suspension is pushing in this direction the required force will be lower compared to the forward movement.

F. As the suspension is moving back to its natural position the required pushing force increasing causing again a positive stiffness between E and F.

G. Once the shuttle is moved beyond the starting point of the locking range (C and/or F), the spring helps pushing in the negative x-direction causing a negative stiffness and the zero force crossing

The hysteresis loop clearly shows the area with contact (B-C-D-E-F-B) where friction causes energy loss. For a higher friction coefficient the hysteresis loop will maintain its shape however line C-D will shift up and line E-F down.
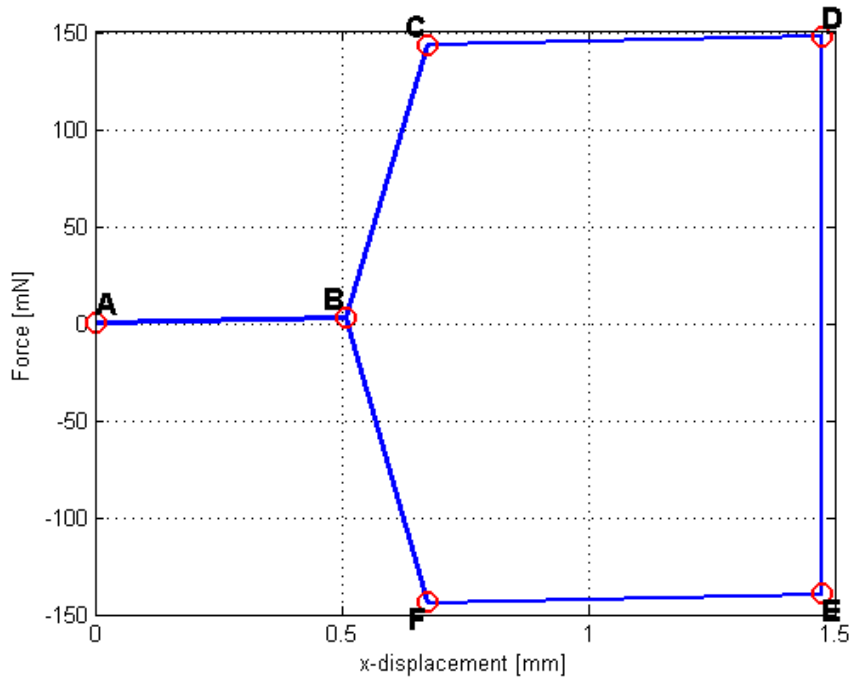
Figure 11.6: Locking Mechanism Hysteresis loop

11.2. TESTING

Prototype dimensions are measured via SEM imaging. Stiffness characteristics of the prototype are measured using a *Futek LSB200 20gr Miniature S-Beam Load Cell* in combination with a *Physik Instrumente (PI) M-406.2DG Precision Linear Stage* to provide a linear movement. A needle is connected to this sensor to actuate the MEMS prototype. The prototype is mounted on a support piece to enable mounting on the force-deflection setup (fig. 11.7). Alignment and lighting during the measurement is accomplished via a two *Dino-Lite USB Microscopes*(fig. 11.8).
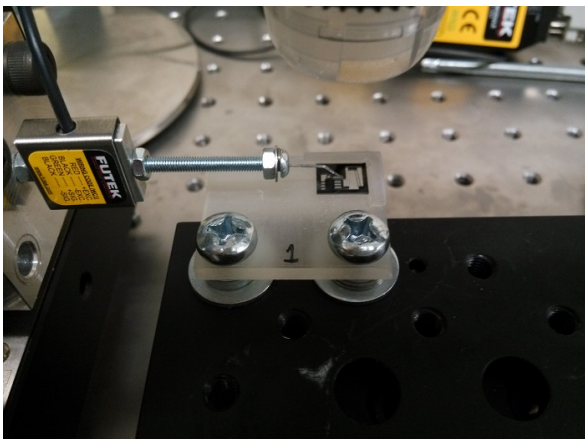
Figure 11.7: Prototype mounted to setup via support piece
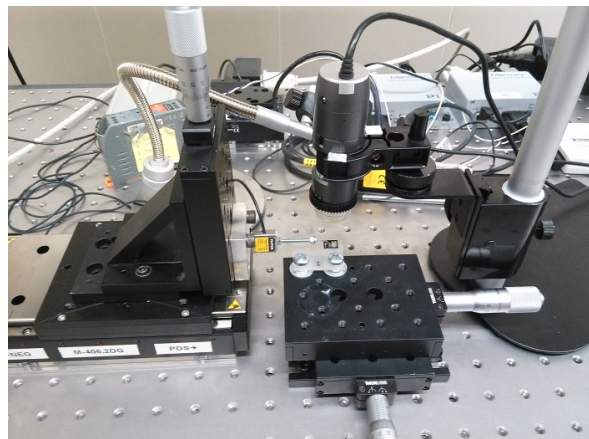
Figure 11.8: Overview of the full test setup

Due to the possibility of the prototypes breaking during SEM imaging it is decided to do force measurements on the MEMS devices before imaging. Two prototypes are produced in the same wafer with matching alignment and are therefore assumed to be identical. Prototype 1 (LS01E1Si001) will be used for testing while prototype 2 (LS01E1Si002) will be unused to see and measure potential wear effects.

To prevent rotation of the shuttle it is actuated in its center.

The measurement needle is not rigid and will therefore influence the results. To correct the measurements for the stiffness of the needle its stiffness is measured.
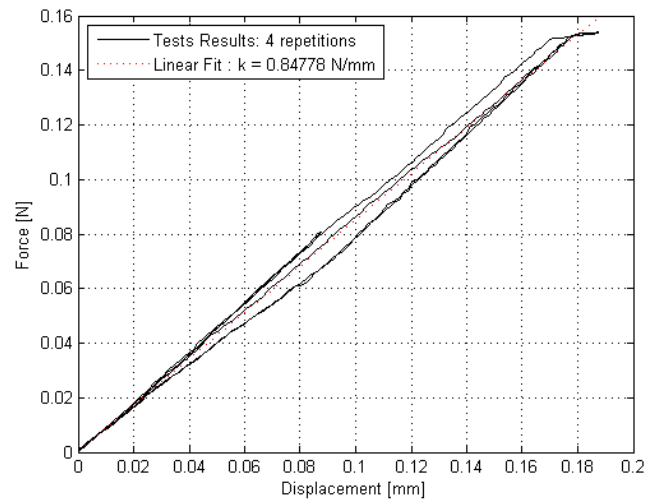
Figure 11.9: Force deflection characteristics of the measurement needle

Figure 11.9 shows that the measurement needle acts as a linear spring with $k_{needle} = 0.8478 N/mm$. Since this stiffness acts in series with the stiffness of interest, the measured stiffness can be corrected to determine the stiffness of the desired components as in fig. 10.9 while $k_1 \neq k_2$ resulting in eq. (11.1).

$$k_{component} = \left(\frac{1}{k_{measured}} - \frac{1}{k_{needle}} \right)^{-1} \tag{11.1}$$

11.3. RESULTS
Two prototypes coded as LS01E1Si001 and LS01E1Si002 are produced(fig. 11.10 and fig. 11.11).
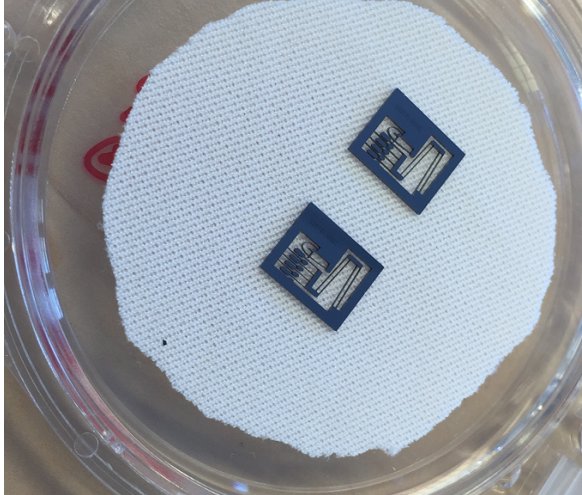
Figure 11.10: LS01E1Si001 and LS01E1Si002 after a DRIE manufacturing process
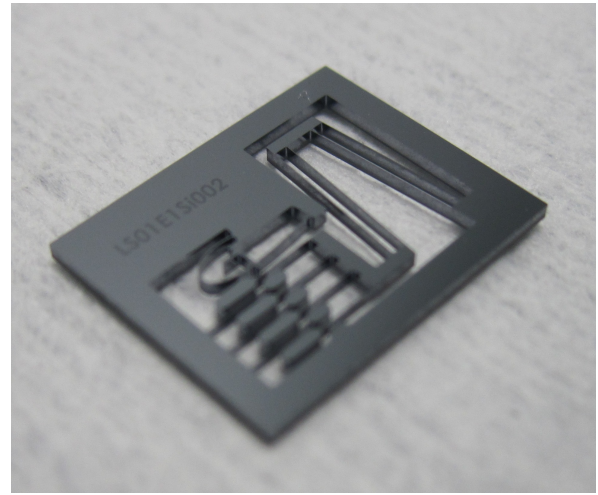
Figure 11.11: Close up of LS01E1Si002

11.3.1. DIMENSIONS
LS01E1Si002 is used for dimensioning of the MEMS prototype. Due to time limitations on the SEM not all dimensions on all individual members can be measured. A small selection of relevant dimensions is measured

and others are derived from this set of dimensions. LS01E1Si001 is only evaluated for wear effects due to this time limitation.

Measurement results of LS01E1Si002 are shown in fig. 11.12 to fig. 11.15.
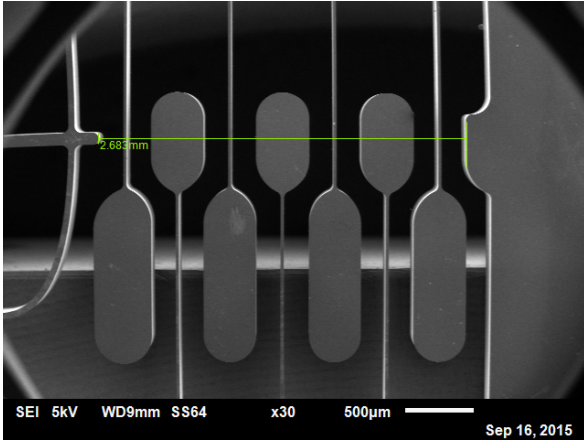
Figure 11.12: SEM image of spring beam, comb fingers and base
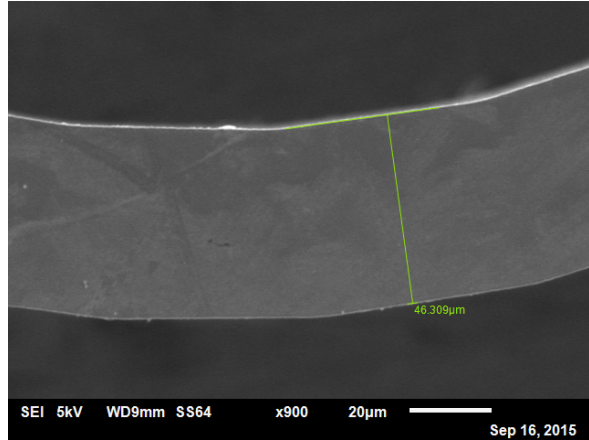
Figure 11.13: SEM of spring beam
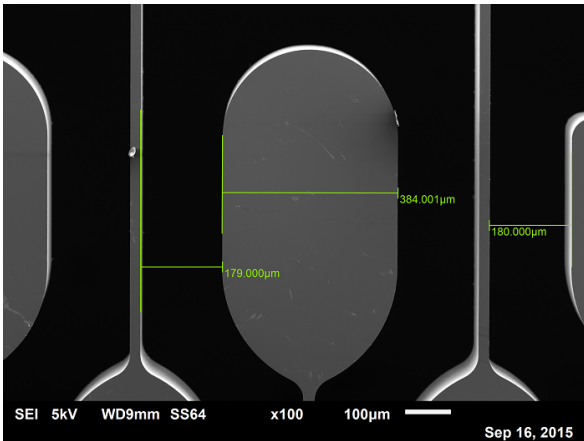
Figure 11.14: SEM image of comb finger tips, beams and spacing
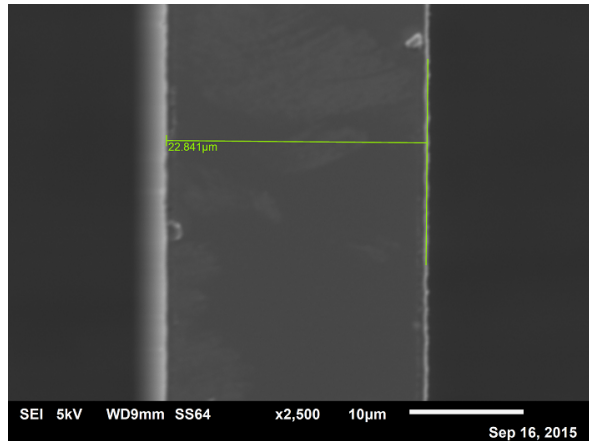
Figure 11.15: SEM of comb finger beam

It can be seen that the final dimension show some deviation from the intended design. Critical elements having a large effect on the locking behavior are the spring dimensions(stiffness), the total prestressing distance of the spring and alignment of the comb fingers.

COMB FINGERS

To ensure perfect alignment of the comb fingers(fig. 11.14) the half-width of a comb finger tip should be equal to the half-width of a comb finger beam + gap between comb finger beam and next comb finger tip. For the given data this alignment can be determined using gap distance $179\mu m$ (eq. (11.2)) or $180\mu m$ (eq. (11.3)).

$$\frac{384.00}{2} - \left(\frac{22.84}{2} + 179\right) = 1.58\mu m \neq 0 \tag{11.2}$$

$$\frac{384.00}{2} - \left(\frac{22.84}{2} + 180\right) = 0.58\mu m \neq 0 \tag{11.3}$$

These misalignment errors are averaged resulting in a misalignment error of $1.08\mu m$ per set of aligning comb finger tips resulting in an additional prestress displacement on the spring of $8 \cdot 1.08 = 8.64\mu m$. This misalignment is also visible for the upper comb finger in the video footage during a test which shows a secondary movement when the comb finger tips align.

The total thickness of all comb finger tips is found to be $6 \cdot 384 + 420 = 2724 \mu m$. Using fig. 11.12 it can be found that the total spring prestress displacement $= 2724 - 2683 = 41 \mu m$ instead of the intended $50 \mu m$.

Figure 11.13 shows the spring beam thickness of $46.31 \mu m$ which is larger than $44 \mu m$ it is designed for. Also note that the spring shape does not show a smooth curve but a discretized curve via straight sections.

SUSPENSION
Due to the limited range of the SEM machine no measurement could be made for the suspension thickness and length. Since the suspension is designed with the same thickness as the comb finger beams it is assumed the dimensions after fabrication are also the same.

11.3.2. WEAR
During testing signs of abrasive wear were noticed in the form of small chips of material appearing on top of the upper comb finger tip. These particles are also found during SEM imaging(fig. 11.16 and fig. 11.17). Wear shown is the result of 8 full locking cycles.
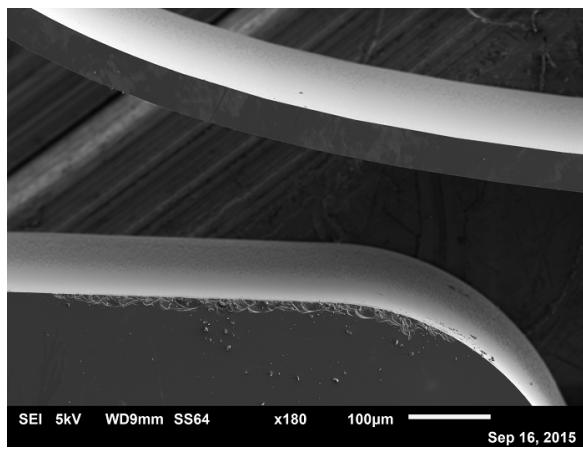
Figure 11.16: SEM image of wear particles on the LS01E1Si001 upper comb finger tip
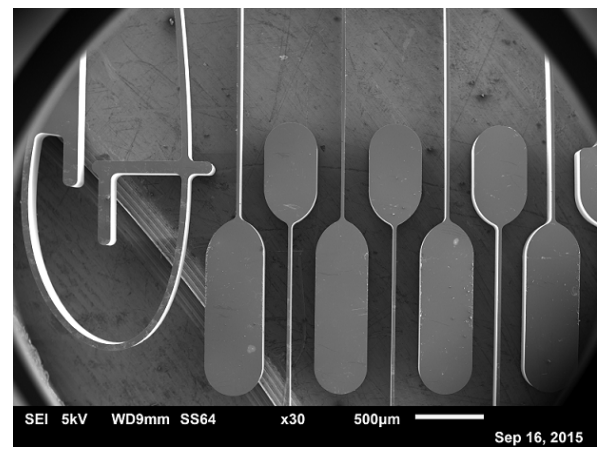
Figure 11.17: SEM image of wear particles on LS01E1Si001

Signs of abrasive wear are also visible on the contact tip of the spring (fig. 11.18 and fig. 11.19).
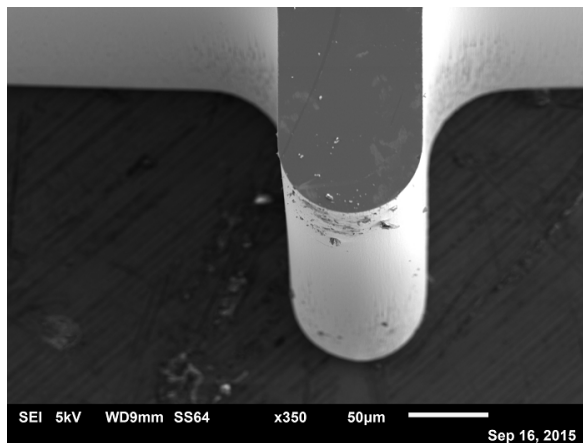
Figure 11.18: SEM image of wear on the LS01E1Si001 spring contact tip above the prototype mid-plane
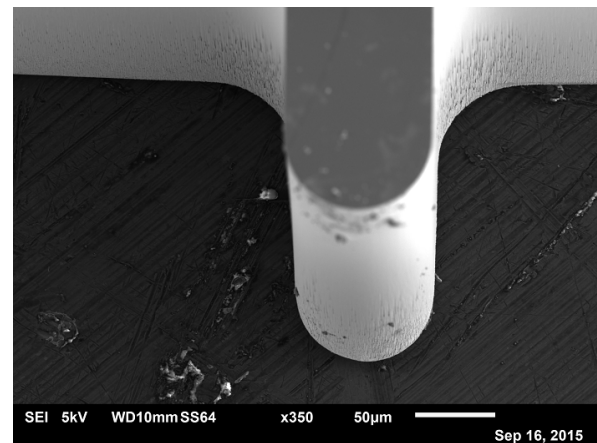
Figure 11.19: SEM image of wear on the LS01E1Si001 spring contact tip below the prototype mid-plane

All pictures show that the majority of the wear is encounter around the upper edge of the device. This can be explained by the in-plane trapezoidal shape of the MEMS prototype which is a known property of the manufacturing process. As a result all contact will occur in a small area increasing the local stress resulting in higher wear. Since the contact force remains equal the locking force of the system will not be affected.

11.3.3. FORCE-DEFLECTION CHARACTERISTICS

Presented measurements are performed on prototype LS01E1Si001 and results are compared with a FEM. Dimensions used in the FEM are modified to the SEM measured dimensions instead of the original intended dimensions. Both the measured stiffness as the stiffness corrected for the needle stiffness according to eq. (11.1) are plotted.

LOCKING SPRING

The spring stiffness is measured by pushing the, assumed rigid, release element in y-direction (fig. 11.20). Results of 20 back and forth movements are plotted in fig. 11.21.
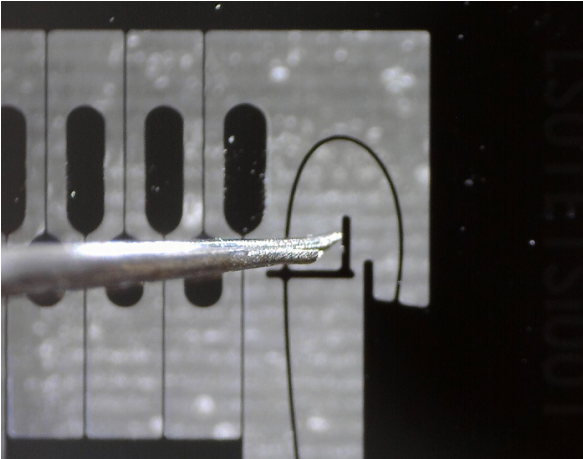
Figure 11.20: Measurement setup of spring testing
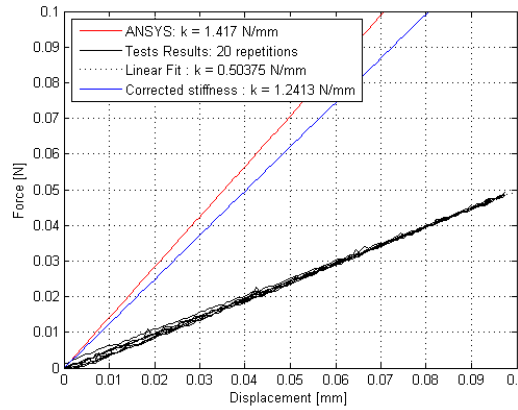
Figure 11.21: Force deflection characteristics of the locking spring in y-direction

The corrected stiffness is found to be 14% lower than the FEA. Variables that could account for this difference are varying material properties, a different spring geometry/length which could not be measured using the SEM or the effect of the discretized curve as seen in fig. 11.13.

Knowing the spring stiffness and prestress displacement, the total spring force can be calculated as $F_{spring} = 1.2413 \cdot 41e^{-3} = 0.0508N$ which is lower than the intended $0.069N$. Although the spring force is lower, the locking device still functions, only with a lower maximum locking force. Assuming $\mu = 0.2$ this would mean $F_{lock} = 8 \cdot 0.0508 \cdot 0.2 = 81mN$.

To confirm the springs performance, its stiffness is also measured in x-direction.
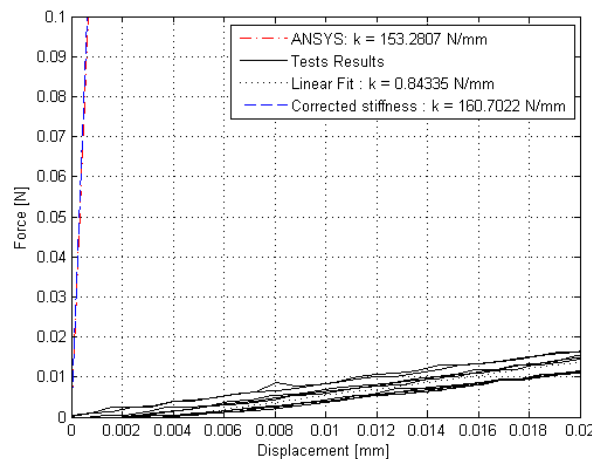
Figure 11.22: Force deflection characteristics of the locking spring in x-direction

Figure 11.22 shows that the corrected results show an offset < 5% compared to the FEM.

SUSPENSION

The suspension stiffness is measured by pushing the shuttle (fig. 11.23). Results of 20 back and forth movements are plotted in fig. 11.24.
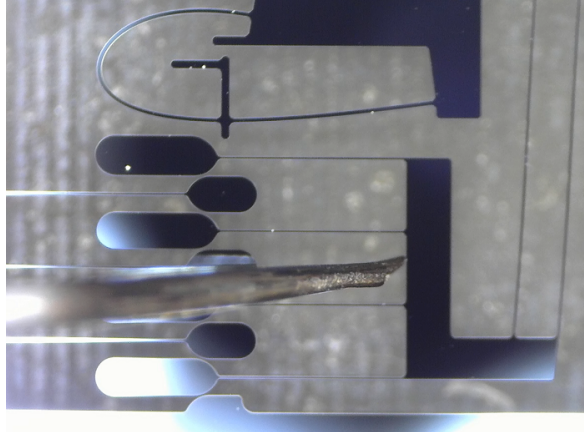
Figure 11.23: Measurement setup of suspenson testing
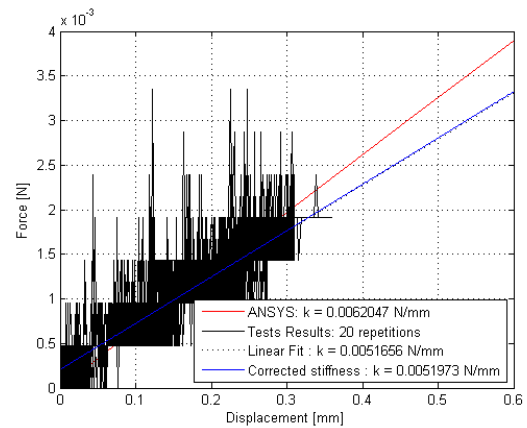
Figure 11.24: Force deflection characteristics of the suspension

The corrected stiffness is found to be 17% lower than the FEA. Variables that could account for this difference are again varying material properties or different suspension dimension since these could not be measured during SEM imaging. Note that a variation in suspension stiffness does not affect the locking system, its value is only required to quantify the total locking capabilities of the system.

LOCKING BEHAVIOR

The force deflection characteristics of a full locking cycle is measured by pushing the shuttle but now for a stroke of $\approx 1.3mm$ (fig. 11.25).
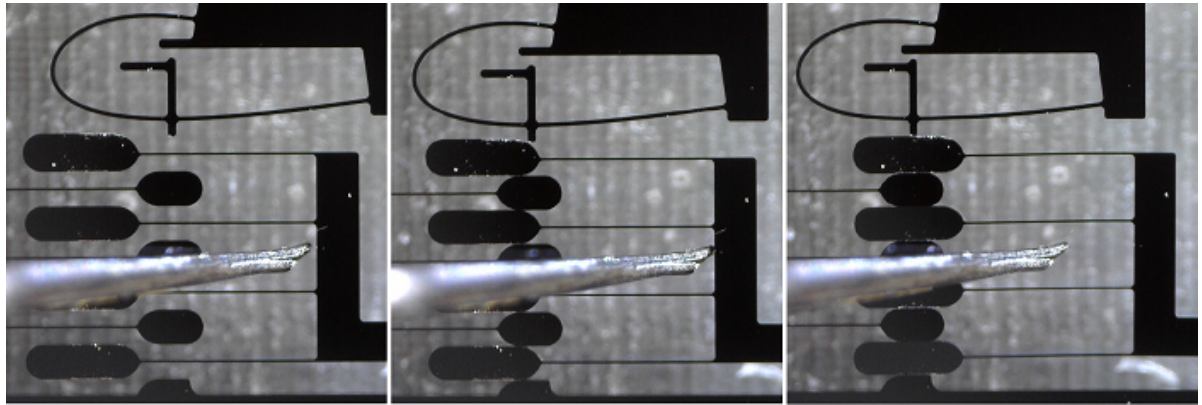
Figure 11.25: Locking movement visualized in 3 steps

First only the suspension is deformed until contact between the upper comb finger and spring contact tip occurs (A-B). In the next phase the spring is prestressed (B-C) and finally the constant locking force is obtained where again only the suspension is deformed (C-D). After one iteration the locking system is unlocked and the measurement is repeated.

Figure 11.26 shows that the measurement is repeatable for consecutive measurements. These measurements are fitted and corrected for the measurement needle stiffness resulting in the real locking behavior. The slope A-B and C-D correspond to the suspension stiffness as measured before. The metric of interest is the force difference between B-C representing the total locking force $F_{lock} = 147mN$.

The expected locking force based on $\mu = 0.2$ was $F_{lock,expected} = 81mN$. The measured $F_{lock} = 147mN > 81mN$ so it can be concluded that this locking mechanism does provide the minimum locking force. Provided
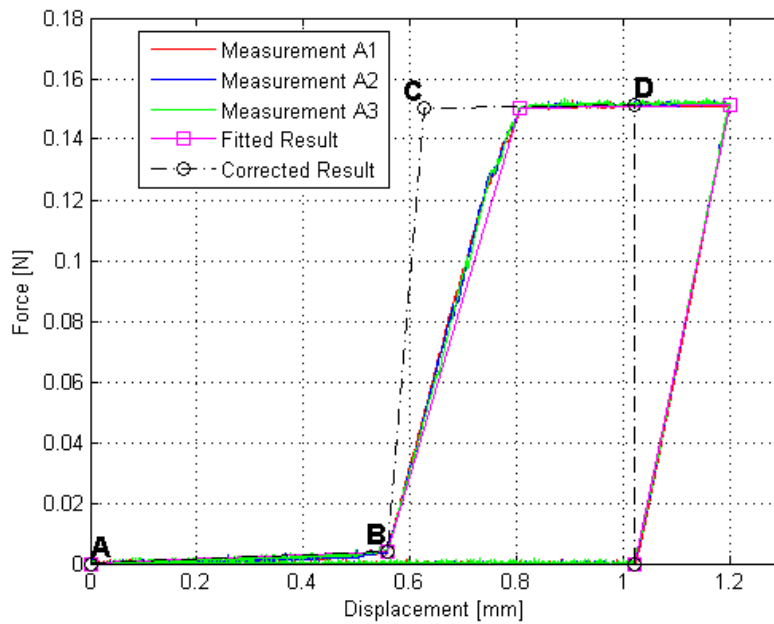
Figure 11.26: Force deflection characteristics of one forward locking movement

that the expected locking force is correct, the friction coefficient during this measurement should be $\mu = \frac{0.147}{8 \cdot 0.0508} = 0.36$.

Static vs. Dynamic Friction Coefficient During the measurement, actuated at $0.1mm/s$, it is possible the dynamic friction coefficient μ_d is measured instead of the static friction coefficient μ_s which is required for this system. Since the static friction coefficient is higher than the dynamic friction coefficient this will not result in a decrease in locking force but will only increase it. This is verified by repeating the previous test but now using steps of $0.1mm$ for a full stroke with a small pause between every step.

Figure 11.27 shows small spikes at the end of the prestressing region. These spikes indicate a difference between μ_d and μ_s and some stick slip behavior, the resolution of the sensor however makes it difficult to quantify this. These spikes are not/barely visible in the region of interest being the locking stroke C-D. For this measurement in the region of interest it is therefore assumed $\mu_d \approx \mu_s$.

Unlocking and/or re-tuning After the system is tuned using a forward movement it is also possible to readjust the system by 1) unlocking the system by lifting the spring(fig. 11.20) allowing the suspension and therefore comb fingers to return to their original position and start the forward procedure again or 2) reversing the actuation direction resulting in a backward movement of the shuttle while maintaining the locked condition.

1. Unlocking the system by lifting the spring is already shown but requires both an x- and y-translation to deliver the tuning and unlocking movement.

2. By reversing the actuation direction only an x-translation is required to initially tune and later readjust the system (fig. 11.28).

   Figure 11.29 shows the hysteresis loop by combining a forward and backward movement. Note the unequal measured stiffness for the the forward and backward in D-E. Both should be equal to the measurement needle stiffness but the backward movement also caused a small addition rotation on the shuttle which is seen in the result of a changed stiffness.

   The shape of the fitted result can also be compared with fig. 11.6 showing great similarities. The final part of the backward movement should show negative stiffness but is not measured since the sensor could only measure pressure.
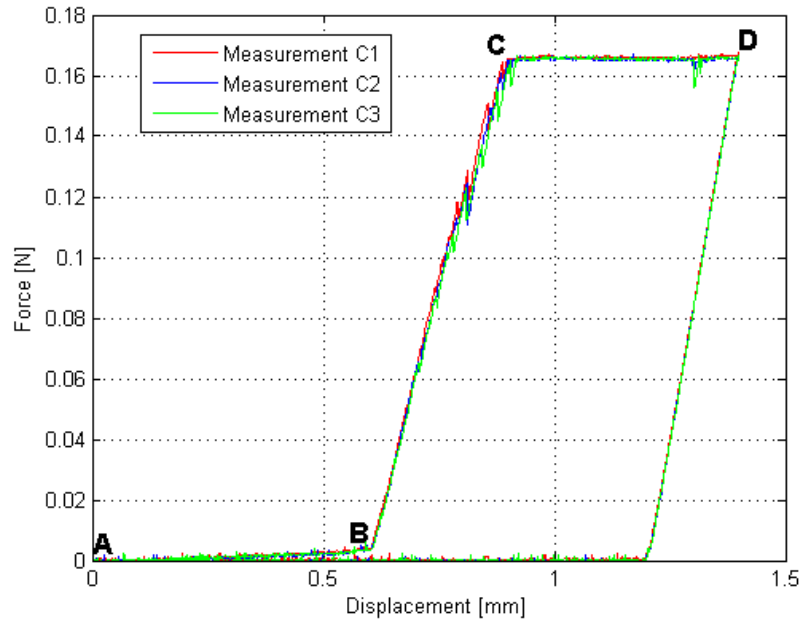
Figure 11.27: Force deflection characteristics of one forward locking movement with 0.1mm steps to evaluated the static vs. dynamic friction coefficient
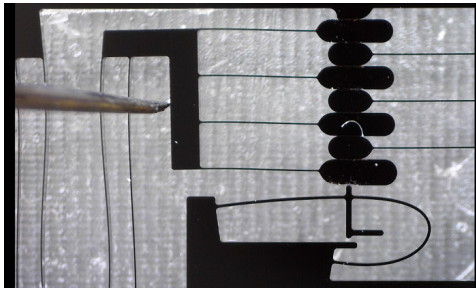
Figure 11.28: Measurement setup of reversed movement tuning
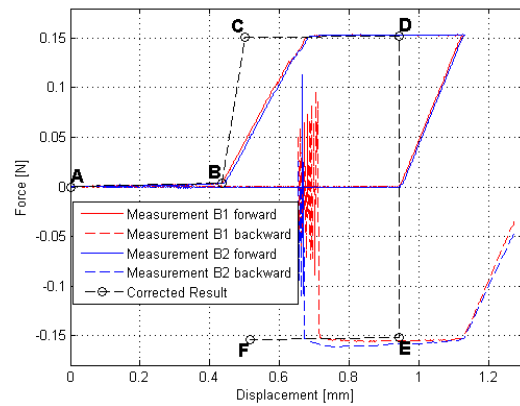
Figure 11.29: Force deflection characteristics of a forward and backward movement

11.4. NORMAL FORCE MEASUREMENT

The estimated spring force is used to calculate the total normal force on the comb fingers and therefore locking force which is correct if comb finger alignment is correct and the prestress displacement is correct. However this is not completely true for this prototype; the prestress displacement is based on a measurement of the gap between the spring contact tip and ground tip and the thickness of the comb finger tips.

- The measurements using the SEM are not 100% accurate resulting in a measurement error.

- Only one comb finger tip is measured and assumed representative for the others. Most likely these are not exactly the same.

- Measurements are done for only one side of the prototype while it is known to be in-plane trapezoidal. Depending on the actual contact point between the comb fingers this will result in a different distance compared to the measurement.

- Video footage showed that the comb fingers did not align perfectly. During the prestress x-movement

this will cause bending in the comb fingers which will act as an additional springs parallel to the main spring increasing the normal force. The combined stiffness of all comb fingers is equal to $0.02 \cdot 8 = 0.16 N/mm$ (main spring = $1.24 N/mm$). The measurement based estimation of the maximum deflection of the comb fingers is approximated at $8 \mu m$ (main spring = $41 \mu m$). The maximum contribution on the normal force is therefore determined 2.5% which is considered very small.

Above mentioned errors cause the calculated spring force, based on the measured prestress displacement, to be a wrong estimation of the normal force. This will not affect the locking system in general but does influence the calculated friction coefficient. Part of the required locking force is delivered by the comb finger springs so the actual normal will be larger than anticipated causing an overestimation of the friction force which should actually be calculated according to eq. (11.4).

$$\mu = \frac{F_C - F_B}{\sum\limits_{i=1}^{8} n_\mu \cdot (F_{spring,i} + F_{combfinger,i})} \tag{11.4}$$

with F_B and F_C the force values of the matching points in fig. 11.26.

An attempt is made to measure the real normal force by y-actuation of the lowest comb finger in locked state and measuring the initial force. Unfortunately the limited space at this point made this impossible. Attempts using the comb fingers above failed because the suspension and shuttle started rotating, instead of a y-translation, before the actual normal force on these points could be measured. Since the influence of the comb fingers on the normal force is calculated to be small (2.5%) it is decided to measure the normal force on the main spring.

Measurement showed an initial force of $0.0518 N$. The normal force based on the measured prestress displacement showed a locking force of $0.0508 N$ which is 2% lower. As mentioned before this discrepancy can be explained by a measurement error of the prestress displacement and deformation of the comb fingers.

11.5. FRICTION COEFFICIENT

Using the corrected normal force the friction coefficient can now be corrected to $\mu = \frac{0.147}{8 \cdot 0.0518} = 0.35$.

Multiple locking cycles are tested on LS01E1SI001 at different instances. Different locking forces are measured which are most likely caused by a varying friction coefficient. Locking forces between $115 mN$ and $159 mN$ are measured corresponding with friction coefficients of 0.27 and 0.38.

11.6. SHOCK RESISTANCE

The current design is subjected to a maximum $F_{internal} = 7 mN$. Given a locking force $F_{lock} = 147 mN$ this leaves $F_{external} = 140 mN$ to absorb shocks. The suspended mass in current prototype consists of a set of comb fingers, shuttle, suspension and intermediate body with a total mass $m = 6.599e^{-6} kg$. Using $F = m \cdot a$ and $a = 9.81 m/s^2$ it is found that shocks up to $2161 G$ are allowed on this locking mechanism.

11.7. CONCLUSION

The MEMS locking system showed a locking force $F_{lock} = 147 mN$ fulfilling the locking requirement. General behavior of the system is as expected. Wear induced by 8 full locking and unlocking cycles is confirmed but did not affect the shape of the locking curve. The locking device in locked state is presented in fig. 11.30.

Variable with the largest and most uncontrollable influence is the friction coefficient. Designing for a minimum friction coefficient has proven to be successful to obtain a minimum locking force. Downside could be higher forces on system components such as the comb fingers, especially during the reversed movement causing buckling of these comb fingers. Friction coefficient for this prototype is measured in range $0.27 - 0.38$.

11.8. RESEARCH SUGGESTIONS

11.8.1. DYNAMIC TESTING

In real life applications the presented locking system will often be subjected to both static and dynamic loads. The current locking system is only tested for static loads below the maximum locking capacity. Influence of,
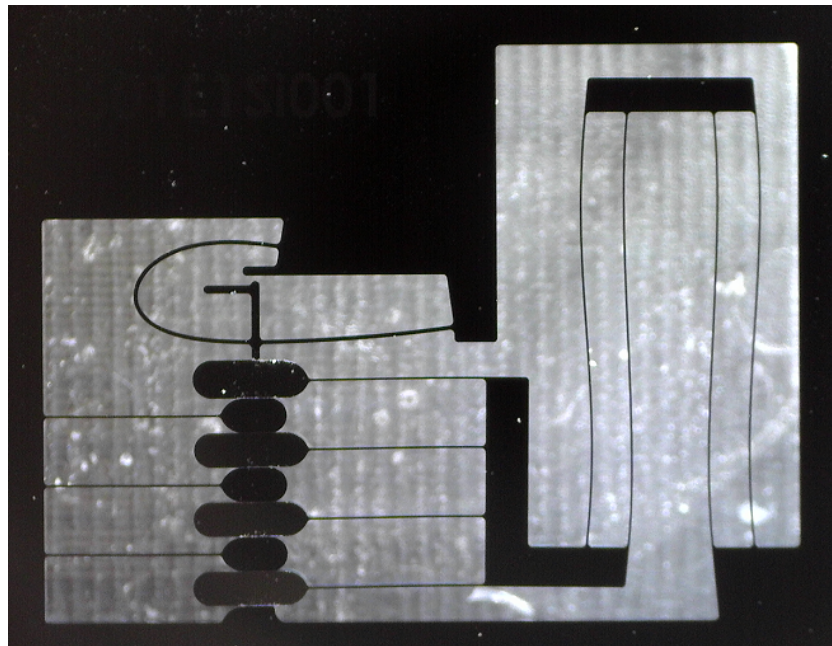
Figure 11.30: LS01E1Si001 in locked state

especially dynamic, loads at the maximum locking capacity are therefore unknown.

Current prototype is designed for a static load of $30mN$ and a dynamic load up to $70mN$. For better measurements on the actual locking system the prototype suspension only delivers a static load of $7mN$. For a valid test the static load should be increased with 23mN. Considered methods are:

- Adding a $23mN$ mass on the shuttle or suspension and performing a dynamic test with the prototype mounted vertically on a shaker. This would result in a device with the designed static force, however the added mass will also influence the dynamic results since the overall mass of the design will be orders of magnitude larger than in the intended design

- Adding a spring, or spring like material to increase the suspension stiffness and therefore static load. First, this method will also influence the dynamic behavior due to the additional mass. Second, adding these small force with sufficient accuracy in a device this small is practically impossible.

Given the issues of performing a dynamic test by adding a static load it is suggested to make a new prototype incorporating the real static loads and intended mass for valid dynamic measurement results.

11.8.2. POSITIONING ACCURACY

The actuation stage, sensors and imaging equipment used do not allow an accurate measurement of the positioning accuracy of the prototype while this could be a key-property of this design.
The measurement for stick-slip behavior did not show the characteristic saw-tooth behavior although this could be present but not within the resolution of the force-sensor. Also an offset is expected when the tuning actuation force is removed. The slip front will flip and a compressive load will be applied on the comb finger beams.

It is very useful to quantify the components in order to make a feed-forward model of the actuator displacement required to obtain a certain frequency change. Dependent on the sensitivity of the frequency to this actuator displacement it might also be interesting to tune the system via a feedback model where the frequency is measured and shuttle moved until the desired frequency is obtained.

12

ALTERNATIVE LOCKING DESIGN

In the thesis paper only a linear increase in locking force is discussed by either increasing the amount of springs (contact forces) or the amount of friction contact points in line with the spring force.

An alternative design where multiple spring are connected in series causing a quadratic increase in locking force as in eq. (12.1) with all springs assumed equal is also possible.

$$F_{lock} = n_F^2 \cdot \mu \cdot F_{spring,y} \tag{12.1}$$

Figure 12.1 shows an example of a locking mechanism design with a quadratic increase in normal and therefore locking force. The lowest cantilever spring beam delivers $1F_{spring,y}$ on the hinged rigid beam. This force acts on both sides of this rigid beam. The next cantilever spring beam adds $1F_{spring,y}$ resulting in $2F_{spring,y}$ on the second hinged rigid beam. The same reasoning applies for cantilevers spring beams added in line up top the top cantilever which is prestressed via a rigid slope resulting in a total force of $1+1+2+2+3 = 9F_{spring,y}$.
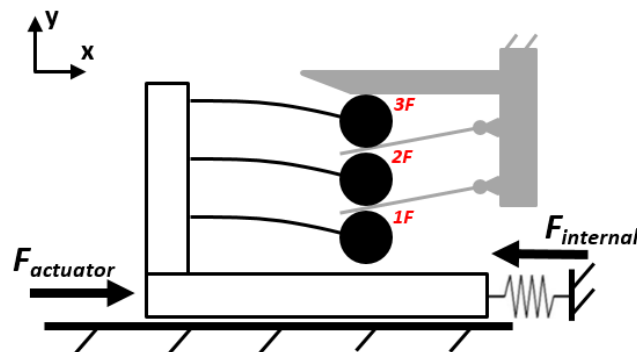
Figure 12.1: Alternative locking mechanism design with quadratic increase in locking force

Note that a large contact tip point is added on the cantilever spring beams. This contact point is added to ensure the effective length of the cantilever spring beam is constant when the shuttle is displaced. Without this contact tip the effective length would decrease when the shuttle moves in the positive x-direction. Size and shape of this contact point is arbitrary as long as it is bigger than the largest tip displacement in y-direction.

Drawback of this design is the uneven locking load on the cantilever spring beams . Depending on the suspension of the shuttle this could cause an additional moment causing undesired rotation. Also the maximum spring and locking force of a cantilever beam is limited and sensitivity to fabrication errors is higher compared to one larger spring with non-deforming comb fingers in line.

A
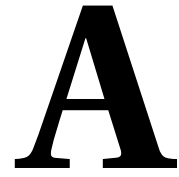
ANSYS APDL Code

A.1. SQUEEZE FILM MODEL

```
FINISH
/CLEAR


!!!!!!!!!!!!!!!!!!!!!!!!!!!!!!!!
! ANSYS Squeeze Film Analysis  !
! Made by: Sjoerd van Bracht   !
! Created: 28-10-2014 !
!!!!!!!!!!!!!!!!!!!!!!!!!!!!!!!!!


! Define element ----------------------------------------------------------------------
/PREP7
/title, Sqeeuze film analysis
ET,1,FLUID136,0 !The default flow regime for FLUID136 and FLUID138 is continuum theory (KEYOPT(1)
!flow regime. For FLUID136, set KEYOPT(1) = 2 to specify the high Knudsen number flow regime with

! Parameters -------------------------------------------------------------------------

l_plate=10e-3  ![m] Plate length
w_plate=500e-6 ![m] Plate width
t_plate=25e-6 ![m] Plate thickness
gap=40e-6 ![m] Gap thickness

p_amb=1e5  ![Pa] Ambient pressure
p_ref=1e5  ![Pa] Reference pressure
velo=1e-3 ![m/s] Arbitrary velocity, the analysis is linear, the magnitude of the velocity can be
freq=25  ![Hz] Frequency
pi=3.14159
omega=2*pi*freq ![rad/s] Frequency

mu=18.3e-6  ![Pa s]=[kg/ms] Viscosity
mfp=64e-9  ![m] mean free path air at ambient pressure (See section 3.4 ANSYS Fluid Analysis Guid
Knud=mfp/gap  ! Knudsen number = mean free fluid path divided by the gap

! Material properties -----------------------------------------------------------------

mp,visc,1,mu
r,1,gap,,,p_amb
rmore,p_ref,mfp

! Build the model ---------------------------------------------------------------------

rectng,0,l_plate,0,w_plate ! Plate domain


! Velocity directly applied to fluid elements --> fluid can be an independent structure
! Velocity determined from mode frequency response from of structure --> fluid elements dependent
TYPE,  1
MAT,  1
REAL,  1
smrtsize,4
AMESH,  all  ! Mesh area plate domain

! Define Constraints ------------------------------------------------------------------
```

```
nsel,s,loc,x,0 ! s= from full, select nodes at x=0,        nsel,.,loc=select nodes by location
nsel,a,loc,x,l_plate ! a = also select, nodes at x=l_plate
nsel,a,loc,y,0
nsel,a,loc,y,w_plate
d,all,pres  ! Fix pressure at outer plate boundary

allsel ! select everything

bfe,all,flue,,velo  ! Apply arbitrary velocity, bfe=element body force load
FINISH



! Solve -------------------------------------------------------------------------------

/SOLU
antyp,harm  ! Full Harmonic analysis
harfrq,freq ! Defines the frequency range in a harmonic analysis. HARFRQ, FREQB(eginning), FREQE(nd)
! If FREQE is blank, the solution is done only at frequency FREQB.
solve ! Static analysis is allowed when frequency is low --> no stiffening effect
FINISH

! Read results-------------------------------------------------------------------------

/POST1
esel,s,type,,1 ! Select elements by type
set,1,1 ! Store "Real" solution
etable,presR,pres  ! Extract "Real" pressure
etable,earea,volu ! Extract element area
smult,forR,presR,earea  ! Compute "Real" force
ssum ! sum over all elements
*get,Fre,ssum,,item,forR! get the total "real" force

set,1,1,,1
etable,presI,pres  ! extract "Imaginary" pressure
smult,forI,presI,earea  ! compute "Imaginary" pressure
ssum
*get,Fim,ssum,,item,forI

K=abs(Fim*omega/velo)  ! Compute equivalent stiffness
C=abs(Fre/velo)   ! Compute damping coefficient

*stat,

!/com, ******* Equivalent stiffness ************************
!*stat,K
!/com, ******* Equivalent damping ************************
!*stat,C

PLNSOL, PRES,, 0 ! Plot pressure ditribution
FINISH
```

A.2. SPRING MODEL

A.2.1. CONTACT VARIABLES

```
FINISH
/CLEAR
/OUTPUT
t_flex=6e-05
*DIM,Coordinates,ARRAY,50,2
*SET,Coordinates(1,1),0
*SET,Coordinates(1,2),0
*SET,Coordinates(2,1),-0.002768
*SET,Coordinates(2,2),0.001462
*SET,Coordinates(3,1),-0.005394
*SET,Coordinates(3,2),0.002596
*SET,Coordinates(4,1),-0.00788
*SET,Coordinates(4,2),0.003426
*SET,Coordinates(5,1),-0.01023
*SET,Coordinates(5,2),0.003976
*SET,Coordinates(6,1),-0.01245
*SET,Coordinates(6,2),0.004262
*SET,Coordinates(7,1),-0.014542
*SET,Coordinates(7,2),0.00431
*SET,Coordinates(8,1),-0.016506
*SET,Coordinates(8,2),0.004136
*SET,Coordinates(9,1),-0.01835
*SET,Coordinates(9,2),0.003764
*SET,Coordinates(10,1),-0.02007
*SET,Coordinates(10,2),0.003208
*SET,Coordinates(11,1),-0.021672
*SET,Coordinates(11,2),0.00249
*SET,Coordinates(12,1),-0.023154
*SET,Coordinates(12,2),0.001626
*SET,Coordinates(13,1),-0.024518
*SET,Coordinates(13,2),0.000632
*SET,Coordinates(14,1),-0.025764
*SET,Coordinates(14,2),-0.000472
*SET,Coordinates(15,1),-0.026892
*SET,Coordinates(15,2),-0.001672
*SET,Coordinates(16,1),-0.0279
*SET,Coordinates(16,2),-0.002952
*SET,Coordinates(17,1),-0.02879
*SET,Coordinates(17,2),-0.0043
*SET,Coordinates(18,1),-0.029558
*SET,Coordinates(18,2),-0.005698
*SET,Coordinates(19,1),-0.030202
*SET,Coordinates(19,2),-0.007134
*SET,Coordinates(20,1),-0.030722
*SET,Coordinates(20,2),-0.008596
*SET,Coordinates(21,1),-0.031114
*SET,Coordinates(21,2),-0.010072
*SET,Coordinates(22,1),-0.031376
*SET,Coordinates(22,2),-0.011548
*SET,Coordinates(23,1),-0.031502
*SET,Coordinates(23,2),-0.013014
*SET,Coordinates(24,1),-0.03149
*SET,Coordinates(24,2),-0.01446
```

```
*SET,Coordinates(25,1),-0.031334
*SET,Coordinates(25,2),-0.015876
*SET,Coordinates(26,1),-0.031032
*SET,Coordinates(26,2),-0.017252
*SET,Coordinates(27,1),-0.030576
*SET,Coordinates(27,2),-0.01858
*SET,Coordinates(28,1),-0.029964
*SET,Coordinates(28,2),-0.01985
*SET,Coordinates(29,1),-0.029186
*SET,Coordinates(29,2),-0.021058
*SET,Coordinates(30,1),-0.028238
*SET,Coordinates(30,2),-0.022192
*SET,Coordinates(31,1),-0.027114
*SET,Coordinates(31,2),-0.023252
*SET,Coordinates(32,1),-0.025804
*SET,Coordinates(32,2),-0.024226
*SET,Coordinates(33,1),-0.024302
*SET,Coordinates(33,2),-0.025114
*SET,Coordinates(34,1),-0.0226
*SET,Coordinates(34,2),-0.025908
*SET,Coordinates(35,1),-0.02069
*SET,Coordinates(35,2),-0.026606
*SET,Coordinates(36,1),-0.018562
*SET,Coordinates(36,2),-0.027204
*SET,Coordinates(37,1),-0.016208
*SET,Coordinates(37,2),-0.0277
*SET,Coordinates(38,1),-0.013618
*SET,Coordinates(38,2),-0.02809
*SET,Coordinates(39,1),-0.01078
*SET,Coordinates(39,2),-0.028374
*SET,Coordinates(40,1),-0.007686
*SET,Coordinates(40,2),-0.02855
*SET,Coordinates(41,1),-0.004324
*SET,Coordinates(41,2),-0.028618
*SET,Coordinates(42,1),-0.000682
*SET,Coordinates(42,2),-0.02858
*SET,Coordinates(43,1),0.00325
*SET,Coordinates(43,2),-0.028436
*SET,Coordinates(44,1),0.007486
*SET,Coordinates(44,2),-0.028186
*SET,Coordinates(45,1),0.012038
*SET,Coordinates(45,2),-0.027832
*SET,Coordinates(46,1),0.016918
*SET,Coordinates(46,2),-0.02738
*SET,Coordinates(47,1),0.02214
*SET,Coordinates(47,2),-0.02683
*SET,Coordinates(48,1),0.027718
*SET,Coordinates(48,2),-0.026186
*SET,Coordinates(49,1),0.033666
*SET,Coordinates(49,2),-0.025454
*SET,Coordinates(50,1),0.04
*SET,Coordinates(50,2),-0.02464
```

A.2.2. Contact Model

```
!%%%%%%%%%%%%%%%%%%%%%%%%%%%%%%%%%%%%%%%%%%%%%%%%%%%%%%%%%%
! Constants

E = 170e9 ![Pa] Modulus of elastisity Si
v = 0.3 ![-] Poisson ratio
rho = 2330 ![kg/m3] Density Si
mu_si = 0.1 ![-] Friction coefficient Si-Si

w_flex = 525e-6       ![m] flexure width (in plane)
n_flexure = 1 ![-] mesh size flexure

pi = 3.1415
x_slope = 500e-6 ![m] 0.5*Length of pretension slope --> defines slope end point relative to N,501

!%%%%%%%%%%%%%%%%%%%%%%%%%%%%%%%%%%%%%%%%%%%%%%%%%%%%%%%%%%
!Define elements and material properties

/PREP7
/TITLE, Friction Locking Beam

! Define element
ET,1,BEAM188 ! Flexures
MP,EX,1,E ! Young's modulus
MP,PRXY,1,v  ! Poisson's ratio
MP,DENS,1,rho      ! Density
SECTYPE,1,beam,RECT  ! Rectangular Beam section
SECDATA , t_flex,w_flex ! Beam thickness, beam width


ET,2,CONTA171  ! Contact Element


! See section 3.9.4 Determining Contact Stiffness and Allowable Penetration

!FKN = 0.5  ! Penalty stiffness in the direction normal to the contact surface (penetration), higher wi
!FKT = 0.1 ! Penalty stiffness tangent ot the contact surface (slip in sticking contact), higher will l
!FTOLN = 1 ! Allowable penetration
!SLTO =  ! Allowable slip


R,1,0,0,FKN, FTOLN,0,0
RMORE,,,, ,,FKT

KEYOPT,2,4,2  ! Detection on nodal point, normal to target surface
KEYOPT,2,2,4  ! Contact algorithm: Pure Lagrange multiplier on contact normal and tangent KEYOPT(2)=4
!KEYOPT,2,5,2 ! Reduce penetration with auto CNOF (contact surface offset)
! Specify a contact surface offset to eliminate small gaps/penetrations due to round-off errors
! Use a negative value to offset the contact surface away from the target surface.
!KEYOPT,2,10,2  ! Detection on nodal point, normal to target surface

!KEYOPT,2,12,2 ! Behavior of contact surface


TB,FRIC,1,,,ISO      ! Activate isotropic friction model (second method: MP,MU,1,mu_si yields same resu
```

```
TBDATA,1,mu_si              ! Define coefficient of friction


ET,3,TARGE169   ! Target Element for 2D elements
KEYOPT,3,2,1   ! Boundary conditions defined by user (0=defined by ANSYS)


!%%%%%%%%%%%%%%%%%%%%%%%%%%%%%%%%%%%%%%%%%%%%%%%%%%%%%%
! Define model

*GET,n_bez,PARM,COORDINATES,DIM,X ! Get length of coordinates vector (amount of coordinates)

*DO,I,1,n_bez ! Make keypoint for every (x,y)
X = COORDINATES(I,1)
Y = COORDINATES(I,2)
K,I,X,Y,,,
*ENDDO

TYPE,1  ! Activate Element 1
SECNUM,1  ! Activate Section Number 1

*DO,I,1,n_bez-1 ! Create lines between all keypoints
L,I,I+1
*ENDDO

LGLUE,ALL

LESIZE,1, , ,n_flexure, ,1, , ,1,  ! Set mesh size for flexure
LMESH,ALL   ! Apply Mesh


*GET,node_flexure_max,NODE,0,NUM,MAXD  ! Find amount of nodes after meshing the mean to select co

TYPE,2  ! Activate Element 2
NSEL,S,NODE,,1,node_flexure_max  ! Select Nodes for Contact Element
ENSYM,0,,0,ALL   ! Reverse Normal Direction
ESURF   ! Create Contact Elements on selected elements
NSEL,ALL   ! Reselect all nodes


! Find coordinate of lowest beam position to determine slope position based on desired prestress
/POST1
NSORT,LOC,Y,0,0
*GET,y_low,SORT,,MIN ! Coordinate with smallest y-value (=lowest)


! Find highest x-value to guarantee enough shuttle displacement
NSORT,LOC,X,0,0
*GET,x_high,SORT,,MAX ! Coordinate with highest x-value

! Find lowest x-value to position shuttle slope
NSORT,LOC,X,0,0
*GET,x_low,SORT,,MIN ! Coordinate with smallest x-value

x_shuttle = x_slope+1.5*(x_high-x_low) ![m] Shuttle displacement based on maximum x-difference in
```

```
! Define center point for shuttle prestress slope arc
alpha2 = atan(y_prestress/(x_slope)) ! Angle of slope between arc start-end points
Lb = (x_slope/2)/cos(alpha2)
beta = asin(Lb/r_arc)


/PREP7
TYPE,3  ! Activate Element 3
N,501,x_low,y_low ! Lower right point
N,502,x_low-x_slope-2*(x_high-x_low),y_low+y_prestress ! End of Sliding surface

N,503,x_low-x_slope,y_low+y_prestress ! Endpoint of curve
N,504,x_low-(r_arc*sin(beta+alpha2)),y_low-(r_arc*cos(beta+alpha2)) ! Arc center point


TSHAP,ARC ! Defines 2-D geometric surfaces for target segment elements
E,503,501,504
NSEL,S,,,501  ! Select node attached to arc-element
ESLN,S,0 ! Select element connected to selected node
ESURF,,REVE ! Reverse normal direction on arc element
NSEL,ALL ! Reselect all nodes
ESLN,ALL ! Reselect all elements


TSHAP,LINE ! Defines simple 2-D and 3-D geometric surfaces for target segment elements
E,503,502 ! Sliding(locking) surface for curved connection


! Detect and store node locations + displacements after solve --> used to check intersections/contact a

*DIM,LOC_Xnodes,ARRAY,node_flexure_max,1 ! Make array to store all node x-coordinates
*DIM,LOC_Ynodes,ARRAY,node_flexure_max,1 ! Make array to store all node y-coordinates
*DO,I,1,node_flexure_max
*GET,X_I,NODE,I,LOC,X ! Get x,y-coordinates
*GET,Y_I,NODE,I,LOC,Y
*SET,LOC_Xnodes(I,1),X_I ! Store x,y-coordinates in array
*SET,LOC_Ynodes(I,1),Y_I
*ENDDO



!%%%%%%%%%%%%%%%%%%%%%%%%%%%%%%%%%%%%%%%%%%%%%%%%%%%%%%%%%%%
! Solve the analysis

/SOLU
ANTYPE,STATIC  ! Static Simulation
SOLCONTROL,ON,ON  ! Contact Detection Control ON
NLGEOM,ON  ! Turn on Large deformation
OUTRES,ALL,ALL  ! Save all results at all iterations
AUTOTS,ON  ! Turn on Automatic TimeStepping


! Constraints

DK,1,ALL ! First keypoint beam
```

```
DK,n_bez,ALL ! Last keypoint beam

TIME, 1 ! Prestressing locking beam
D,501,UX,x_shuttle
D,502,UX,x_shuttle
D,503,UX,x_shuttle
D,504,UX,x_shuttle

! Not necessary with KEYOPT 2=0 for ET3
D,501,UY,0
D,502,UY,0
D,503,UY,0
D,504,UY,0
D,501,ROTZ,0
D,502,ROTZ,0
D,503,ROTZ,0
D,504,ROTZ,0


SOLVE
FINISH

!%%%%%%%%%%%%%%%%%%%%%%%%%%%%%%%%%%%%%%%%%%%%%%%%%%%%%%%%%%
! Read results

/POST1
CurMax = 0 ! Dummy value to store maximum stress
SET,FIRST   ! Read first data set
*GET,NoSets,ACTIVE,0,SET,NSET,LAST,1 ! Number of data sets written for time step 1

*DO,I,1,NoSets
*GET,SEQV_max,SECR,ALL,S,EQV,MAX ! Equivalent stress value

*IF,SEQV_max,GT,CurMax,THEN
CurMax = SEQV_max ! Maximum equivalent stress till current time step
Index_max = I ! Data set at maximum stress

*ENDIF
SET,NEXT ! Read next data set
*ENDDO

SET,,, ,,, ,NoSets
*GET,SEQV_end,SECR,ALL,S,EQV,MAX ! Equivalent stress value at final position


*DIM,UX_nodes,ARRAY,node_flexure_max,1 ! Make array to store all node x,y-displacement data
*DIM,UY_nodes,ARRAY,node_flexure_max,1 ! Make array to store all node x,y-displacement data
*DO,I,1,node_flexure_max ! Get x,y-displacements
*GET,UX_I,NODE,I,U,X
*GET,UY_I,NODE,I,U,Y
*SET,UX_nodes(I,1),UX_I !Store x,y-displacement in array
*SET,UY_nodes(I,1),UY_I
*ENDDO


*VOPER,X_LOC,LOC_Xnodes,ADD,UX_nodes, , ,
```

```
*VOPER,Y_LOC,LOC_Ynodes,ADD,UY_nodes, , ,

!%%%%%%%%%%%%%%%%%%%%%%%%%%%%%%%%%%%%%%%%%%%%%%%%%%%%%%%%%
! Plotting, printing and saving

!PLDISP,1 ! Plot deformed shape

!SET,,, ,,, ,Index_max  ! Plot stresses at 'Index_max'or 'NoSets'
!PLESOL, S,EQV, 0,1.0
!/ESHAPE,1
!/REPLOT


/POST26

NSOL,2,501,U,X, UX_shuttle

RFORCE,3,501,F,X, FX_shuttle
RFORCE,4,501,F,Y, FY_shuttle

RFORCE,5,1,F,X,FX_left
RFORCE,6,1,F,Y,FY_left

RFORCE,7,node_flexure_max-2,F,X, FX_right
RFORCE,8,node_flexure_max-2,F,Y, FY_right


!%%%%%%%%%%%%%%%%%%%%%%%%%%%%%%%%%%%%%%%%%%%%%%%%%%%%%%%%%
! Write stresses to file

*CREATE,scratch,gui
/OUTPUT,'Locking_beam_results_max_stress','txt','C:\Users\Sjoerd\Documents\ME2490-35 Graduation\Optimiz
*VWRITE, 'NoSets','Index_max','SEQV_max','SEQV_end'
%C, %C, %C, %C
     *VWRITE, NoSets, Index_max, Curmax, SEQV_end
%G, %G, %G, %G
/OUTPUT,TERM
*END
/INPUT,scratch,gui


!%%%%%%%%%%%%%%%%%%%%%%%%%%%%%%%%%%%%%%%%%%%%%%%%%%%%%%%%%
! Write Fx-data to file

*CREATE,scratch,gui
*DEL,VAR_export
*DIM,VAR_export,TABLE,NoSets,7 ! *DIM, Par, Type, IMAX, JMAX
 VGET,VAR_export(1,0),2
 VGET,VAR_export(1,1),3
 VGET,VAR_export(1,2),4
 VGET,VAR_export(1,3),5
 VGET,VAR_export(1,4),6
 VGET,VAR_export(1,5),7
 VGET,VAR_export(1,6),8
```

```
/OUTPUT,'Locking_beam_results_Fx','txt','C:\Users\Sjoerd\Documents\ME2490-35 Graduation\Optimizat

*VWRITE,'UX_shuttle','FX_shuttle','FY_shuttle','FX_left','FY_left','FX_right','FY_right'
%C, %C, %C, %C, %C, %C, %C
*VWRITE,VAR_export(1,0),VAR_export(1,1),VAR_export(1,2),VAR_export(1,3),VAR_export(1,4),VAR_expor
%G, %G, %G, %G, %G, %G, %G
/OUTPUT,TERM
*END
/INPUT,scratch,gui
```

A.2.3. Equivalent Contact Model

```
!%%%%%%%%%%%%%%%%%%%%%%%%%%%%%%%%%%%%%%%%%%%%%%%%%%%%%
! Constants

w_flex = 525e-6      ![m] flexure width (in plane)
n_flexure = 1 ![-] mesh size flexure

mu_si = 0.1 ![-] Friction coefficient Si-Si

!%%%%%%%%%%%%%%%%%%%%%%%%%%%%%%%%%%%%%%%%%%%%%%%%%%%%%
!Define elements and material properties

/PREP7
/TITLE, Friction Locking Beam

! Define element
ET,1,BEAM188 ! Flexure
MPTEMP,,,,,,,,
MPTEMP,1,0
MPDATA,EX,1,,169e9  ![Pa] Modulus of elastisity Si
MPDATA,EY,1,,169e9
MPDATA,EZ,1,,130e9
MPDATA,PRXY,1,,0.064 ![-] Poisson ratio
MPDATA,PRYZ,1,,0.36
MPDATA,PRXZ,1,,0.28
MPDATA,GXY,1,,50.9e9
MPDATA,GYZ,1,,79.6e9
MPDATA,GXZ,1,,79.6e9
MP,DENS,1,2330 ![kg/m3] Density Si
MP,Mu,1,mu_si
SECTYPE,1,beam,RECT  ! Rectangular Beam section
SECDATA , t_flex,w_flex ! Beam thickness, beam width

!%%%%%%%%%%%%%%%%%%%%%%%%%%%%%%%%%%%%%%%%%%%%%%%%%%%%%
! Define model

*GET,n_bez,PARM,COORDINATES,DIM,X ! Get length of coordinates vector (amount of coordinates)

*DO,I,1,n_bez ! Make keypoint for every (x,y)
X = COORDINATES(I,1)
Y = COORDINATES(I,2)
K,I,X,Y,,,
*ENDDO

TYPE,1  ! Activate Element 1
SECNUM,1  ! Activate Section Number 1

*DO,I,1,n_bez-1 ! Create lines between all keypoints
L,I,I+1
*ENDDO

LGLUE,ALL

LESIZE,1, , ,n_flexure, ,1, , ,1,  ! Set mesh size for flexure
LMESH,ALL  ! Apply Mesh
```

```
*GET,node_flexure_max,NODE,0,NUM,MAXD  ! Find amount of nodes after meshing

/POST1
! Find coordinate of lowest beam position to apply prestress force
NSORT,LOC,Y,0,0
*GET,y_low,SORT,,MIN ! Lowest y-value
*GET,y_low_coordinate,SORT,0,IMIN ! Coordinate with smallest y-value (=lowest)


! Detect and store node locations + displacements,
! after solving --> used to check intersections/contact after solving

*DIM,UX_nodes,ARRAY,node_flexure_max,1 ! Make array to store all node x-coordinates
*DIM,UY_nodes,ARRAY,node_flexure_max,1 ! Make array to store all node y-coordinates
*DO,I,1,node_flexure_max
*GET,X_I,NODE,I,LOC,X ! Get x,y-coordinates
*GET,Y_I,NODE,I,LOC,Y
*SET,UX_nodes(I,1),X_I ! Store x,y-coordinates in array
*SET,UY_nodes(I,1),Y_I
*ENDDO


!%%%%%%%%%%%%%%%%%%%%%%%%%%%%%%%%%%%%%%%%%%%%%%%%%%%%%%%%%%
! Solve the analysis

/SOLU
ANTYPE,STATIC  ! Static Simulation
SOLCONTROL,ON,ON  ! Contact Detection Control ON
NLGEOM,ON  ! Turn on Large deformation
OUTRES,ALL,ALL  ! Save all results at all iterations
AUTOTS,OFF  ! Turn Automatic TimeStepping on or off (default=on)
NSUBST,10 ! Number of substeps to be taken this load step


! Constraints
DK,1,ALL ! First keypoint beam
DK,n_bez,ALL ! Last keypoint beam


! Prestressing locking beam + applying equivalent friction force
F_lock = 0.5 ![N] Maximum applied prestressing force (=F_locky)

F,y_low_coordinate,FY,F_lock ! Apply x-force on current lowest beam point
F,y_low_coordinate,FX,-20e-3 ! Apply beam reaction force on lowest beam point

SOLVE
FINISH

!%%%%%%%%%%%%%%%%%%%%%%%%%%%%%%%%%%%%%%%%%%%%%%%%%%%%%%%
! Read results

/POST1
*GET,NoSets,ACTIVE,0,SET,NSET,LAST,1 ! Number of data sets written for loadstep 1
*DIM,max_stress_vec,ARRAY,NoSets,1 ! Make array to store all maximum stresses
```

```
SET,FIRST   ! Read first data set
*DO,I,1,NoSets
*GET,SEQV_max,SECR,ALL,S,EQV,MAX ! Equivalent stress value
*SET,max_stress_vec(I,1),SEQV_max ! Store maximum equivalent stress in array
SET,NEXT ! Read next data set
*ENDDO


*DIM,DX_nodes,ARRAY,node_flexure_max,1 ! Make array to store all node x,y-displacement data
*DIM,DY_nodes,ARRAY,node_flexure_max,1 ! Make array to store all node x,y-displacement data
*DO,I,1,node_flexure_max ! Get x,y-displacements
*GET,UX_I,NODE,I,U,X
*GET,UY_I,NODE,I,U,Y
*SET,DX_nodes(I,1),UX_I ! Store x,y-displacement in array
*SET,DY_nodes(I,1),UY_I
*ENDDO

*VOPER,X_LOC,UX_nodes,ADD,DX_nodes, , , ! Add displacement vector to original coordinates to obtain co
*VOPER,Y_LOC,UY_nodes,ADD,DY_nodes, , ,


!%%%%%%%%%%%%%%%%%%%%%%%%%%%%%%%%%%%%%%%%%%%%%%%%%%%%%%%%%%%%
! Plotting and defining variables

!PLDISP,1 ! Plot deformed shape

!SET,LAST ! Plot stresses at last substep
!PLESOL, S,EQV, 0,1.0
!/ESHAPE,1
!/REPLOT


/POST26
RFORCE,2,1,F,X,FX_left
RFORCE,3,1,F,Y,FY_left

RFORCE,4,node_flexure_max-2,F,X, FX_right
RFORCE,5,node_flexure_max-2,F,Y, FY_right

NSOL,6,y_low_coordinate,U,X, UX_lowest_point
NSOL,7,y_low_coordinate,U,Y, UY_lowest_point


!%%%%%%%%%%%%%%%%%%%%%%%%%%%%%%%%%%%%%%%%%%%%%%%%%%%%%%%%%%%%
! Save specific arrays to file

*CREATE,scratch,gui
*CFOPEN,'C:\Users\Sjoerd\Documents\ME2490-35 Graduation\ANSYS - Equivalent Contact\Optimization_GA_limi
*VWRITE
('x-coordinates',x,'y-coordinates') ! Writes a column header
*VWRITE,X_LOC(1),Y_LOC(1), , , , , , ,
(F,',',F) ! F - real numbers, fixed point format Fw.d where w is an integer constant denoting the field
*CFCLOS  ! E - real numbers, exponent notation
*END ! nX - n times horizontal skip (space), / - vertical skip (newline)
/INPUT,scratch,gui
```

```
*CREATE,scratch,gui
*CFOPEN,'C:\Users\Sjoerd\Documents\ME2490-35 Graduation\ANSYS - Equivalent Contact\Optimization_G
*VWRITE
('Maximum Stress') ! Writes a column header
*VWRITE,max_stress_vec(1) , , , , , ,
(E) ! F - real numbers, fixed point format Fw.d where w is an integer constant denoting the field
*CFCLOS  ! E - real numbers, exponent notation
*END ! nX - n times horizontal skip (space), / - vertical skip (newline)
/INPUT,scratch,gui


!%%%%%%%%%%%%%%%%%%%%%%%%%%%%%%%%%%%%%%%%%%%%%%%%%%%%%%%%
! Write Fx-data(variables) to file

*CREATE,scratch,gui
*DEL,VAR_export
*DIM,VAR_export,TABLE,NoSets,6 ! *DIM, Par, Type, IMAX, JMAX
 VGET,VAR_export(1,0),2
 VGET,VAR_export(1,1),3
 VGET,VAR_export(1,2),4
 VGET,VAR_export(1,3),5
 VGET,VAR_export(1,4),6
 VGET,VAR_export(1,5),7


/OUTPUT,'Results_Fx','txt','C:\Users\Sjoerd\Documents\ME2490-35 Graduation\ANSYS - Equivalent Con

*VWRITE,'FX_left','FY_left','FX_right','FY_right','UX_lowest_point','UX_lowest_point'
%C, %C, %C, %C, %C, %C
*VWRITE,VAR_export(1,0),VAR_export(1,1),VAR_export(1,2),VAR_export(1,3),VAR_export(1,4),VAR_expor
%G, %G, %G, %G, %G, %G
/OUTPUT,TERM
*END
/INPUT,scratch,gui
```

A.3. Prototype Suspension

```
FINISH
/CLEAR
/OUTPUT


!%%%%%%%%%%%%%%%%%%%%%%%%%%%%%%%%%%%%%%%%%%%%%%%%%%%%%%%
! Constants

w_flex = 525e-6     ![m] flexure width (in plane)
t_flex= 20e-6
L_flex = 5e-3

dx = 1.5e-3 ![m]
alpha = 5.4 ![deg]

!%%%%%%%%%%%%%%%%%%%%%%%%%%%%%%%%%%%%%%%%%%%%%%%%%%%%%%%
!Define elements and material properties

/PREP7
/TITLE, LS01E01Si001 Suspension

! Define element
ET,1,BEAM188 ! Flexure
MPTEMP,,,,,,,,
MPTEMP,1,0
MPDATA,EX,1,,169e9  ![Pa] Modulus of elastisity Si
MPDATA,EY,1,,169e9
MPDATA,EZ,1,,130e9
MPDATA,PRXY,1,,0.064 ![-] Poisson ratio
MPDATA,PRYZ,1,,0.36
MPDATA,PRXZ,1,,0.28
MPDATA,GXY,1,,50.9e9
MPDATA,GYZ,1,,79.6e9
MPDATA,GXZ,1,,79.6e9
MP,DENS,1,2330 ![kg/m3] Density Si
SECTYPE,1,beam,RECT  ! Rectangular Beam section
SECDATA , t_flex,w_flex ! Beam thickness, beam width



ET,2,MPC184 !Rigid elements
KEYOPT,2,1,1



!%%%%%%%%%%%%%%%%%%%%%%%%%%%%%%%%%%%%%%%%%%%%%%%%%%%%%%%
! Define model

TYPE,1  ! Activate Element 1
SECNUM,1  ! Activate Section Number 1

angle = (alpha/360)*2*3.1415

K,1,0,0
K,2,L_flex*sin(angle),L_flex*cos(angle)
K,3,0.467e-3,0
K,4,0.467e-3+L_flex*sin(angle),L_flex*cos(angle)
```

```
K,5,0.467e-3 +1.92e-3,0
K,6,0.467e-3 +1.92e-3-L_flex*sin(angle),L_flex*cos(angle)
K,7,0.467e-3 +1.92e-3 + 0.467e-3,0
K,8,0.467e-3 +1.92e-3 +0.467e-3 -L_flex*sin(angle),L_flex*cos(angle)

K,9,-2.7e-3,0

L,1,2
L,3,4
L,5,6
L,7,8
L,1,9

LESIZE,ALL, , ,20, ,1, , ,1,  ! Set mesh size for flexure
LMESH,ALL   ! Apply Mesh


TYPE,2
L,2,4
L,4,6
L,6,8
L,1,3

LSEL,S,LINE,,6 ,9
LESIZE,ALL, , ,1
LMESH,ALL


!%%%%%%%%%%%%%%%%%%%%%%%%%%%%%%%%%%%%%%%%%%%%%%%%%%%%%%%%%%%
! Solve the analysis

/SOLU
ANTYPE,STATIC  ! Static Simulation
SOLCONTROL,ON,ON  ! Contact Detection Control ON
NLGEOM,ON  ! Turn on Large deformation
OUTRES,ALL,ALL  ! Save all results at all iterations
AUTOTS,OFF  ! Turn Automatic TimeStepping on or off (default=on)
NSUBST,10 ! Number of substeps to be taken this load step

! Constraints
DK,5,ALL ! First keypoint beam
DK,7,ALL ! First keypoint beam

DK,1, ,dx, , , ,UX, , , , ,  ! move the shuttle

DK,9, ,0, , , ,UY, , , , ,
DK,9, ,0, ,0,ROTZ, , , , , ,

SOLVE
FINISH

!%%%%%%%%%%%%%%%%%%%%%%%%%%%%%%%%%%%%%%%%%%%%%%%%%%%%%%%%%%%
! Read results

/POST1
PLDISP,1 ! Plot deformed shape
```

```
SET,LAST ! Plot stresses at last substep
PLESOL, S,EQV, 0,1.0
/ESHAPE,1
/REPLOT

!ANTIME,10,0.5, ,1,2,0,1

/POST26
NSOL,2,1,U,Y, UY
NSOL,3,1,U,X, UX
RFORCE,4,1,F,X,FX
NSOL,5,85,U,Y, UY_contact

/AXLAB,X,x-displacement [m]
/AXLAB,Y,y-displacement [m]
XVAR,3
PLVAR,2,

PRVAR,2,3,4,5
```

B

MATLAB Scripts

B.1. OPTIMIZATION

B.1.1. LOCKEXEOPTIM

```matlab
1   clear all; close all; clc;
2
3   Pop_Size = 10;        %Population size for GA
4
5   load('Feasible_initial_parameters.mat')
6   %remove y_prestress
7   feasible_parameters = [feasible_parameters(:,1) ...
        feasible_parameters(:,[3,4,5,6,7,8,9,10])];
8   r = randi(length(feasible_parameters),1,Pop_Size);  % Select random initial ...
        population indices for GA
9   Init_Pop = feasible_parameters(r,:);                % Initial population for GA
10
11  x_min = -2e-3;
12  x_max = 4e-3;
13  y_min = -3e-3;
14  y_max = 2e-3;
15
16  %x0 = [t_flex;  x2; y2; x3; y3; x4; y4; x5; y5];
17  lb = [20e-6;    x_min;y_min;    x_min;y_min;    x_min;y_min;    180e-6;y_min]; % ...
        Lower bounds of x
18  ub = [100e-6;   x_max;y_max;    x_max;y_max;    x_max;y_max;    x_max;y_max]; % Upper ...
        bounds of x
19  %% Genetic Algorithm
20  options = ...
        gaoptimset('InitialPopulation',Init_Pop,'PopulationSize',Pop_Size,'PlotFcns',{@gaplotbestf,@gaplot
21  %[x,fval,exitflag,output,population] = ...
        ga(@LockObjGA_constrained,9,[],[],[],[],lb,ub,@LockConGA,options);
22  [x,fval,exitflag,output,population] = ...
        ga(@LockObjGA_unconstrained,9,[],[],[],[],lb,ub,[],options);
23  save('LockGAResults.mat','x','fval','exitflag','output','population')
24
25  fprintf('The number of generations was : %d\n', output.generations);
26  fprintf('The number of function evaluations was : %d\n', output.funccount);
27  fprintf('The best function value found was : %g\n', fval);
28
29  %% Result analysis
30  %[id,F_lock,stress_real,y_prestress,t_flex,y,x2,y2,x3,y3,x4,y4,x5,y5]
31  load par_vec
32  % j=1;
33  % for i=1:length(par_vec)
34  %     if par_vec(i,1) == 0
35  %         par_vec_converged(j,1:13) = par_vec(i,1:13);
36  %         j=j+1;
37  %     end
38  % end
39
40  k=1;
41  for i=1:length(par_vec)
42      x_par_vec = par_vec(i,[5,6,7,8,9,10,11,12,13]);
43      if isequal(x_par_vec,x)
44          a(k)=i;
45          k=k+1;
46      end
47  end
48
49  F_lock_max = par_vec(a(1),2)
50  y_prestress = par_vec(a(1),4)
51
52  %find(par_vec_f_value(:,3)==fval)
```

B.1.2. LOCKOBJGA UNCONSTRAINED

```matlab
1   function f = LockObjGA_unconstrained(x)
```

```matlab
2  %% Genetic Algorithm objective function
3
4  t_flex = x(1);
5  x2 = x(2);
6  y2 = x(3);
7  x3 = x(4);
8  y3 = x(5);
9  x4 = x(6);
10 y4 = x(7);
11 x5 = x(8);
12 y5 = x(9);
13
14
15 F_lock_req = 0.1;            %[N] Required locking force
16 y_prestress_req = 40e-6;    %[m] Required prestress
17
18 stress_limit = 200e6;       %[Pa] Maximum allowed stress
19
20 [id,F_lock_max,y_prestress] = LockAnalysis(t_flex,x2,y2,x3,y3,x4,y4,x5,y5,stress_limit);
21
22 if id ==0
23     % Clamping force ≥ Minimum clamping force
24     cF = 1/F_lock_req;                      %[1/N] Direction coefficient for f1 objective
25     cF2 = cF/4;                             %[-] Weight factor for objective increase ...
           when F_lock is already fulfilled
26
27     if F_lock_max ≤ F_lock_req
28         f1 = cF*F_lock_max;            %[N]
29     elseif F_lock_max > F_lock_req
30         f1_add = cF2*(F_lock_max-F_lock_req);
31         f1 = cF*F_lock_req + f1_add;
32     end
33
34     % Prestress ≥ Minimum prestress displacement
35     cy = 1/y_prestress_req;                 %[1/m] Direction coefficient for f2 objective
36     cy2 = cy/8;                             %[-] Weight factor for objective increase ...
           when F_lock is already fulfilled
37
38     if y_prestress ≤ y_prestress_req
39         f2 = cy*y_prestress;          %[m]
40     elseif y_prestress > y_prestress_req
41         f2_add = cy2*(y_prestress-y_prestress_req);
42         f2 = cy*y_prestress_req + f2_add;
43     end
44
45 else
46     f1 = -5;
47     f2 = -5;
48 end
49
50 if f1==-5 && f1==-5
51     f = -f1-f2;
52 else
53     f=abs(min([f1 f2])/max([f1 f2])*max([f1 f2]))*(-f1-f2);
54 end
55
56 % f1
57 % f2
58 % f
59 %% Save all evaluated parameters to file
60 global par_vec_f_value
61 if exist('par_vec_f_value','var') == 0
62     delete('par_vec_f_value.mat')
63     par_vec_f_value(1,1:3) = [f1,f2,f];
64 else
65     [rows,¬] = size(par_vec_f_value);
66     par_vec_f_value(rows+1,1:3) = [f1,f2,f];
67 end
68 save('par_vec_f_value.mat','par_vec_f_value')
69 end
```

B.1.3. LOCKANALYSIS

```matlab
 1  function ...
        [id,F_lock_max,y_prestress]=LockAnalysis(t_flex,x2,y2,x3,y3,x4,y4,x5,y5,stress_limit)
 2  % Function used to analyse different locking geometries.
 3  % 1) Bezier curve is created based multiple Bezier points
 4  % 2) If Bezier curve is accepted, ANSYS is used to analyse the characteristics
 5  % 3) Key-characteristics are determined/extracted to check perfomance
 6  % 4) Relevant data is stored in vectors and written to result-file
 7  %
 8  % If id = 0 --> Bezier-curve is accepted + ANSYS converged to a solution
 9  % If id = 1 --> ANSYS did not converge
10  % If id = 2 --> Bezier-curve is intersecting
11  % If id = 3 --> Bezier curve is too flat to prestress
12
13  %% Create Berzier curve with initial point (x,y)=(0,0)
14
15  points = [0 x2 x3 x4 x5 ; 0 y2 y3 y4 y5]';
16  [bezcurve] = bezier_(points);
17  x_bez = bezcurve(:,1); %[m] x-coordinates from bezier curve
18  y_bez = bezcurve(:,2); %[m] y-coordinates from bezier curve
19
20  % remove digits of precision > 10^-7 (not written to ANSYS anyways)
21  x_bez = round(x_bez*10^7)/(10^7);
22  y_bez = round(y_bez*10^7)/(10^7);
23
24  [x_bez,y_bez] = overlap_coord(x_bez,y_bez); %function to remove similar coordinates ...
        in series
25
26  %bezier_curce = [x_bez y_bez zeros(length(x_bez),1)]
27
28  y_low = min(y_bez);        %[m] Find coordinate of lowest beam position
29
30  % Plot beam shape evaluated by ANSYS
31  close(figure(2));
32  figure(2)
33  axis equal
34  scatter(points(:,1),points(:,2),'bo')
35  hold on
36  plot(x_bez,y_bez,'r','Linewidth',2)
37  grid on
38
39  xlabel('x [m]')
40  ylabel('y [m]')
41  axis([-2e-3 4e-3 -3e-3 2e-3])
42  title('Evaluated Locking Beam')
43
44  %% Check if created line does not intersect with itself
45  % id-numbers are written to results-file and can be used for results
46  % analysis and see potential errors/problems/phenomena
47
48  [id] = intersections(x_bez,y_bez);   % id=0(no intersections), id=2(intersections)
49  if id ≠ 2                            % only evaluate when no initial intersection is found
50      [id]=Thickness_bounds(t_flex,x_bez,y_bez);   % id=0 or id=4
51  end
52
53  if id == 0    % no curve intersection --> run ANSYS
54      [id] = run_ansys(t_flex,x_bez,y_bez);
55  end
56
57  %% Evaluate the results
58  F_lock_max = 0;
59  y_prestress = 0;
60  stress_real = 0;
61
62  if id==1        % ANSYS non-convergent -> no feasible solution -> no buckling_beam.txt
63      display('ANSYS did not converge')
64
65  elseif id==2    % Curve intersection
66      display('Intersection in initial Bezier-curve')
```

```matlab
67
68  elseif id==3      % Curve not high enough
69      display('Bezier-curve too flat to prestress')
70
71  elseif id==4      % Beam boundaries are intersecting (beam thickness + mask clearance)
72      display('Intersection in boundaries')
73
74  elseif id==0      % ANSYS convergent +no intersections -> calculate stroke
75      % Import data from ANSYS file
76      filetoRead = ['Results_Fx' ,'.txt'];
77      filetoRead2 = ['Results_xy_locations' ,'.txt'];
78      filetoRead3 = ['Results_max_stress_vec' ,'.txt'];
79
80      % Deleting the first row (headers)
81      Data = dlmread(filetoRead,',',1,0);
82      Data2 = dlmread(filetoRead2,',',1,0);
83      Data3 = dlmread(filetoRead3,',',1,0);
84
85  %% Define all outputs
86      Fx_left = Data(:,1);          %[N]
87      Fy_left = Data(:,2);          %[N]
88      Fx_right = Data(:,3);         %[N]
89      Fy_right = Data(:,4);         %[N]
90      Ux_lowest_point = Data(:,5);%[m]
91      Uy_lowest_point = Data(:,6);%[m]
92
93      stress_max = Data3;           %[Pa] maximum stress per substep
94
95  %% Loop to structure nodes in correct order to plot and check structure for ...
        intersections after deformation
96  %      i_vec = 1:1:length(Data2);
97  %      i_vec_new(1) = i_vec(1);
98  %      i_vec_new(2) = i_vec(2);
99  %
100 %      j=1; k=0;
101 %      for i=3:length(i_vec)
102 %          i_vec_new(i) = i_vec(i+j);
103 %
104 %          if   j==1 && k==0
105 %              j=1;
106 %              k=1;
107 %          elseif j==1 && k==1
108 %              j=-2;
109 %              k=0;
110 %          elseif j==-2
111 %              j=1;
112 %          end
113 %      end
114 %
115 %      for i=1:length(Data2)
116 %          j = i_vec_new(i);
117 %          x_new(i)= Data2(j,1);   % x-coordinates in correct order
118 %          y_new(i)= Data2(j,2);   % y-coordinates in correct order
119 %      end
120
121 %% Analysis Output Characteristics
122      % Check for intersections after deformation
123 %      [id] = intersections(x_new',y_new');   % id=0(no intersections), ...
        id=2(intersections)
124 %      if id ≠ 2  %only evaluate when no initial intersection is found
125 %          [id]=Thickness_bounds(t_flex,x_new,y_new);  % id=0 or id=4
126 %      end
127
128      if id==2 || id==4
129          F_lock_max = 0;
130
131      else
132          F_lock = -Fy_left-Fy_right; %[N] Beam force on shuttle
133
134          %Interpolation on ANSYS data
135          p = polyfit([0;F_lock],[0;stress_max],4);
```

```
136            F_lock_fit = 0:0.001:max(F_lock);
137            stress_max_fit = polyval(p,F_lock_fit);
138
139            p2 = polyfit([0;F_lock],[0;Uy_lowest_point],4);
140            Uy_lowest_point_fit = polyval(p2,F_lock_fit);
141
142    %% Plot stress and required prestress as function of locking force
143    %          close(figure(3));
144    %          figure(3)
145    %          subplot(2,1,1)
146    %          plot([0;F_lock],[0;stress_max/10^6],'o')
147    %          hold on
148    %          plot(F_lock_fit,stress_max_fit/10^6,'r')
149    %          xlabel('F_{lock} [N]')
150    %          ylabel('Maximum stress [MPa]')
151    %          grid on
152    %
153    %          subplot(2,1,2)
154    %          plot(F_lock_fit,Uy_lowest_point_fit*10^6)
155    %          xlabel('F_{lock} [N]')
156    %          ylabel('y\_prestress [\mum]')
157    %          grid on
158
159    %% Output data
160            pos = find(stress_max_fit-stress_limit<0, 1, 'last');    % maximum index ...
                    where stress is below maximum
161            F_lock_max = F_lock_fit(pos);              %[N] maximum locking force within ...
                    stress limit
162            stress_real = stress_max_fit(pos);
163            y_prestress = Uy_lowest_point_fit(pos); %[m] required prestress for this ...
                    locking force
164        end
165    end
166
167    %% Save all evaluated parameters to file
168    global par_vec
169    if exist('par_vec','var') == 0
170        delete('par_vec.mat')
171        par_vec(1,1:13) = ...
               [id,F_lock_max,stress_real,y_prestress,t_flex,x2,y2,x3,y3,x4,y4,x5,y5];
172    else
173        [rows,¬] = size(par_vec);
174        par_vec(rows+1,1:13) = ...
               [id,F_lock_max,stress_real,y_prestress,t_flex,x2,y2,x3,y3,x4,y4,x5,y5];
175    end
176    save('par_vec.mat','par_vec')
177    end
```

B.1.4. RUN ANSYS

```
1   % This function loads all the variables and compiles the variable part of the input ...
        for Ansys.
2   % The Vars.txt containing the first part of the ansys code is combined with
3   % the Constant.txt part. This code is given to ANSYS by a DOS command.
4
5   function [id] = run_ansys(t_flex,x_bez,y_bez)
6   % Write variables to Vars.txt
7   i_bez = length(x_bez);
8
9   vars = {'FINISH'
10  '/CLEAR'
11  '/OUTPUT'
12  horzcat('t_flex=',num2str(t_flex));
13  horzcat('*DIM,Coordinates,ARRAY,',num2str(i_bez),',2')};
14  fid = fopen('Vars.txt', 'w');
15  for i=1:length(vars)
16      fprintf(fid,'%s\r\n', vars{i});
17  end
```

```matlab
18   fclose(fid);
19
20   for i=1:i_bez
21       vars2 = {...
22           horzcat('*SET,Coordinates(',num2str(i),',1),',num2str(x_bez(i)));
23           horzcat('*SET,Coordinates(',num2str(i),',2),',num2str(y_bez(i)))};
24       fid2 = fopen('Vars.txt', 'a');
25       for j=1:length(vars2)
26           fprintf(fid2,'%s\r\n', vars2{j});
27       end
28       fclose(fid2);
29   end
30
31
32   %% Combine Vars.txt + Constant.txt (=model)
33   system('copy Vars.txt+Constant.txt CompleteAnsys.txt');
34
35   %% Execute ansys
36   % Delete .lock file in case it exists. This file blocks the startup of
37   % ANSYS if it was previously closed in a wrong way.
38   if exist('Quad8.lock','file')
39       delete('Quad8.lock')
40   end
41
42   if exist('Results_Fx.txt','file')
43       delete('Results_Fx.txt')
44   end
45
46   if exist('Results_xy_locations.txt','file')
47       delete('Results_xy_locations.txt')
48   end
49
50   if exist('Results_max_stress_vec.txt','file')
51       delete('Results_max_stress_vec.txt')
52   end
53
54   dos( ' "C:\Program Files\ANSYS Inc\v161\ansys\bin\winx64\ANSYS161.exe" -b -j Quad8 ...
55       -dir "C:\Users\Sjoerd\Documents\ME2490-35 Graduation\ANSYS - Equivalent ...
56       Contact\Optimization_GA_limited" -i "C:\Users\Sjoerd\Documents\ME2490-35 ...
57       Graduation\ANSYS - Equivalent Contact\Optimization_GA_limited\CompleteAnsys.txt" ...
58       -o "C:\Users\Sjoerd\Documents\ME2490-35 Graduation\ANSYS - Equivalent ...
59       Contact\Optimization_GA_limited\output.out"');
55
56
57   id = 1; % 0=false, 1=true
58   if exist('Results_Fx.txt','file')
59       id = 0;  %Als deze file wordt geschreven is MATLAB geconvergeerd=goed
60   end
61   end
```

B.1.5. INTERSECTIONS

```matlab
1    function [id] = intersections(x1,y1,x2,y2)
2    %Function returns id = 0 when there are no intersections
3    %Function returns id = 2 when there are intersections
4
5    %INTERSECTIONS Intersections of curves.
6    %   Computes the (x,y) locations where curve(s) intersect. The curves
7    %   can be broken with NaNs or have vertical segments.
8    %
9    %   [X0,Y0] = intersections(X1,Y1,X2,Y2);
10   %
11   % You can also get intersections of a curve with itself.  Simply pass in
12   % only one curve, i.e.,
13   %
14   %   [X0,Y0] = intersections(X1,Y1);
15   %
16   % Theory of operation:
```

```
17  %
18  % Given two line segments, L1 and L2,
19  %
20  %   L1 endpoints:  (x1(1),y1(1)) and (x1(2),y1(2))
21  %   L2 endpoints:  (x2(1),y2(1)) and (x2(2),y2(2))
22  %
23  % we can write four equations with four unknowns and then solve them.  The
24  % four unknowns are t1, t2, x0 and y0, where (x0,y0) is the intersection of
25  % L1 and L2, t1 is the distance from the starting point of L1 to the
26  % intersection relative to the length of L1 and t2 is the distance from the
27  % starting point of L2 to the intersection relative to the length of L2.
28  %
29  % So, the four equations are
30  %
31  %    (x1(2) - x1(1))*t1 = x0 - x1(1)
32  %    (x2(2) - x2(1))*t2 = x0 - x2(1)
33  %    (y1(2) - y1(1))*t1 = y0 - y1(1)
34  %    (y2(2) - y2(1))*t2 = y0 - y2(1)
35  %
36  % Rearranging and writing in matrix form,
37  %
38  %  [x1(2)-x1(1)        0        -1   0;      [t1;       [-x1(1);
39  %        0        x2(2)-x2(1)  -1   0;   *    t2;   =    -x2(1);
40  %   y1(2)-y1(1)        0         0  -1;       x0;        -y1(1);
41  %        0        y2(2)-y2(1)   0  -1]       y0]        -y2(1)]
42  %
43  % Let's call that A*T = B.  We can solve for T with T = A\B.
44  %
45  % Once we have our solution we just have to look at t1 and t2 to determine
46  % whether L1 and L2 intersect.  If 0 ≤ t1 < 1 and 0 ≤ t2 < 1 then the two
47  % line segments cross and we can include (x0,y0) in the output.
48  %
49  % In principle, we have to perform this computation on every pair of line
50  % segments in the input data.  This can be quite a large number of pairs so
51  % we will reduce it by doing a simple preliminary check to eliminate line
52  % segment pairs that could not possibly cross.  The check is to look at the
53  % smallest enclosing rectangles (with sides parallel to the axes) for each
54  % line segment pair and see if they overlap.  If they do then we have to
55  % compute t1 and t2 (via the A\B computation) to see if the line segments
56  % cross, but if they don't then the line segments cannot cross.  In a
57  % typical application, this technique will eliminate most of the potential
58  % line segment pairs.
59
60
61  % Input checks.
62  error(nargchk(2,5,nargin))
63
64  % Adjustments when fewer than five arguments are supplied.
65  switch nargin
66      case 2
67          robust = true;
68          x2 = x1;
69          y2 = y1;
70          self_intersect = true;
71      case 3
72          robust = x2;
73          x2 = x1;
74          y2 = y1;
75          self_intersect = true;
76      case 4
77          robust = true;
78          self_intersect = false;
79      case 5
80          self_intersect = false;
81  end
82
83
84  % Force all inputs to be column vectors.
85  x1 = x1(:);
86  y1 = y1(:);
87
```

```
88   % Compute number of line segments in each curve and some differences we'll
89   % need later.
90   n1 = length(x1) - 1;
91   n2 = length(x2) - 1;
92   xy1 = [x1 y1];
93   xy2 = [x2 y2];
94   dxy1 = diff(xy1);
95   dxy2 = diff(xy2);
96
97   % Determine the combinations of i and j where the rectangle enclosing the
98   % i'th line segment of curve 1 overlaps with the rectangle enclosing the
99   % j'th line segment of curve 2.
100  [i,j] = find(repmat(min(x1(1:end-1),x1(2:end)),1,n2) <= ...
101      repmat(max(x2(1:end-1),x2(2:end)).',n1,1) & ...
102      repmat(max(x1(1:end-1),x1(2:end)),1,n2) >= ...
103      repmat(min(x2(1:end-1),x2(2:end)).',n1,1) & ...
104      repmat(min(y1(1:end-1),y1(2:end)),1,n2) <= ...
105      repmat(max(y2(1:end-1),y2(2:end)).',n1,1) & ...
106      repmat(max(y1(1:end-1),y1(2:end)),1,n2) >= ...
107      repmat(min(y2(1:end-1),y2(2:end)).',n1,1));
108
109  % Force i and j to be column vectors, even when their length is zero, i.e.,
110  % we want them to be 0-by-1 instead of 0-by-0.
111  i = reshape(i,[],1);
112  j = reshape(j,[],1);
113
114  % Find segments pairs which have at least one vertex = NaN and remove them.
115  % This line is a fast way of finding such segment pairs.  We take
116  % advantage of the fact that NaNs propagate through calculations, in
117  % particular subtraction (in the calculation of dxy1 and dxy2, which we
118  % need anyway) and addition.
119  % At the same time we can remove redundant combinations of i and j in the
120  % case of finding intersections of a line with itself.
121  if self_intersect
122      remove = isnan(sum(dxy1(i,:) + dxy2(j,:),2)) | j <= i + 1;
123  else
124      remove = isnan(sum(dxy1(i,:) + dxy2(j,:),2));
125  end
126  i(remove) = [];
127  j(remove) = [];
128
129  % Initialize matrices.  We'll put the T's and B's in matrices and use them
130  % one column at a time.  AA is a 3-D extension of A where we'll use one
131  % plane at a time.
132  n = length(i);
133  T = zeros(4,n);
134  AA = zeros(4,4,n);
135  AA([1 2],3,:) = -1;
136  AA([3 4],4,:) = -1;
137  AA([1 3],1,:) = dxy1(i,:).';
138  AA([2 4],2,:) = dxy2(j,:).';
139  B = -[x1(i) x2(j) y1(i) y2(j)].';
140
141  % Loop through possibilities.  Trap singularity warning and then use
142  % lastwarn to see if that plane of AA is near singular.  Process any such
143  % segment pairs to determine if they are colinear (overlap) or merely
144  % parallel.  That test consists of checking to see if one of the endpoints
145  % of the curve 2 segment lies on the curve 1 segment.  This is done by
146  % checking the cross product
147  %
148  %    (x1(2),y1(2)) - (x1(1),y1(1)) x (x2(2),y2(2)) - (x1(1),y1(1)).
149  %
150  % If this is close to zero then the segments overlap.
151
152  % If the robust option is false then we assume no two segment pairs are
153  % parallel and just go ahead and do the computation.  If A is ever singular
154  % a warning will appear.  This is faster and obviously you should use it
155  % only when you know you will never have overlapping or parallel segment
156  % pairs.
157
158
```

```
159        overlap = false(n,1);
160        warning_state = warning('off','MATLAB:singularMatrix');
161        % Use try-catch to guarantee original warning state is restored.
162        try
163            lastwarn('')
164            for k = 1:n
165                T(:,k) = AA(:,:,k)\B(:,k);
166                [last_warn] = lastwarn;
167                lastwarn('')
168                if strcmp(last_warn,'MATLAB:singularMatrix')
169                    % Force in_range(k) to be false.
170                    T(1,k) = NaN;
171                    % Determine if these segments overlap or are just parallel.
172                    overlap(k) = rcond([dxy1(i(k),:);xy2(j(k),:) - xy1(i(k),:)]) < eps;
173                end
174            end
175            warning(warning_state)
176        catch err
177            warning(warning_state)
178            rethrow(err)
179        end
180        % Find where t1 and t2 are between 0 and 1 and return the corresponding
181        % x0 and y0 values.
182        in_range = (T(1,:) ≥ 0 & T(2,:) ≥ 0 & T(1,:) ≤ 1 & T(2,:) ≤ 1).';
183        % For overlapping segment pairs the algorithm will return an
184        % intersection point that is at the center of the overlapping region.
185        if any(overlap)
186            ia = i(overlap);
187            ja = j(overlap);
188            % set x0 and y0 to middle of overlapping region.
189            T(3,overlap) = (max(min(x1(ia),x1(ia+1)),min(x2(ja),x2(ja+1))) + ...
190                min(max(x1(ia),x1(ia+1)),max(x2(ja),x2(ja+1)))).'/2;
191            T(4,overlap) = (max(min(y1(ia),y1(ia+1)),min(y2(ja),y2(ja+1))) + ...
192                min(max(y1(ia),y1(ia+1)),max(y2(ja),y2(ja+1)))).'/2;
193            selected = in_range | overlap;
194        else
195            selected = in_range;
196        end
197        xy0 = T(3:4,selected).';
198
199        % Remove duplicate intersection points.
200        [xy0,index] = unique(xy0,'rows');
201        x0 = xy0(:,1);
202        y0 = xy0(:,2);
203
204        if isempty([x0 y0])
205            id = 0;
206        else
207            id = 2;
208        end
209    end
```

B.1.6. THICKNESS BOUNDS

```
1  function [id]=Thickness_bounds(t_flex,x_bez,y_bez)
2  % Function to create boundary region around calculated Bezier curve.
3  % Bounds are based on material thickness and required gap between line segments
4  % If bounds are not violated, output id = 0, else output id = 4
5
6  dist_sep = 2*t_flex + 180e-6;    %[m] minimal required seperation between lines
7
8  for i=1:length(x_bez)-1
9
10 % Input
11 Ax = x_bez(i);
12 Ay = y_bez(i);
13 Bx = x_bez(i+1);
14 By = y_bez(i+1);
```

```
15
16   mid_x = (Bx+Ax)/2;
17   mid_y = (By+Ay)/2;
18
19   LAB = sqrt((Bx-Ax)^2 + (By-Ay)^2);  %[m] length evaluated segment
20   d = dist_sep/LAB;                   %[-] correction factor to scale offset to dist_sep
21
22   %% Calculation
23   vx = Bx - Ax;
24   vy = By - Ay;
25
26   X = vy*d/sqrt(1+vx^2);
27   Y = -vx/vy*X;
28
29   % Side 1 of line LAB
30   Cx(i) = X + mid_x;
31   Cy(i) = Y + mid_y;
32
33   % Side 2 of line LAB
34   Dx(i) = mid_x - X;
35   Dy(i) = mid_y - Y;
36
37   % Plotting
38   % figure(1);hold on; axis equal;
39   %
40   % plot(Ax,Ay,'ro',Bx,By,'bo',Cx(i),Cy(i),'go',Dx(i),Dy(i),'yo',mid_x,mid_y,'ko');  % ...
          Point: Start, End, End normal side 1, End normal side 2, Mid point
41   % plot([Ax Bx],[Ay By],'-k');              % Original line segment
42   % plot([mid_x Cx(i)],[mid_y Cy(i)],'r:');       % Normal side 1
43   % plot([mid_x Dx(i)],[mid_y Dy(i)],'g:');       % Normal side 2
44   % grid on
45   end
46
47   % figure(2);hold on;axis equal
48   % plot(x_bez,y_bez,'k',Cx,Cy,'b--',Dx,Dy,'b--')
49   % grid on
50
51   id = 0;
52   [id] = intersections(Cx',Cy');
53   if id≠2
54       [id] = intersections(Dx',Dy');
55       if id≠2
56           [id] = intersections(x_bez,y_bez,Cx',Cy');
57           if id≠2
58               [id] = intersections(x_bez,y_bez,Dx',Dy');
59           end
60       end
61   end
62
63   if id==2
64       id=4;   % Change id output (different id for intersecting line and boundary ...
              violation)
65   end
66   end
```

B.2. DATA ANALYSIS

B.2.1. STIFFNESS ANALYSIS

```matlab
1   clc;clear all;close all
2
3   %% ANSYS Results
4       stress_limit = 200e6;
5
6   % Import data from ANSYS file
7       filetoRead = ['Results_Fy' ,'.txt'];
8       filetoRead2 = ['Results_xy_locations_Fy' ,'.txt'];
9       filetoRead3 = ['Results_max_stress_vec_Fy' ,'.txt'];
10
11      % Deleting the first row (headers)
12      Data = dlmread(filetoRead,',',1,0);
13      Data2 = dlmread(filetoRead2,',',1,0);
14      Data3 = dlmread(filetoRead3,',',1,0);
15
16  %% Define all outputs
17      Fx_left = Data(:,1);        %[N]
18      Fy_left = Data(:,2);        %[N]
19      Fx_right = Data(:,3);       %[N]
20      Fy_right = Data(:,4);       %[N]
21      Ux_lowest_point = Data(:,5);%[m]
22      Uy_lowest_point = Data(:,6);%[m]
23
24      stress_max = Data3;         %[Pa] maximum stress per substep
25
26      F_lock = -Fy_left-Fy_right; %[N] Beam force on shuttle
27
28          %Interpolation on ANSYS data
29          p = polyfit([0;F_lock],[0;stress_max],4);
30          F_lock_fit = 0:0.001:max(F_lock);
31          stress_max_fit = polyval(p,F_lock_fit);
32
33          p2 = polyfit([0;F_lock],[0;Uy_lowest_point],4);
34          Uy_lowest_point_fit = polyval(p2,F_lock_fit);
35
36          pos = find(stress_max_fit-stress_limit<0, 1, 'last');    % maximum index ...
                  where stress is below maximum
37          F_lock_max = F_lock_fit(pos);            %[N] maximum locking force within ...
                  stress limit
38          stress_real = stress_max_fit(pos);
39          y_prestress = Uy_lowest_point_fit(pos); %[m] required prestress for this ...
                  locking force
40
41
42      k_ANSYS = F_lock_fit(end)/(Uy_lowest_point_fit(end)*1000);  %[N/mm]
43
44
45
46  %% Test results for LS01E1Si001
47
48  % Read and Define all Data
49  filetoRead2 = ['LS01E1Si001_16_spring_measurement_20x' ,'.txt'];
50
51  % Deleting the first row (headers)
52  Data2 = dlmread(filetoRead2,'\t',0,0);    %R=0 and C=0 specifies the first value in ...
        the file
53
54  f_c = 0.047;        %[N/V] Sensor calibration factor
55
56  x1 = Data2(:,2);    %[mm]
57  x1 = x1 - x1(1);    %[mm] Adjust displacement to start at 0mm
58
59  F1 = -f_c*Data2(:,3); %[N]
60  F1 = F1 - F1(1);
61
62  %Remove all data entries before first contact
```

```matlab
63  k = find(x1>0.05);
64  x1 = x1(k)-x1(k(1));
65  F1 = F1(k);
66
67  R = corrcoef(x1,F1);
68
69  %Data fitting + confindence intervals
70  x_vec = [0:0.001:0.6];
71  fitresult = fit(x1,F1,'poly1');
72  p_values = coeffvalues(fitresult);
73  ci = confint(fitresult,0.95);
74  lower_fit = ci(1,2) + ci(1,1)*x_vec;
75  fit = p_values(2) + p_values(1)*x_vec;
76  upper_fit = ci(2,2) + ci(2,1)*x_vec;
77
78  k_test = p_values(1);
79  k_needle = 0.8478;
80  k_real = (1/k_test - 1/k_needle)^(-1);
81  F_real = x_vec*k_real;
82
83  k_lower = ci(1,1);
84  k_upper = ci(2,1);
85  k_real_lower = (1/k_lower - 1/k_needle)^(-1);
86  F_real_lower = x_vec*k_real_lower;
87  k_real_upper = (1/k_upper - 1/k_needle)^(-1);
88  F_real_upper = x_vec*k_real_upper;
89
90  hold on
91  plot(Uy_lowest_point_fit*1000,F_lock_fit, 'r-.',x_vec,fit,'k',x_vec,F_real,'b:')%,...
92      %x_vec,lower_fit,'k:',x_vec,upper_fit,'k:',x_vec,F_real_lower,'b:',x_vec,F_real_upper,'b:')
93  xlabel('Displacement [mm]')
94  ylabel('Force [N]')
95  grid on
96  legend(['FEM: k = ' num2str(k_ANSYS) ' N/mm'],['\mu test results : k = ' ...
97      num2str(k_test) ' N/mm'],['\mu corrected stiffness : k = ' num2str(k_real) ' ...
98      N/mm'],'Location','NorthWest')
97  axis([0 0.1 0 0.1])
98
99  % k_real_lower - k_real
100 % k_real_upper - k_real
101
102 % k_lower - k_test
103 % k_upper - k_test
104
105 %% Plot with original data
106 % hold on
107 % plot(x1,F1,'k',x_vec,fit,'k:',x_vec,F_real,'b--',x_vec,lower_fit,x_vec,upper_fit)
108 % xlabel('Displacement [mm]')
109 % ylabel('Force [N]')
110 % grid on
111 % legend(['FEM: k = ' num2str(k_ANSYS) ' N/mm'],'Tests Results',['Linear Fit : k = ' ...
112      num2str(k_test) ' N/mm'],['Corrected stiffness : k = ' num2str(k_real) ' ...
113      N/mm'],'Location','NorthWest')
112 % axis([0 0.1 0 0.1])
```

B.2.2. Full Stroke Analysis

```matlab
1   clc;clear all;close all
2
3   %% Test results for LS01E1Si001
4
5   % Read and Define all Data
6   filetoRead = ['LS01E1Si001_25_0_01_full_stroke' ,'.txt'];
7   filetoRead2 = ['LS01E1Si001_26_0_01_full_stroke' ,'.txt'];
8   filetoRead3 = ['LS01E1Si001_27_0_01_full_stroke' ,'.txt'];
9
10  % Deleting the first row (headers)
```

```matlab
11  Data = dlmread(filetoRead,'\t',0,0);    %R=0 and C=0 specifies the first value in the ...
        file
12  Data2 = dlmread(filetoRead2,'\t',0,0);   %R=0 and C=0 specifies the first value in ...
        the file
13  Data3 = dlmread(filetoRead3,'\t',0,0);   %R=0 and C=0 specifies the first value in ...
        the file
14
15
16  % Sensor calibration: gain + shift
17  f_c = 0.047;        %[N/V] Sensor calibration factor
18
19  x1 = Data(:,2);     %[mm]
20  x1 = x1 - x1(1);    %[mm] Adjust displacement to start at 0mm
21  F1 = -f_c*Data(:,3);%[N] volt to newton conversion
22  F1 = F1 - F1(1);    %[N] Force shift to start at F=0
23
24  x2 = Data2(:,2);     %[mm]
25  x2 = x2 - x2(1);     %[mm] Adjust displacement to start at 0mm
26  F2 = -f_c*Data2(:,3);%[N] volt to newton conversion
27  F2 = F2 - F2(1);     %[N] Force shift to start at F=0
28
29  x3 = Data3(:,2);     %[mm]
30  x3 = x3 - x3(1);     %[mm] Adjust displacement to start at 0mm
31  F3 = -f_c*Data3(:,3);%[N] volt to newton conversion
32  F3 = F3 - F3(1);     %[N] Force shift to start at F=0
33
34  % Remove all data entries before first contact
35  value = 0.1;
36  u = find(x1>value);
37  x1 = x1(u)-x1(u(1));
38  F1 = F1(u);
39
40  u2 = find(x2>value);
41  x2 = x2(u2)-x2(u2(1));
42  F2 = F2(u2);
43
44  u3 = find(x3>value);
45  x3 = x3(u3)-x3(u3(1));
46  F3 = F3(u3);
47
48  % Manual data fitting
49  Ax = 0;
50  Ay = 0;
51  Bx = 0.556;
52  By = 0.003835;
53  Cx = 0.805;
54  Cy = 0.1504;
55  Dx = 1.199;
56  Dy = 0.1515;
57  DEx = 1.020;
58  DEy= 0;
59
60  x_test = [Ax Bx Cx Dx DEx Ax];
61  y_test = [Ay By Cy Dy DEy Ay];
62
63  k_needle = 0.8478;
64  k1 = (By-Ay)/(Bx-Ax);
65  k_real1 = (1/k1 - 1/k_needle)^(-1);
66  k2 = (Cy-By)/(Cx-Bx);
67  k_real2 = (1/k2 - 1/k_needle)^(-1);
68  k3 = (Dy-Cy)/(Dx-Cx);
69  k_real3 = (1/k3 - 1/k_needle)^(-1);
70  k4 = (Dy-DEy)/(Dx-DEx);
71  k_real4 = (1/k4 - 1/k_needle)^(-1);
72
73  x_cor = [Ax Bx Cx-(Dx-DEx) DEx DEx Ax];
74  y_cor = [Ay By Cy Dy DEy Ay];
75
76  %% Plotting
77  plot(x_test,y_test,'ro:',x_cor,y_cor,'bo-.',x1,F1,'k',x2,F2,'k',x3,F3,'k','LineWidth',1)
78  xlabel('Displacement [mm]')
```

```matlab
79  ylabel('Force [N]')
80  grid on
81  legend('Fitted Result','Corrected Result','Test results','Location','NorthWest')
82  axis([0 1.3 0 0.18])
83
84  coords = [Ax Ay;Bx By;Cx-(Dx-DEx) Cy;DEx Dy];
85
86  text(coords([1,4],1), coords([1,4],2), ['A';'D'],...
87      'VerticalAlignment','bottom', ...
            'HorizontalAlignment','left','FontWeight','bold','FontSize',14)
88
89  text(coords([2,3],1), coords([2,3],2), ['B';'C'],...
90      'VerticalAlignment','bottom', ...
            'HorizontalAlignment','right','FontWeight','bold','FontSize',14)
```

BIBLIOGRAPHY

[1] M. Andrews, I. Harris, and G. Turner. A comparison of squeeze-film theory with measurements on a microstructure. *Sensors and Actuators A: Physical*, 36(1):79–87, 1993.

[2] D. J. Bell, T. J. Lu, N. A. Fleck, and S. M. Spearing. Mems actuators and sensors: observations on their performance and selection for purpose. *Journal of Micromechanics and Microengineering*, 15(7):S153, 2005.

[3] R. G. Christian. The theory of oscillating-vane vacuum gauges. *Vacuum*, 16(4):175–178, 1966.

[4] S Enderling, J. Hedley, L. Jiang, R. Cheung, C. Zorman, M. Mehregany, and A.J. Walton. Characterization of frequency tuning using focused ion beam platinum deposition. *Journal of Micromechanics and Microengineering*, 17(2):213, 2007.

[5] W. S. Griffin, H. H. Richardson, and S. Yamanami. A study of fluid squeeze-film damping. *Journal of Fluids Engineering*, 88(2):451–456, 1966.

[6] H. Hosaka, K. Itao, and S. Kuroda. Damping characteristics of beam-shaped micro-oscillators. *Sensors and Actuators A: Physical*, 49(1–2):87–95, 1995.

[7] D. Joachim and Lin Liwei. Selective polysilicon deposition for frequency tuning of mems resonators. In *Micro Electro Mechanical Systems, 2002. The Fifteenth IEEE International Conference on*, pages 727–730, 2002.

[8] J.M. Kirby. *Micro- and Nanoscale Fluid Mechanics. Transport in Microfluidic Devices*. Cambridge University Press, New York, United States of America, 2010.

[9] K. Kokubun, M. Hirata, H. Murakami, Y. Toda, and M. Ono. A bending and stretching mode crystal oscillator as a friction vacuum gauge. *Vacuum*, 34(8–9):731–735, 1984.

[10] M.J. Novack. *Design and fabrication of thin film micromachined accelerometer*. M.s. thesis, 1992.

[11] J. B. Starr. Squeeze-film damping in solid-state accelerometers. In *Solid-State Sensor and Actuator Workshop, 1990. 4th Technical Digest., IEEE*, pages 44–47, 1990.

[12] H. Sumali and T.G. Carne. Air-drag damping on micro-cantilever beams.

[13] Z. Xiongxing, P. Shoujun, and Z. Jinlong. Air damping effects of mems parallel-plate structure using ansys thin film analysis. *Advanced Materials Research*, 403-408:4588–4592, 2012.